

**In-Cylinder Combustion Analysis of a Yamaha R6 FSAE Engine:
Achieving Improved Engine Performance and Efficiency
through Burn Rate Combustion Diagnostics**

by

Jacob Timothy Fredrick

A thesis submitted to the Graduate Faculty of
Auburn University
in partial fulfillment of the
requirements for the Degree of
Master of Science

Auburn, Alabama
May 9, 2011

Keywords: internal, combustion, reciprocating, engine, burn rate analysis, FSAE

Copyright 2011 by Jacob Timothy Fredrick

Approved by

Peter D. Jones, Chair, Woltosz WEMS Professor of Mechanical Engineering
Daniel W. Mackowski, Associate Professor of Mechanical Engineering
Jay M. Khodadadi, Alumni Professor of Mechanical Engineering
Roy W. Knight, Assistant Professor of Mechanical Engineering

Abstract

The actual three-dimensional, turbulent combustion process that occurs in a modern, spark-ignited internal combustion engine is very complex and difficult to model. However, since cylinder pressure is directly related to the combustion event, in-cylinder pressure traces sampled and averaged over multiple cycles can be utilized to provide the burn rate of the air and fuel mixture in the cylinder with respect to crankshaft position. A design of experiment was created to examine the influence of ignition timing, fuel rail pressure, injection timing, and air to fuel ratio on the start of combustion, burn duration, and combustion centroid at various engine operating points. Once the factors controlling the three burn rate profile parameters were understood, they were used to manipulate the combustion event and improve engine performance and efficiency. Through the in-cylinder pressure analysis performed, an indicated specific fuel consumption of 0.469 lbm/hp-hr and an indicated mean effective pressure of 43 psi were realized for the 15% load, 3,000 rpm operating point. An indicated specific fuel consumption of 0.356 lbm/hp-hr and an indicated mean effective pressure of 88 psi were achieved for the 60% load, 3,000 rpm operating point. The study was performed on a 599 cc Yamaha R6, four stroke, inline four cylinder, naturally aspirated, spark ignition engine with a restricted intake for use in Formula SAE competition.

Acknowledgements

I am very grateful to my parents, Tim and Wanda Fredrick, who have pushed me to give nothing but my best in everything. It is by their example that I acquired the discipline and determination necessary to succeed in graduate school. I would also like to show my appreciation to my teammates on Auburn FSAE. They have been a great group to work with, and I'm fortunate to have been one of their teammates. In particular, I would like to thank Dr. Peter Jones, Brian Keyser, and Sean Baker for their dedication, support, and expertise given throughout this experiment as well as Kistler and BEI Encoders for their generous sponsorship of this research. In addition, the service of Dr. Daniel Mackowski, Dr. Jay Khodadadi, and Dr. Roy Knight on my advisory committee was much appreciated. I would also like to acknowledge Paul Wiczynski, Chris Byus, Ryan Siefring, Arvind Suresh, Pete Woon, Joe Reynolds, and Chris Pollitt for the exposure to internal combustion engine testing they granted me in my time at Cummins, Inc. Last, but certainly not least, I would like to thank Greg Nelson for all of the guidance he gave me during my young engineering career at Harley-Davidson Motor Company and for encouraging and greatly influencing my decision to pursue my Master's Degree in Mechanical Engineering here at Auburn University.

Table of Contents

Abstract	ii
Acknowledgements	iii
List of Tables	vi
List of Figures	vii
List of Abbreviations	x
Chapter 1: Background	1
2.1 Spark Ignition Engine Pre-Mixed Flame Development	5
2.2 Calculating Performance and Efficiency Indicators from the P-V Diagram	6
2.3 Quantifying Combustion Variability	8
Chapter 2: Working Principles of the System.....	5
Chapter 3: Modeling Techniques and Equations	10
3.1 Combustion Modeling Approaches	10
3.2 Derivation of the Mass Fraction Burn Rate	13
Chapter 4: Instrumentation & Programming	20
4.1 Piezoelectric Pressure Sensors	20
4.2 Incremental Angular Encoders	27
4.3 Data Acquisition	28
4.4 Data Integrity and Analysis	30
Chapter 5: Component Machining & Dynamometer Setup.....	34

5.1 Cylinder Head Drilling Procedure	34
5.2 Angular Encoder Component Machining and Dynamometer Setup	39
Chapter 6: Design of Experiment	42
6.1 15% Load, 3,000 RPM DOE	42
6.2 60% Load, 3,000 RPM DOE	47
Chapter 7: Experimental Results	54
7.1 15% Load, 3,000 RPM Experimental Results	54
7.2 60% Load, 3,000 RPM Experimental Results	60
Chapter 8: Conclusions	68
References.....	70
Appendix.....	72
LabView 2009 Data Acquisition Block Diagram.....	72
LabView 2009 Data Acquisition Front Panel.....	73
MATLAB R2009a Data Analysis Code	74
MATLAB R2009a JANAF Table Thermodynamic Data Code	87

List of Tables

Table 1-1: Yamaha R6 engine specifications	1
Table 4-1: Measurement task and recommended crank degree resolution.....	27
Table 4-2: Test readiness and verification instructions	31
Table 6-1: 15% load, 3,000 RPM DOE matrix.....	42
Table 6-2: 15% load, 3,000 RPM SOC ANOVA	44
Table 6-3: 15% load, 3,000 RPM combustion centriod ANOVA	45
Table 6-4: 15% load, 3,000 RPM combustion duration ANOVA	46
Table 6-5: 60% load, 3,000 RPM DOE matrix.....	47
Table 6-6: 60% load, 3,000 RPM SOC ANOVA	48
Table 6-7: 60% load, 3,000 RPM combustion centriod ANOVA	50
Table 6-8: 60% load, 3,000 RPM combustion duration ANOVA	51
Table 7-1: 15% load, 3,000 RPM performance and efficiency comparison.....	58
Table 7-2: 60% load, 3,000 RPM performance and efficiency comparison.....	64

List of Figures

Figure 1-1: Location of combustion on in-cylinder pressure trace.....	2
Figure 1-2: Combustion energy release aspects.....	3
Figure 2-1: Four-Stroke P-V Diagram.....	6
Figure 3-1: Cylinder control volume	14
Figure 4-1: Kistler 5001 charge amplifier and 6052A high temperature pressure sensor	21
Figure 4-2: Standard deviation of pressure as a function of crankshaft position.....	23
Figure 4-3: Variation in pressure readings from 40 degrees ATDC to EVO	24
Figure 4-4: Thermal shock distortion on the log-log P-V diagram	24
Figure 4-5: Thermal shock effect on the mass fraction burned curve	25
Figure 4-6: National Instruments USB-6210 data acquisition unit	29
Figure 4-7: MoTeC M400 ECU.....	29
Figure 4-8: IMEP control chart.....	31
Figure 4-9: Data analysis program flowchart	33
Figure 5-1: Tilt table and cylinder head jig adjustment on mill	35
Figure 5-2: Mill setup for second cylinder head machining operation.....	36
Figure 5-3: Pressure sensor communication passage.....	37
Figure 5-4: Mounting sleeve location in cylinder head	37
Figure 5-5: Disassembled upper crankcase, transmission, & power cylinder components....	38
Figure 5-6: Disassembled lower crankcase, cylinder head, & clutch components.....	38

Figure 5-7: Crankshaft encoder assembly.....	39
Figure 5-8: Crankshaft encoder bracket construction	40
Figure 5-9: Crankshaft encoder mating shaft.....	41
Figure 5-10: Engine dynamometer test stand	41
Figure 6-1: 15% load, 3,000 RPM SOC half-normal plot	43
Figure 6-2: 15% load, 3,000 RPM combustion centroid half-normal plot	44
Figure 6-3: 15% load, 3,000 RPM combustion duration half-normal plot.....	45
Figure 6-4: 15% load, 3,000 RPM DOE mass fraction burned curves.....	46
Figure 6-5: 60% load, 3,000 RPM SOC half-normal plot	48
Figure 6-6: 60% load, 3,000 RPM combustion centroid half-normal plot	49
Figure 6-7: 60% load, 3,000 RPM combustion duration half-normal plot.....	50
Figure 6-8: 60% load, 3,000 RPM DOE mass fraction burned curves.....	51
Figure 6-9: Mass fraction burned dependency on ignition timing.....	52
Figure 6-10: Mass fraction burned dependency on lambda	53
Figure 7-1: 15% load, 3,000 RPM ISFC as a function of SOC placement.....	54
Figure 7-2: 15% load, 3,000 RPM IMEP as a function of SOC placement	55
Figure 7-3: 15% load, 3,000 RPM ignition delay	55
Figure 7-4: 15% load, 3,000 RPM ISFC as a function of combustion centroid placement....	56
Figure 7-5: 15% load, 3,000 RPM IMEP as a function of combustion centriod placement ..	57
Figure 7-6: 15% load, 3,000 RPM combustion centroid placement characteristics	57
Figure 7-7: 15% load, 3,000 RPM fired and motored cycle.....	58
Figure 7-8: 15% load, 3,000 RPM P-V diagram	59
Figure 7-9: 15% load, 3,000 RPM log-log P-V diagram.....	59

Figure 7-10: 15% load, 3,000 RPM mass fraction burned curve.....	60
Figure 7-11: 60% load, 3,000 RPM ISFC as a function of SOC placement.....	61
Figure 7-12: 60% load, 3,000 RPM IMEP as a function of SOC placement	61
Figure 7-13: 60% load, 3,000 RPM ignition delay.....	62
Figure 7-14: 60% load, 3,000 RPM ISFC as a function of combustion centroid placement..	62
Figure 7-15: 60% load, 3,000 RPM IMEP as a function of combustion centriod placement	63
Figure 7-16: 60% load, 3,000 RPM combustion centriod placement characteristics.....	63
Figure 7-17: 60% load, 3,000 RPM fired and motored cycle.....	64
Figure 7-18: 60% load, 3,000 RPM P-V diagram	65
Figure 7-19: 60% load, 3,000 RPM log-log P-V diagram.....	66
Figure 7-20: 60% load, 3,000 RPM mass fraction burned curve.....	66

List of Abbreviations

Acronyms

AF	air to fuel ratio
ANOVA	analysis of variance
BDC	bottom dead center
COV	coefficient of variation
CR	compression ratio
DOE	design of experiment
ECM	engine control module
FSAE	Formula Society of Automotive Engineers
IMEP	indicated mean effective pressure
ISFC	indicated specific fuel consumption
LNV	lowest normalized value
LPP	location of peak pressure
MAP	manifold absolute pressure
MBT	max brake torque
NA	naturally aspirated
PCP	peak cylinder pressure
P-V	pressure vs. volume diagram
SI	spark ignition

SOC	start of combustion
STD	standard deviation
TDC	top dead center

Symbols

a	Wiebe function efficiency parameter
A	instantaneous combustion chamber surface area
A_{ch}	cylinder head combustion chamber surface area
A_f	area of flame front
A_p	piston crown surface area
B	cylinder bore
c_v	specific heat at constant volume
c_{vch}	charge specific heat at constant volume
c_{vr}	residual specific heat at constant volume
C	Woschni heat transfer calibration constant
C_1	average cylinder gas velocity empirical calibration parameter
C_2	average cylinder gas velocity empirical calibration parameter
e	Reynolds number exponent
ff	turbulent flame factor
h	heat transfer coefficient averaged over combustion chamber surface area
i	index of summation
i_t	ignition timing in terms of crank angle BTDC

l	connecting rod length
L	piston stroke
m	mass
	Wiebe function form factor
m_b	burned mass
m_{ch}	charge mass
m_f	mass of fuel inducted per cycle
m_r	residual mass
n	upper bound of summation
N	crankshaft rotational speed
P	instantaneous cylinder pressure
P_m	instantaneous motored cylinder pressure
P_r	working fluid reference pressure
Q	heat transfer
Q_{ht}	spatially averaged combustion chamber heat transfer
Q_{HV}	heating value of fuel
r	crankshaft throw
s	distance between crankshaft axis and piston pin axis
S_p	mean piston speed
t	time
T	mean gas temperature
T_r	working fluid reference temperature

T_{wall}	mean combustion chamber wall temperature
u	specific internal energy
u_{bg}	specific internal energy of burned exhaust gas
u_{ch}	specific internal energy of unburned charge
U	internal energy
U_1	laminar flame speed
U_t	turbulent flame speed
V	instantaneous cylinder volume
V_c	cylinder clearance volume
V_d	displaced cylinder volume
V_r	working fluid reference volume
V_s	swirl velocity
W	work transfer
$W_{c,i}$	indicated work per cycle
x_b	mass fraction burned
η_f	fuel conversion efficiency
θ	crank angle
θ_o	start of combustion crank angle
$\Delta\theta$	crank angle duration of combustion
λ	relative air/fuel ratio
ρ_u	density of unburned gas

ω characteristic charge velocity

Subscripts

i index of summation

min minimum

Chapter 1: Background

Measuring pressure inside the cylinder of a reciprocating engine was first utilized around the late 1700's when James Watt and others were developing steam engines. The early engine indicators used during that time were primitive mechanical devices. Although the measurement technology has advanced greatly, the goal is still the same: understand the energy release process in the cylinder to optimize power and efficiency. Utilizing in-cylinder pressure measurements is a widely used, established method of developing internal combustion engines in industry, but has yet to be used by Formula SAE (Society of Automotive Engineers) teams due to the cost and complications associated with performing combustion diagnostics. Therefore, being able to comprehend how design choices affect the in-cylinder energy release is a substantial advantage over the competition. The specifications for the Yamaha R6 engine under study are listed in Table 1-1. To comply with FSAE rules, the engine was run with a 20 millimeter restriction between the throttle and plenum.

Table 1-1: Yamaha R6 engine specifications

Engine Configuration	Inline four cylinder, 4-stroke
Engine Displacement	599 cc
Compression Ratio	13.1:1
Valves per Cylinder	4
Bore x Stroke	67 x 42.5 mm
Intake Valve Opening	39 degrees BTDC
Intake Valve Closing	65 degrees ABDC
Exhaust Valve Opening	64 degrees BBDC
Exhaust Valve Closing	24 degrees ATDC

There are two main approaches to analyzing cylinder pressure data. One is a burn rate analysis and the other is a heat release analysis. The burn rate analysis performed in this experiment is the standard choice for use with gasoline engines and produces a normalized quantity on a scale of 0 to 100 percent mass fraction burned. Heat release analysis is commonly used with diesel engine combustion studies and produces an absolute energy quantity [1]. The heat release analysis tends to be more sensitive to measurement errors than the burn rate analysis since the magnitudes of the errors are reduced by normalizing.

The pressure rise in an internal combustion reciprocating engine is due to three main factors: combustion, change in cylinder volume, and heat transfer to or from the containing surfaces [2]. The pressure change due to cylinder volume can be taken out of the equation by comparing the engine motoring curve (engine is externally powered) to the firing curve. The difference in pressure between these two diagrams is the effect of combustion. The crankshaft position where the two curves first start to diverge is the start of combustion (SOC).

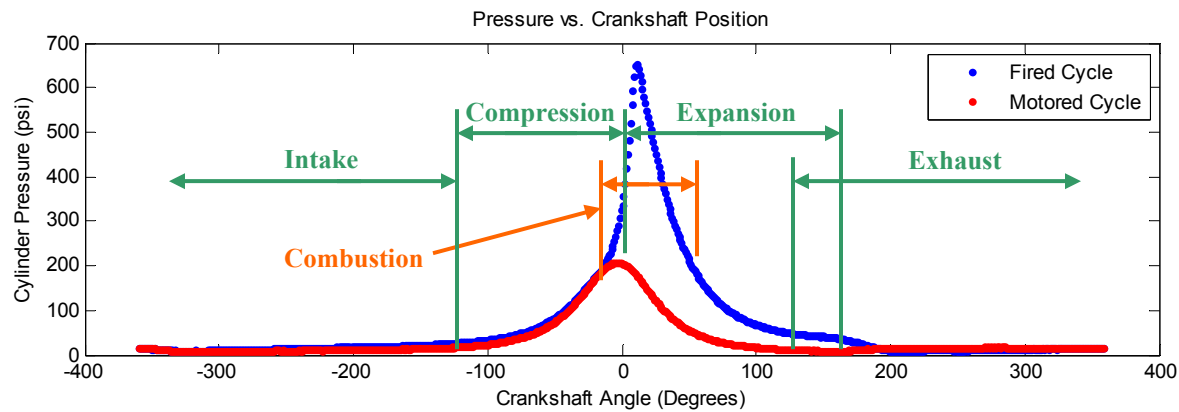


Figure 1-1: Location of combustion on in-cylinder pressure trace

The effect of heat transfer in all of this is something that can be estimated using various methods. Quite often the heat transfer is modeled as convective heat transfer while employing a heat transfer coefficient that includes the effects of radiation. The amount of

heat transfer happening in the cylinder is very complex to model since it is dependent on the in-cylinder combustion species, swirl and squish, and flame front geometry. The empirically based and proven Woschni correlation [3], which is still a preferred way to model the in-cylinder heat transfer, was utilized in this analysis.

A First Law of Thermodynamics energy balance performed on the cylinder provides a differential equation from which the in-cylinder energy release profile can be calculated. The energy-release aspects of combustion can be characterized by the parameters shown in Figure 1-2. The SOC, combustion duration, and centroid of combustion (crankshaft angle where 50% burn occurs, often abbreviated CA50) are the critical parameters. A shorter burn duration will provide a higher torque output and reduced combustion variability. The placement of the centroid and SOC has a great effect on ISFC (indicated specific fuel consumption) and IMEP (indicated mean effective pressure). The mass burn rate at the centroid location is also important to note.

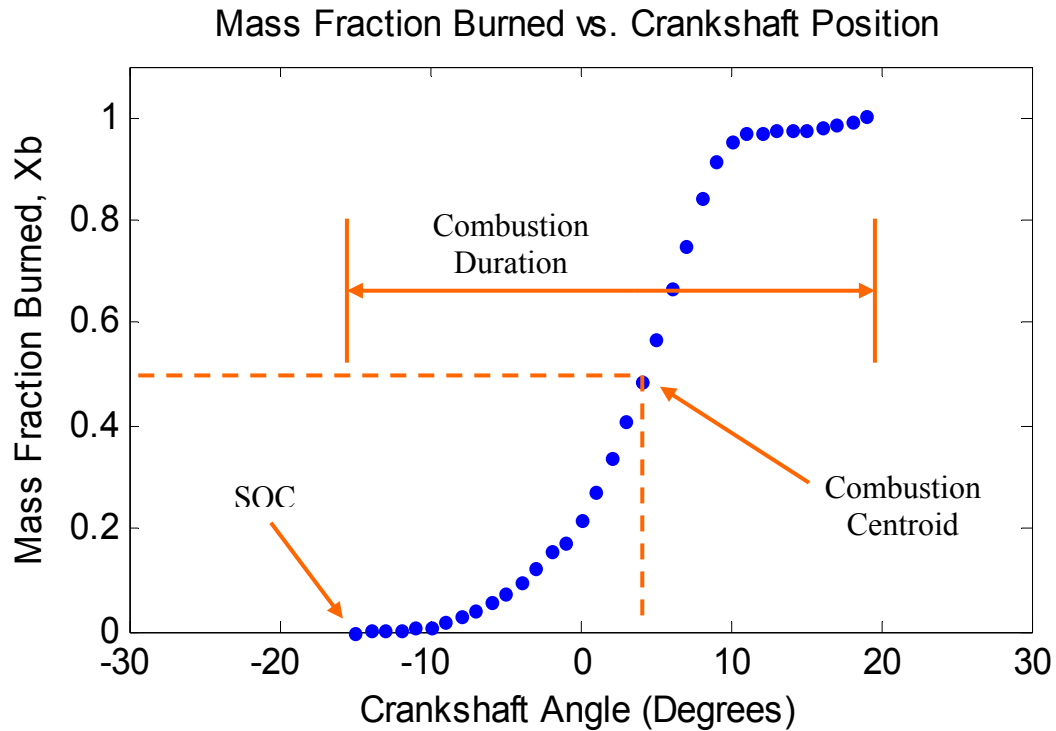


Figure 1-2: Combustion energy release aspects

Combustion in internal combustion engines occurs in a three-dimensional, time dependent, turbulent flow with a fuel containing a blend of hydrocarbons which have poorly understood combustion chemistry [4]. Even while running at constant speed, load, and temperature, there will be considerable variations in performance from cycle-to-cycle. Cycle-to-cycle and cylinder-to-cylinder variation are due to variations in the amount of air and fuel delivered, spark plug, injector signal wire resistance (from temperature variation), valve timing (spring rate variation, natural frequency, etc.), fuel density (temperature and/or air bubbles), and buildup on the injector tip. This variability can result in compromised spark timing, torque and power, lower fuel economy, and engine roughness. Taking the average of the pressure traces over a span of 100 cycles is the common practice used to minimize the effects of the variations on test measurements.

Although the combustion process in an internal combustion engine is quite complicated and riddled with variation, utilizing in-cylinder pressure traces to perform a quasi-steady, closed loop analysis offers insight on what is happening inside the cylinder. By examining the key combustion performance parameters (IMEP, combustion phasing, cyclic variation, and energy release), cylinder pressure combustion analysis allows for the evaluation of various air handling, fueling strategies, combustion chamber shapes, compression ratios, spark plug parameters, valve timing, and ignition timing in order to make sound design decisions that maximize the engine's potential for improved performance, economy, drivability, reliability, and cost.

Chapter 2: Working Principles of the System

2.1 Spark Ignition Engine Pre-Mixed Flame Development

The Yamaha R6 engine under study is naturally aspirated (NA) meaning that it draws air into the intake system at atmospheric temperature and pressure. Once the air-fuel mixture has been inducted into the cylinder and compressed, combustion initiates at the spark plug and a plasma channel is created which is roughly at 60,000 K, 300 bar and expands at supersonic velocity [5]. The chemical reactions only become possible on the kernel surface at temperatures below 3,000 K. Within roughly 0.1 ms, the kernel has grown to a diameter of 1 mm, and grows at a laminar velocity. The kernel eventually becomes wrinkled and turbulent after its diameter reaches the local integral scale of turbulence. The kernel must reach a critical diameter (the local integral scale of turbulence) in order for self-sustained combustion to begin. It is because of these events early on in the combustion process that ignition delay exists. Turbulent combustion is a wrinkled flame that behaves as a laminar flame locally. The laminar flame speed is dependent on the type of fuel, AF ratio, and pressure and temperature of the mixture [6].

The ignition delay and laminar flame speed come into play when determining spark timing. For a given mixture of fuel and air inside of a cylinder, there exists an optimum spark timing for which the engine will produce maximum torque. This timing is referred to as maximum brake torque (MBT) timing. It is a compromise between starting combustion

too early in the compression stroke when the work transfer is actually to the cylinder gases (as well as potentially subjecting the cylinder to knock) and completing combustion too late in the expansion stroke, thus lowering peak expansion stroke pressures. Knock is the pre-ignition of the end gas (mixture on the opposite side of the flame front from the spark plug) that produces a very violent and undesired detonation and supersonic pressure oscillations that are very destructive to an engine's power cylinder components. The end gas auto-ignites from abnormally high temperatures and pressures in the cylinder caused by aggressive timing. Ignition timing is a balance between the work transferred to the piston before TDC and the work transferred to the piston before BDC. The specific timing is dependent on engine speed and load.

2.2 Calculating Performance and Efficiency Indicators from the P-V Diagram

In-cylinder pressure data acquired over the operating cycle of an engine can be used to calculate the work transfer from the gas to the piston. A pressure-volume (P-V) diagram of the engine cycle is very useful in calculating the indicated work per cycle. It is simply the integral of the P-V diagram given by Eq. (2.1) [6].

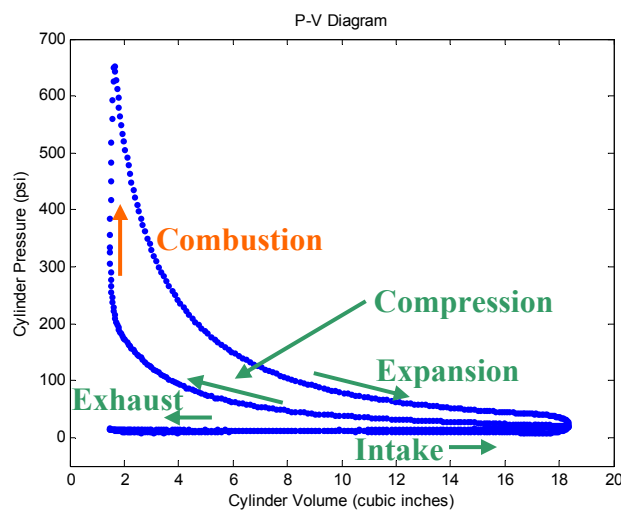


Figure 2-1: Four-Stroke P-V Diagram

$$W_{c,i} = \oint PdV \quad (2.1)$$

Gross indicated work per cycle is only the work done on the piston over the positive work loop bound by the compression and expansion strokes. Net indicated work per cycle includes the losses in the pumping loop (charge induction and exhaust) as well. The pumping loop is negative in NA engines since some amount of work is required to intake charge and exhaust burnt combustion gases. Indicated quantities only include the impact of the compression, combustion, and expansion processes on engine performance. It is a measure of the available power and torque at the crankshaft and does not include frictional losses through the drivetrain. A useful way to compare closed-cycle engine performance between different engines is to calculate the IMEP by Eq. (2.2) [6]. IMEP takes the engine's displacement into account in order to provide a fair comparison between engines of different sizes.

$$IMEP = \frac{W_{c,i}}{V_d} \quad (2.2)$$

The fuel conversion efficiency is the ratio of work output to the total available energy of the inducted fuel and is defined by Eq. (2.3) [6]. The indicated specific fuel consumption (ISFC) is the fuel flow rate per unit power output. Eq. (2.4) expresses this quantity on a per cycle basis.

$$\eta_f = \frac{W_{c,i}}{m_f Q_{HV}} \quad (2.3)$$

$$ISFC = \frac{m_f}{W_{c,i}} \quad (2.4)$$

Tuning for MBT can be accomplished by examining the average IMEP versus the crankshaft angle corresponding to the centroid of combustion and SOC. To achieve the maximum efficiency, each cylinder should be optimized individually if the ECM (engine control module) is capable of providing different ignition timings to individual cylinders. However, there will always be some phasing efficiency loss that exists.

2.3 Quantifying Combustion Variability

Combustion variability can be quantified by examining the IMEP of each cycle. The most basic approach is to calculate the standard deviation (STD) of the IMEP which gives a representation of cyclic variation and engine stability. The variability can also be expressed as a coefficient of variation (COV) by relating the STD as a percentage of the mean IMEP in Eq. (2.6) [7].

$$STD \text{ IMEP} = \sqrt{n \sum_{i=1}^n \frac{(IMEP_i - \bar{IMEP})^2}{(n-1)}} \quad (2.5)$$

$$COV \text{ IMEP} = \frac{STD \text{ IMEP}}{\bar{IMEP}} \cdot 100\% \quad (2.6)$$

Typically COV's of IMEP above 3-5% will result in drivability issues that are detectable by the driver. Misfires and partial burns can be detected by calculating the lowest normalized value (LNV) of IMEP in Eq. (2.7) [7]. The lowest IMEP is normalized by the mean IMEP. An LNV less than 80% indicates a partial burn, and a LNV less than 0% indicates a misfire.

$$LNV \text{ IMEP} = \frac{IMEP_{min}}{\bar{IMEP}} \cdot 100\% \quad (2.7)$$

Misfires occur when the flame propagation is never initiated properly. This may be due to insufficient ignition energy, conditions at the spark plug at the time of ignition,

excessive residuals, AF ratios outside of combustion limits, high compression pressures, low temperatures, high mean flow around the spark plug, and excessive plug fouling. Partial burns occur when the flame never fully propagates across the combustion chamber. Partial burns can be a result of burn durations that are too long, low compression pressures, retarded spark timing, and poorly mixed charge. Partial burns can also cause irregular misfires [7].

Chapter 3: Modeling Techniques and Equations

3.1 Combustion Modeling Approaches

Many different types of combustion models have been conceived. They are all subject to a tradeoff between the simplicity of the model and the accuracy of the results that it produces. There are three categories of approaches to model the combustion process [3]:

- Zero-Dimensional Models
 - Use empirical heat-release model
 - Time is the only independent variable
- Quasi-Dimensional Models
 - Use a separate submodel for turbulent combustion
- Multi-Dimensional Models
 - Numerically solve equations for mass, momentum, energy, and species conversion to predict flame propagation
 - 1, 2, or 3-dimensional

The zero and quasi-dimensional models are simplistic, easy to employ into an engine model, and are quite useful for parametric engine modeling. However, they are not linked to combustion chamber geometry explicitly. When combustion chamber geometry is important or being developed, a multi-dimensional model should be used.

A rather well known zero-dimensional combustion model was nicely presented by Heywood [6]. The model uses the three zones including an unburned gas zone, an adiabatic burned gas core, and a burned gas thermal boundary layer. Conservation of mass and energy are utilized to determine the conditions in the burned and unburned gas. In order to do this, however, the mass fraction burned must be calculated. This can be done with the Wiebe function [6]. The function can be fitted to experimental data to greatly reduce the number of combustion model inputs into engine simulation software.

$$x_b = 1 - \exp\left[-a\left(\frac{\theta - \theta_o}{\Delta\theta}\right)^{m+1}\right] \quad (3.1)$$

Where:

θ = crank angle

θ_o = start of combustion

$\Delta\theta$ = total combustion duration

a = efficiency parameter

m = form factor

Ferguson also utilizes the Wiebe function in his engine model [8]. Ferguson's model is much more complex and includes the effects of heat loss, blow by, and equivalence ratio. Ultimately, six ordinary differential equations are required to be simultaneously, numerically integrated. The six ordinary differential equations are the change of pressure, burned and unburned temperature, work, heat loss, and enthalpy loss with respect to crank angle.

The requirement for arbitrarily determined burn rate information for these models is not very convenient. Quasi-dimensional models try to predict the burn rate information by assuming a spherical flame front geometry, and by using information about the turbulence as an input. The equation at the forefront of this technique proposed by Stone [4] is shown in

Eq. (3.2). The product of the density of the unburned gas, area of flame front, and turbulent flame speed equals the product of the density of the unburned gas, area of flame front, and laminar flame speed multiplied by a turbulent flame factor (ff).

$$\frac{dm_b}{dt} = \rho_u A_f U_t = \rho_u A_f U_1 ff \quad (3.2)$$

This simple approach can be made much better with additional turbulence consideration. The effects of ignition delay and the pressure rise due to compression on the length scale of turbulence as well as squish and swirl need to be analyzed as well.

Since even very complex multi-dimensional models in commercial codes have trouble producing accurate simulations, a very powerful tool needed for the improvement of combustion analysis is the incorporation of experimental cylinder pressure data. The pressure inside of the cylinder is directly related to the combustion process which makes it very useful in determining the mass fraction burn profile. One of the earliest models was created by Rassweiler and Withrow in 1936 [9]. Despite its simplicity, it is still widely used. The approach only requires cylinder pressure and volume geometric details. However, this leads to several shortcomings. The model assumes that the polytropic constant is constant, while in reality, it varies from compression to expansion and changes during the combustion process. Since the model is ultimately a scaling relationship, it doesn't take into account incomplete combustion or the accuracy of cylinder pressure and mass flow rate data. Therefore, the effect of heat transfer is not included in the model. The flow of cylinder charge into crevices such as between the piston, rings, liner, head gasket gap, and spark plug threads is also ignored.

Because of the shortcomings of the Rassweiler and Withrow model, other two region models with a burned and unburned gas region have since been proposed. However, they are

computationally complicated and time-consuming. A simple, more accurate one-zone model was created by Gatowski in 1984 [10]. Cheung and Heywood then tested the validity, accuracy, and robustness of the model in 1993 [11]. This experiment uses a similar approach that tracks the charge mass burned and residual mass fraction on the basis of an individual cycle. It permits the investigation of partial burns, misfires, and heat losses through empirical correlations. The degree of burn rate variability from cycle-to-cycle can also be more accurately quantified.

3.2 Derivation of the Mass Fraction Burn Rate

Since an internal combustion engine is not a closed system, it is not a heat engine in the thermodynamic sense of the term. An engine is best analyzed as an open system that exchanges heat and work with the surrounding environment. The reactants (fuel and air mixture) flow into the cylinder, and the products (exhaust gases) flow out [6]. An equation for the energy-release of a reciprocating internal combustion SI engine can be derived from the First Law of Thermodynamics [12].

$$\frac{dU}{dt} = \frac{dQ}{dt} - \frac{dW}{dt} = \frac{dQ}{dt} - P \frac{dV}{dt} \quad (3.3)$$

Where:

$\frac{dU}{dt}$ = time rate of change of internal energy of the system

$\frac{dQ}{dt}$ = time rate of change of heat transfer (heat-release from combustion
minus the heat transfer to chamber walls)

$\frac{dW}{dt}$ = time rate change of work done by the system

$P \frac{dV}{dt}$ = time rate change of work done under quasi-static expansion

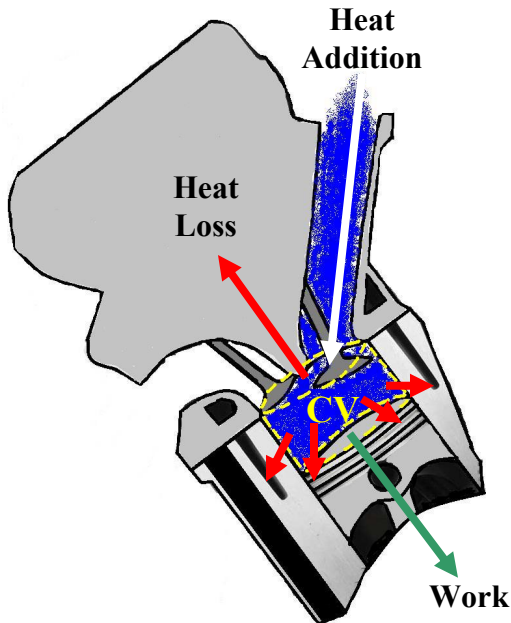


Figure 3-1: Cylinder control volume

The temperature changes which occur around minimum and maximum cylinder volumes are not primarily a result of heat transfer interactions [6]. During combustion, the temperature rise occurs to stabilize the internal energy as the species change from reactants to products. The heat transfer model used by Heywood [6] that is based off of the Woschni correlation [3] is a convective heat-transfer rate to the combustion chamber walls shown in Eq. (3.4). It includes the effects of piston movement, swirl, and combustion. This relationship is correlated with experimental data and gives an estimation of the heat flux.

$$\frac{dQ_{ht}}{dt} = Ah(T - T_{wall}) \quad (3.4)$$

Where:

A = instantaneous combustion chamber surface area

h = heat transfer coefficient averaged over the chamber surface area

T = mean cylinder gas temperature

T_{wall} = mean chamber wall temperature

The heat transfer coefficient (in W/m²K) is calculated by taking the cylinder bore as the characteristic length, calculating the average in-cylinder gas velocity, utilizing the ideal gas law, and including curve fit parameters in Eq. (3.5) [6]. The mean cylinder charge temperature can be calculated through the ideal gas law since the molecular weight of the reactants and products are nearly identical [13]. This gives a temperature very close to the actual mass averaged cylinder temperature.

$$h = 3.26CB^{e-1}P^e\omega^eT^{0.75-1.62e} \quad (3.5)$$

Where:

e = Reynolds number exponent (unit less data fit parameter)

B = cylinder bore [m]

P = cylinder pressure [Pa]

T = mean cylinder gas temperature [K]

C = calibration constant (unit less correction factor)

ω = characteristic charge velocity (piston movement, swirl, and combustion)

Eq. (3.6) [6] calculates the average cylinder gas velocity (in meters per second), which includes the effects of swirl in higher-speed engines. It has been shown to provide acceptable velocity predictions in both compression and spark ignition four-stroke, water-cooled engines. Three separate equations emerge for the combustion and expansion period, gas exchange period, and the rest of the cycle.

$$\omega = \left[C_1 S_p + C_2 \frac{V_d T_r}{P_r V_r} \right] (P - P_m) \quad (3.6)$$

Where:

$C_1 = 2.28$, $C_2 = 3.24 \times 10^{-3}$ - combustion and expansion period

$$C_1 = 6.28 + 0.417 \frac{V_s}{S_p}, \quad C_2 = 0 \text{ - gas exchange period} \quad (3.7)$$

$$C_1 = 2.28 + 0.308 \frac{V_s}{S_p}, \quad C_2 = 0 \text{ - rest of the cycle} \quad (3.8)$$

$$S_p = 2LN \text{ - mean piston speed [m/s]} \quad (3.9)$$

(L = piston stroke, N = crankshaft rotational speed)

V_s = swirl velocity [m/s]

V_d = displaced volume [m^3]

T_r = working fluid temperature at start of combustion [K]

P_r = working fluid pressure at start of combustion [Pa]

V_r = working fluid volume at start of combustion [m^3]

P_m = motored cylinder pressure [Pa]

P = cylinder pressure [Pa]

The time rate of change of work transfer done by the system can be calculated by converting the rate of change of cylinder volume with respect to time to the rate of change of cylinder volume with respect to crankshaft angle.

$$P \frac{dV}{dt} = P 2\pi N \frac{dV}{d\theta} \quad (3.10)$$

To calculate the cylinder volume, piston position, and combustion chamber area at any crankshaft position, the following three equations can be utilized respectively [6].

$$V = V_c + \frac{\pi B^2}{4} (l + r - s) \quad (3.11)$$

$$s = r \cos \theta + (l^2 - r^2 \sin^2 \theta)^{1/2} \quad (3.12)$$

$$A = A_{ch} + A_p + \pi B(l + r - s) \quad (3.13)$$

Where:

V_c = cylinder clearance volume

B = cylinder bore

l = connecting rod length

r = crankshaft throw

s = distance between crankshaft axis and piston pin axis

A_{ch} = cylinder head combustion chamber surface area

A_p = piston crown surface area

The internal energy of the cylinder gases can be split by the burned and fresh charge mass fractions. Then the time rate of change of internal energy can be related to the change in crankshaft angle.

$$U = mu = mx_b u_{bg} + m(1 - x_b)u_{ch} \quad (3.14)$$

$$\frac{dU}{dt} = 2\pi N \frac{d}{d\theta} [mx_b u_{bg} + m(1 - x_b)u_{ch}] \quad (3.15)$$

Where:

$m = m_{ch} + m_r$ - mass of fresh charge plus residual mass

x_b = mass fraction burned

u_{bg} = specific internal energy of burned exhaust gas

u_{ch} = specific internal energy of unburned charge

The product rule can be used to expand Eq. (3.15) by relating the rate of change of mass and internal energy to the rate of change of crankshaft angle.

$$\frac{dU}{dt} = 2\pi N \left[(x_b u_{bg} + (1 - x_b)u_{ch}) \frac{dm}{d\theta} + m \frac{d}{d\theta} [x_b u_{bg} + (1 - x_b)u_{ch}] \right] \quad (3.16)$$

$$\frac{d}{d\theta} \left[x_b u_{bg} + (1-x_b) u_{ch} \right] = \\ u_{bg} \frac{dx_b}{d\theta} + x_b \frac{du_{bg}}{dT} \frac{dT}{d\theta} - u_{ch} \frac{dx_b}{d\theta} + (1-x_b) \frac{du_{ch}}{dT} \frac{dT}{d\theta} \quad (3.17)$$

If blowby is ignored, the equation is simplified greatly. Taking $dm/d\theta = 0$ reduces the rate of change of internal energy equation further. The definition of specific heat at constant volume given by Eq. (3.19) can be used to simplify the equation even more. This reveals the heat-release in Eq. (3.20).

$$\frac{dU}{dt} = 2\pi N \left\{ m(u_{bg} - u_{ch}) \frac{dx_b}{d\theta} + m \left[x_b \frac{du_{bg}}{dT} + (1-x_b) \frac{du_{ch}}{dT} \right] \frac{dT}{d\theta} \right\} \quad (3.18)$$

$$c_v(T) = \frac{du}{dT} \quad (3.19)$$

$$\frac{dU}{dt} = 2\pi N \underbrace{\left\{ m(u_{bg} - u_{ch}) \frac{dx_b}{d\theta} + mc_v \frac{dT}{d\theta} \right\}}_{heat-release} \quad (3.20)$$

Now equations (3.4), (3.10), and (3.20) can be combined to form a relation for the mass fraction burn rate with respect to the change in crankshaft angle.

$$2\pi N \left\{ m(u_{bg} - u_{ch}) \frac{dx_b}{d\theta} + mc_v \frac{dT}{d\theta} \right\} = Ah(T - T_{wall}) - P2\pi N \frac{dV}{d\theta} \quad (3.21)$$

Eq. (3.21) can be solved for the mass fraction burn rate with respect to change in crankshaft position relation shown below.

$$\frac{dx_b}{d\theta} = \boxed{\frac{\left(\frac{dQ_{ht}}{dt} - P \frac{dV}{dt} \right)}{2\pi N} - (m_{ch} c_{vch} + m_r c_{vr}) \frac{dT}{d\theta}} \quad (3.22)$$

A Taylor Series was utilized to numerically integrate the differential equation and obtain the mass fraction burned curve with respect to crankshaft position. The thermodynamic properties of the unburned and burned gas mixtures necessary to calculate the burn rate were acquired from a separate program written by Dr. Peter Jones [14] which uses polynomial curve fits from the NASA Equilibrium Code for JANAF table thermodynamic data.

Chapter 4: Instrumentation & Programming

4.1 Piezoelectric Pressure Sensors

By the late 1800's the need for engine indicators capable of accurately measuring cylinder pressure in internal combustion engines with higher peak cylinder pressures gave way to optical indicators. Devices like the planimeter were later invented to find the area of the P-V diagrams created by the indicators. The electronic age gave way to new engine indicator devices becoming commercially available. Most of them consisted of a cathode ray oscilloscope with additional hardware for measuring cylinder pressure and crankshaft position. Improvements in digital electronics allowed for high-speed analogue to digital conversions with electronic storage. Once data processing via a computer was possible, better instrumentation and signal conditioning systems gave way to more accurate data and analysis. These advanced electronic systems are now standard equipment for manufacturers and researchers of internal combustion engines, and the analysis methods used are widely used and proven.

Piezoelectric pressure sensors are the preferred equipment in acquiring reciprocating engine cylinder pressure. They are constructed of quartz which makes them very durable even in the harshest of environments, and they are capable of measuring highly dynamic pressures in the combustion chamber with great accuracy and repeatability. When the quartz crystal (SiO_2) deforms due to a pressure change in the cylinder, it sends a charge to the

charge amplifier through low noise co-axial cables. The charge is a result of the change in electric polarization which is proportional to the mechanical deformation. This is called the piezoelectric effect which was discovered by Jacques Curie in 1880 [15]. The charge amplifier which was patented by Kistler in the 1950's, converts the charge into a voltage that the data acquisition unit can read. However, the pressure signal is AC coupled. This means that the shape of the signal and relative amplitude are known, but the DC offset is not. Because of this, a procedure known as pegging is needed. Cylinder pressure pegging takes the pressure signal and corrects it to some known pressure at a given crank angle in order to convert it into an absolute pressure. Most often the MAP (manifold absolute pressure) at BDC will be used to correct the pressure signal as was done in this experiment, but the important thing is to be consistent in whatever approach is used. The magnitude of PCP (peak cylinder pressure) is so much greater than that of the air handling events that the data can contain large errors in the pumping loss loop in the P-V diagram without a pegging method. Absolute pressure is necessary to accurately obtain PCP, polytropic coefficients, temperature estimates, burn rate calculations, and pumping losses. However, it is not necessary to determine the location of peak pressure (LPP), IMEP, or the COV of IMEP [7].

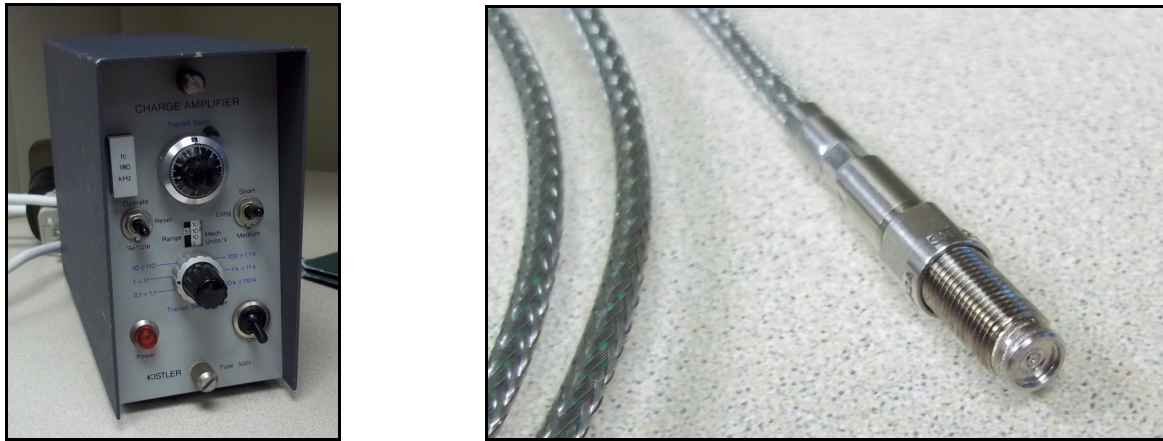


Figure 4-1: Kistler 5001 charge amplifier and 6052A high temperature pressure sensor

There are two types of piezoelectric pressure sensors, dry and wet transducers. The wet transducers utilize water cooling to minimize the effect of thermal shock on the pressure transducer. Thermal shock is the short-term drift of the sensor from exposure to hot combustion gases. As the temperature of the transducer body changes, it deforms, causing a fake signal to be superimposed on the real signal. This will show up as distortion in the cylinder pressure trace and will be evident in the mass fraction burned rate (particularly in the tail) and in the expansion and exhaust events on the log-log P-V diagram. The larger thread size of the water cooled design makes the sensor more difficult to fit into a small bore cylinder head (like passenger car engines). Modern dry sensors are designed to minimize the effects of thermal shock through various crystal cuts, and offer a temperature range for which the transducer sensitivity published on the calibration certificate is valid. However, it can never be completely compensated for and was experienced during this experiment.

The smaller size of dry transducers, allows for minimal intrusion on the actual combustion chamber geometry. The smaller crystal size also results in a lower natural frequency. This enhances the transducer's ability to measure knock and combustion noise as well as its ability to acquire measurements at higher engine speeds [15]. However, they are subject to greater changes in sensitivity at higher operating temperatures due to the sensor's construction-related factors like diaphragm deformation.

The degree of error due to thermal shock is also associated with the operating point in the engine's map is being run (ignition timing, engine speed and load). Changes in engine load will also result in zero-shift of the pressure signal in dry transducers. This is an issue when switching from fired to motored curves and vice versa [15]. Thermal shock can be detected by a simple test. The variation of pressure at -180° and +180° crank angles (in

relation to TDC) can be compared. If the variation at $+180^\circ$ is much greater than at -180° , thermal shock is occurring. Thermal shock will also cause unreasonably low pressure readings in the P-V diagram pumping loop. Locating the transducer's measuring face near the intake valves substantially reduces the heat flow load on the transducer when compared to mounting it near the exhaust valves. In this experiment, the transducer was mounted in between the intake and exhaust valve. Figure 4-2 shows a typical plot for the standard deviation of the pressure trace for the 15% load, 3,000 RPM case. Little difference was seen in the variation of pressure between the -180° and $+180^\circ$ crankshaft positions. The major variation occurred shortly after TDC.

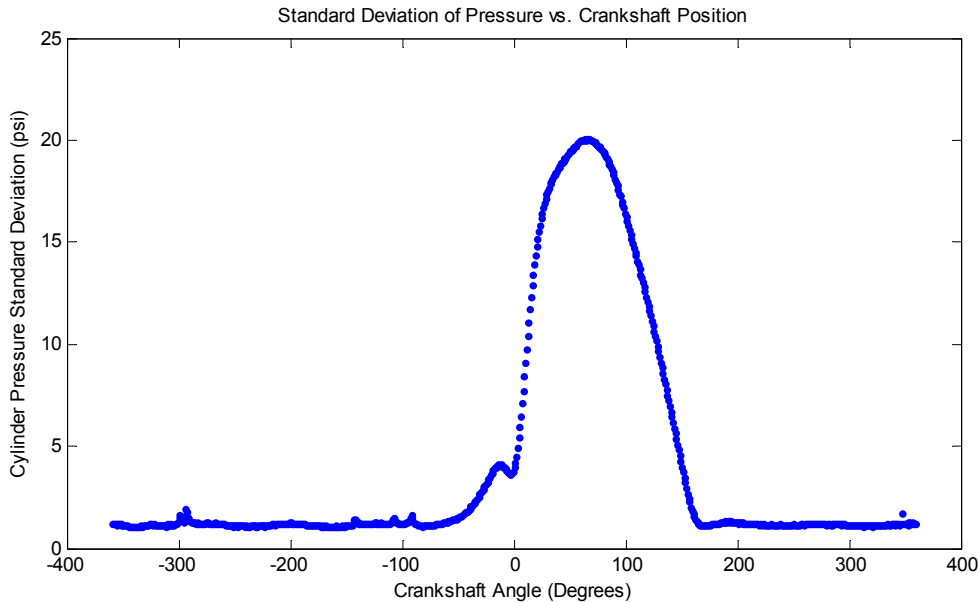


Figure 4-2: Standard deviation of pressure as a function of crankshaft position

It seems as though thermal shock effects from the burned gases have the most influence on random sensor variation during the expansion stroke in between 40 degrees ATDC and exhaust valve opening (EVO, 64 degrees BBDC). Figure 4-3 displays the mean, median, and mode of 100 consecutive pressure traces in which this phenomenon can clearly be seen.

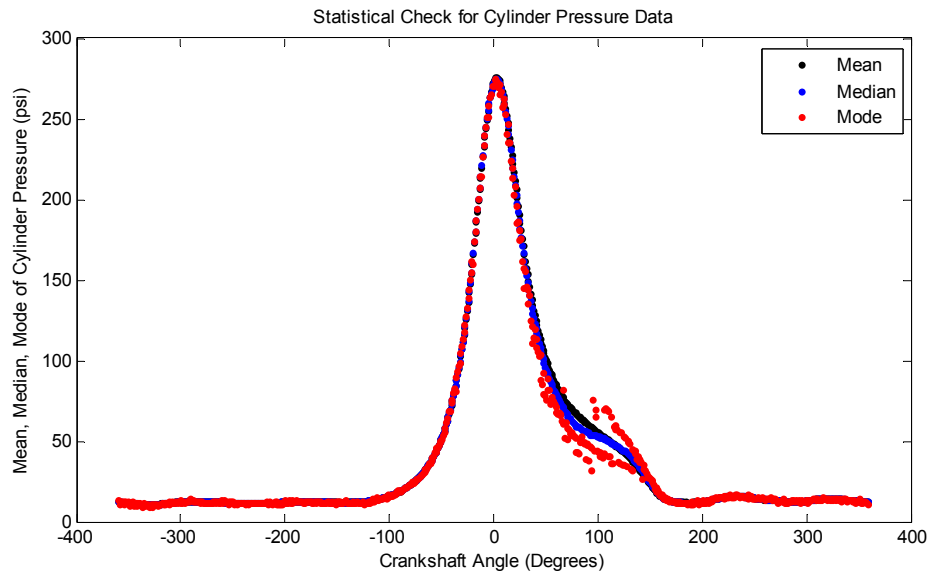


Figure 4-3: Variation in pressure readings from 40 degrees ATDC to EVO

The variations seen in the expansion stroke pressure values were evident in other plots as well. The log-log P-V diagrams all had some distortion in the later portions of the expansion stroke and into the beginning of the exhaust event as seen in Figure 4-4. The expansion stroke should have a linear slope slightly higher than the compression stroke slope. However, with the thermal shock present, the ideal values for the expansion polytropic exponents were not realized due to unwanted curvature at the end of the expansion stroke.

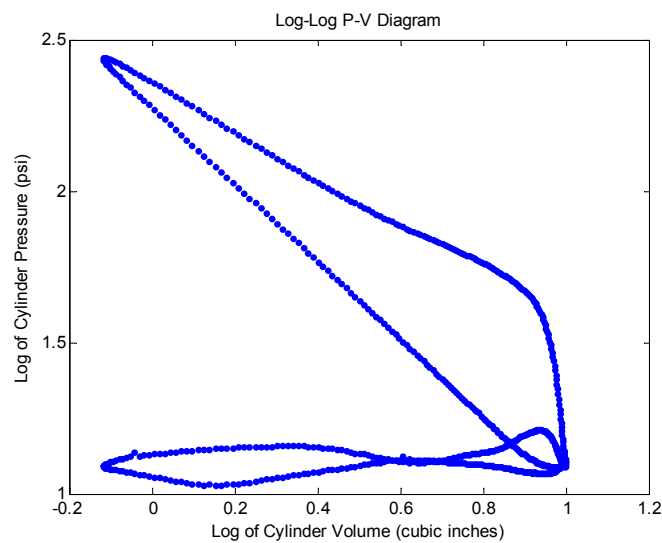


Figure 4-4: Thermal shock distortion on the log-log P-V diagram

The thermal shock also affected the mass fraction burned curve. The thermal shock to the pressure sensor resulted in the mass fraction burned curves lacking a tail at the end of combustion (EOC). This can be seen in Figure 4-5 where experimental data has been fitted to a Wiebe function for reference. However, since this experiment was mainly concerned with the location of SOC and the combustion centroid, the problematic readings near EOC were tolerable.

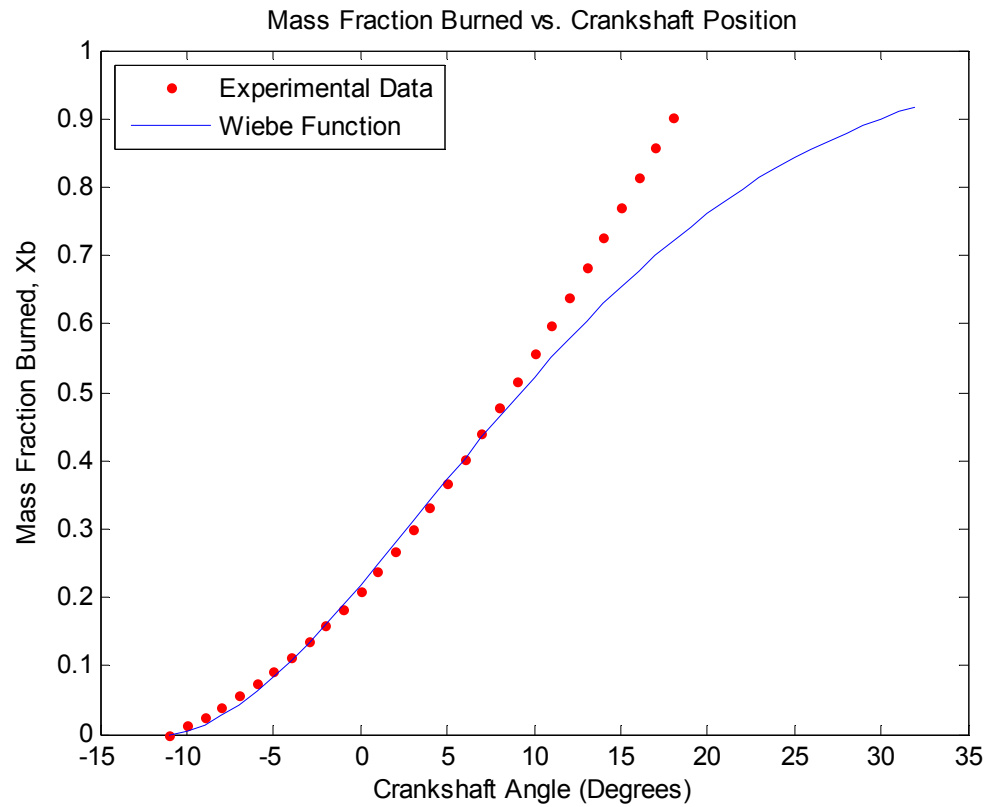


Figure 4-5: Thermal shock effect on the mass fraction burned curve

Errors in the cylinder pressure readings can also arise from transducer drift which is the undesirable change in transducer output over time that is not a function of the measured variable. The transducer will drift to ± 10 volts over some period of time on the order of hours, minutes, or even seconds depending on the condition of the cabling, connections, and charge amplifier used. Any condensation that is allowed to collect in the cables and

connections will cause excessive drift. The cables can be baked for two hours at 125°C to eliminate any condensation. Dirty or corroded connections can also add paths for current leakage from the measurement system. These must be kept very clean with contact cleaner to avoid issues. A well maintained measurement system will take hours to experience this drift and not effect measurements. A well implemented pegging procedure will eliminate the effects of long-term drift as well. Typically, the resistance between the center conductor and the outer shield should be kept greater than 10^{13} ohms [7]. The choice of the charge amplifier's time constant is also important. Both drift and time constant simultaneously affect the voltage output of the charge amplifier [17]. One or the other will dominate. Charge amplifiers will have short, medium, and long time constant settings to choose from. Most often the short time constant is utilized for monitoring the cylinder pressure of a modern engine. There was very little sensor drift experienced throughout this experiment.

Electrical noise will also cause issues in acquiring good data. A filter is sometimes required to be implemented into the data acquisition to smooth the pressure trace and eliminate noise spikes in the data. The noise will also be visible in the P-V diagram in the form of oscillations, especially in the low pressure regions of the diagram like the pumping loop. However, care must be taken not to filter the pressure signal so much that knock is no longer detectable. Mechanical noise from the engine's reciprocating parts can also cause problems with transducer readings. Accelerations as high as 1000 g's are commonly encountered in modern engines [15]. Even a transducer that is over-torqued the slightest bit will exhibit a changed sensitivity which throws off the calibration of the transducer.

4.2 Incremental Angular Encoders

The angular encoder that monitors crankshaft position mounts to the side of the engine with a specially machined bracket. The optical encoder used detects radial position using a light gate and optical pickup. This type of encoder has become the industry standard when accurate crankshaft displacement measurements are required. The optical signal received by the optical pickup is converted into a digital voltage signal which the data acquisition unit can read. The encoder utilized for this testing had a resolution of 360 pulses per revolution which is preferred for general combustion work. Encoders with up to 3600 pulses per revolution may be required when analyzing engine knock or combustion noise.

Table 4-1 below gives Rogers' [15] recommended resolution for various combustion work.

Table 4-1: Measurement task and recommended crank degree resolution

Task	Resolution (crank degrees)
Knock	<0.2
IMEP, Friction Measurements	1
Combustion Noise	<0.2
Heat Release Calculations	1
Calculation of Polytropic	1
Injection Timing Curve Edges	0.1
Direct Analysis of Pressure Curve	1
Rotational Vibration Analysis	<1

The encoder's shaft is coupled to the crankshaft through a bellows assembly to accommodate any angular misalignment due to the mating shaft run out. However, any mechanical resonance in the shaft encoder can cause oscillations to show up in the mass

fraction burned curve. Large diameter bellows can help to reduce these effects, but have a shorter life than smaller diameter bellows. The data processing program must know the angular offset of the encoder relative to true TDC. The encoder sends two pulses to count every degree increment and to determine the direction of rotation. Another pulse occurs once every cycle on the third channel to reset the degree position counter in the data acquisition program. The zero point that the encoder sees must be phased to true TDC. The encoder also only records 360 degree positions before resetting while a 4-stroke engine cycle operates over a duration of 720 degrees. Therefore, the data processing program had logic embedded in it to determine which revolution is which in the engine's cycle. TDC is most often found by locating the PCP on the motored pressure trace. PCP actually occurs slightly before TDC due to heat transfer. This phasing difference is called the "loss angle". This can be anywhere from 0 to 0.5 degrees at lower engine speeds and up to 3 degrees at higher speeds. The loss angle was found by adjusting the pressure trace so that the compression stroke polytropic exponent on the log-log P-V diagram matched the calculated ratio of specific heats.

4.3 Data Acquisition

It is necessary for the in-cylinder analysis that the in-cylinder pressure signal be coupled with crankshaft angular position since most of the information derived from the pressure trace is related to cylinder volume and crankshaft position. Therefore, the data acquisition program is setup to use each pulse from the crankshaft encoder (per single degree increment) as a trigger to acquire a cylinder pressure data point, and then write them both to a ASCII file format. This allows for cylinder pressure data to be captured in the angular domain. The data can then be scanned at a constant rate fast enough to avoid aliasing and

sampled at a variable frequency that automatically matches engine speed. The user simply puts in the maximum sample rate necessary in order to not miss any events along with the number of cycles to sample. According to common sampling theorems, the data must be sampled at a frequency at least twice that of the highest frequency component of the signal of interest. A sample frequency of up to ten times the highest frequency component may be necessary to avoid aliasing the signal [15]. The National Instruments USB-6210 data acquisition unit utilized to acquire the cylinder pressure and crankshaft position data was fully capable of providing such a sample frequency with a maximum scan rate of 250kS/s. A MoTeC M400 ECU acquired all the other data pertinent to monitoring engine operation.



Figure 4-6: National Instruments USB-6210 data acquisition unit



Figure 4-7: MoTeC M400 ECU

4.4 Data Integrity and Analysis

Daily instrumentation checks are necessary to achieve high data integrity from day-to-day. It is a good idea to record combustion data at the same test condition each day to ensure that there are no instrumentation issues [7]. Ideally, the chosen test condition should be fairly representative of the test points being run that day, and the combustion data at motored and fired conditions should always be taken in the same order. An engine warm-up procedure must also be created and strictly followed. Coolant and oil temperatures should also be kept constant. The intake and exhaust restrictions should also be kept the same when verifying the chosen test condition each day.

Data from the daily instrumentation checks can be used to construct a control chart. Typically, control charts are created for monitoring data such as IMEP, PMEP, polytropic coefficients, PCP, and LPP during both the firing and motoring condition check. PCP measurements provide a good cylinder pressure transducer check while the LPP confirms encoder phasing in relation to TDC. Data such as the MAP, AF ratios, and the heat-release centroid should be recorded for the firing condition check [7]. The daily test readiness and verification instructions that were performed before every extensive test are listed in Table 4-2. An example of a control chart for IMEP is shown in Figure 4-8.

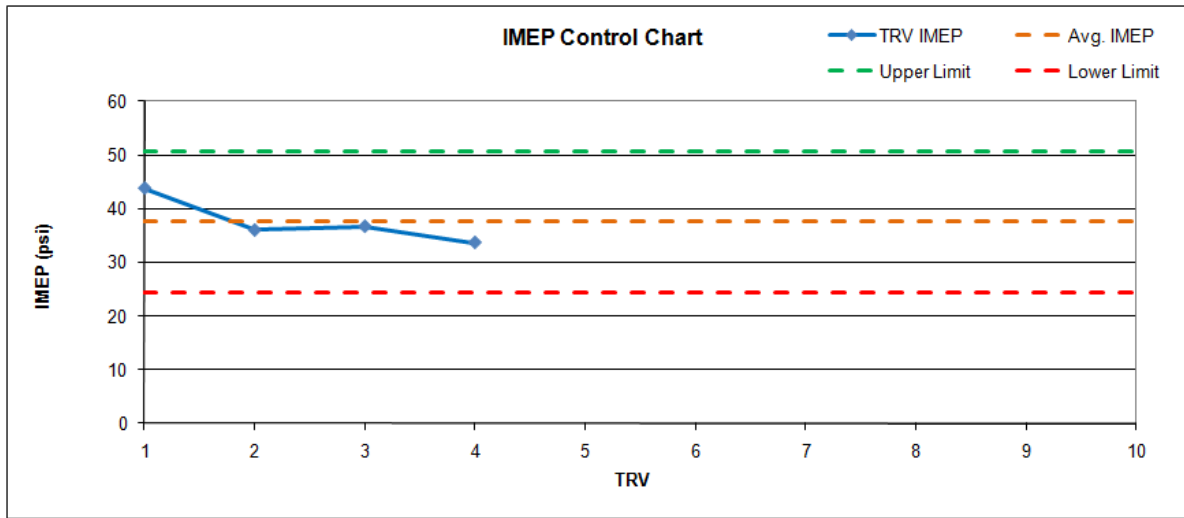


Figure 4-8: IMEP control chart

Table 4-2: Test readiness and verification instructions

1	Check that pressure transducer does not drift over a ten minute period
2	Warm up engine at idle until engine coolant temperature is at 75 °C for five minutes
3	Shut down engine, disconnect the cylinder #1 spark plug and injector connectors
4	Motor engine at 3,000 rpm, 75 °C coolant temperature
5	Take data point
6	Shut down engine, reconnect spark plug and injector
7	Examine LPP (location of peak pressure)
8	Take engine to 3,000 rpm, 15% load, 75 °C coolant temperature, ignition timing: 15 deg. BTDC, rail pressure: 60 psi. injection timing: 150 degrees BTDC, lambda: 0.96
9	Take data point
10	Shut down engine
11	Compare variation in pressure STD between -180° and +180° ATDC data points
12	Examine IMEP

During this experiment, there was no way to control the atmospheric pressure, temperature, and humidity. The variations in atmospheric conditions are primarily responsible for the variations in performance. To counter act this, any data used for

comparison on performance and efficiency plots was all recorded on the same day to avoid outside factors such as the weather having an influence on the results.

The data analysis program shown in Figure 4-9 processes the data. Since the cycle-to-cycle variation in the pressure readings can be high, around 100 cycles were analyzed and averaged into a single data set to be used in the analysis. Because the sample sizes are quite large, it is important to monitor the standard deviation of the pressure data. Samples that display high standard deviations in the pressure data are a red flag that something is wrong. This allowed for the detection of the thermal shock experienced by the sensor throughout the experiment. It can also indicate when the engine may not be in a steady state condition. Both fired and motored cylinder pressure traces were used in a series of calculations to provide data integrity plots, P-V and log-log P-V diagrams, and the burn rate profile. The P-V diagram is integrated using the trapezoid method to provide indicated work, MEP, power, torque, and SFC. The log-log P-V diagram is utilized to determine the polytropic exponent of compression and expansion as an error check. If a differing value from what is expected is obtained, this may indicate an incorrect compression ratio or TDC location input. If the compression line has a curve to it, that indicates the engine has not been allowed to obtain a stable operating temperature and heat transfer effects are playing a role. The log-log P-V also displays the intake, compression, expansion, and exhaust portions of a given cycle more clearly than a standard P-V diagram. The program returns other values of interest as well, such as the PCP and LPP of the motored and fired pressure curves, thermal shock test, STD, COV and LNV of IMEP, and the SOC, combustion centroid and duration.

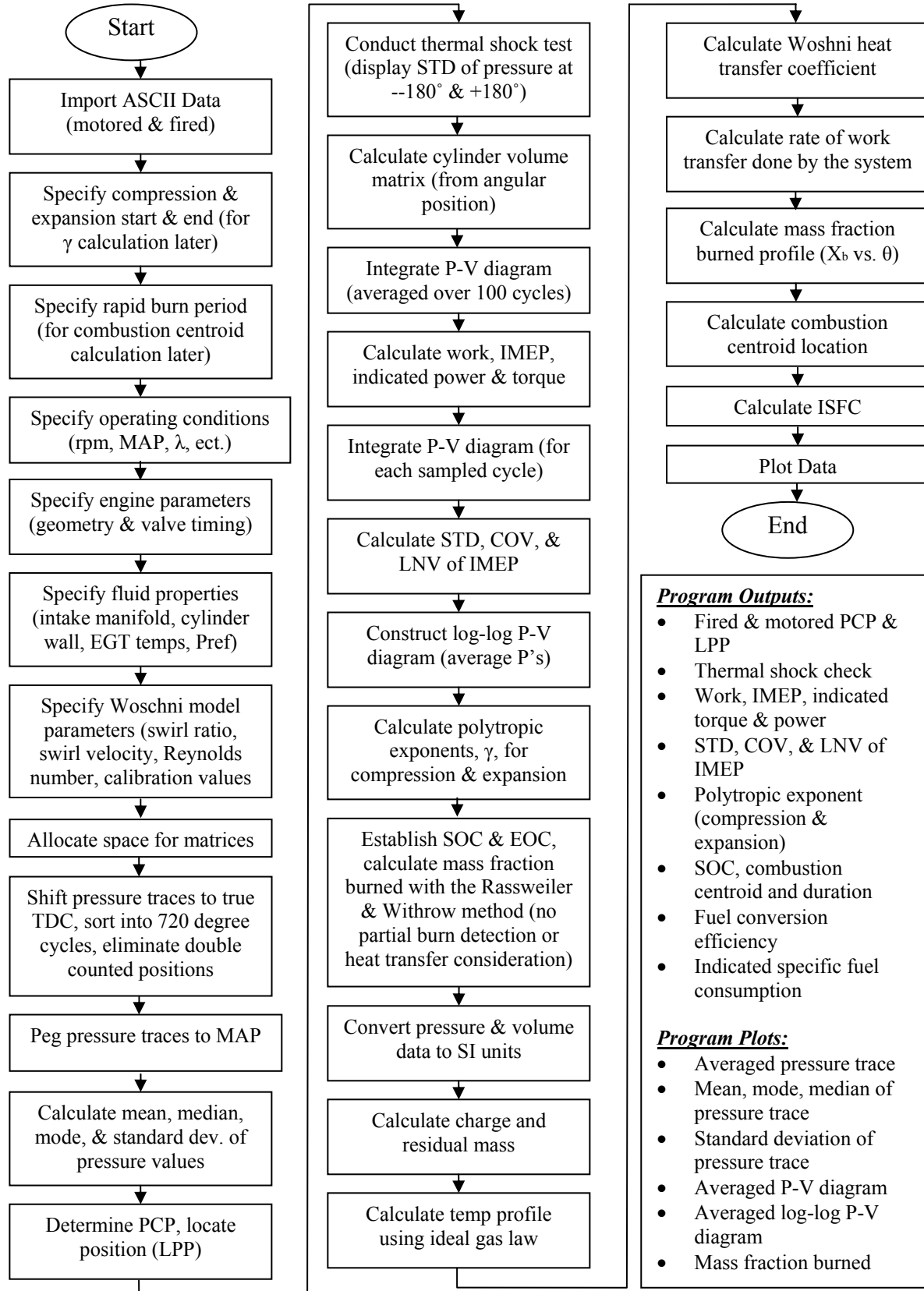


Figure 4-9: Data analysis program flowchart

Chapter 5: Component Machining & Dynamometer Setup

5.1 Cylinder Head Drilling Procedure

In most cases, the combustion chamber of an internal combustion engine can be accessed rather easily with either a special spark plug or glow plug which has a piezoelectric sensor already integrated into the plug. However, these units can be quite expensive so the Kistler 6052A sensor was utilized instead. This sensor requires that the cylinder head be drilled and fitted with a special sensor mounting sleeve. The sleeve allows the transducer to access the combustion chamber by sealing the water jacket passages that the transducer mounting hole must be drilled through. It also separates the transducer from the cylinder head material. This isolates the transducer from deformation stresses in the head that can cause a shift in sensitivity during operation.

When mounting the pressure transducer in the head, a flush mount with minimal communication passage length is preferable. Although a large communication passage reduces the effects of thermal shock on the transducer, it is also susceptible to errors from pressure waves developing in the passage. The longer the passage, the less responsive the pressure sensor is to the actual cylinder pressure due to the ringing effect. The shortest passageway and smallest possible cavity volume along with the largest passage diameter is desired to provide the highest natural frequency. Care must be taken when drilling the transducer passage that no portion of the casting becomes so thin that a premature structural failure of the head results.

Since dimensional drawings of the Yamaha R6 cylinder head were not available, much planning went into the machining process. First a pilot hole was drilled from the combustion chamber out to ensure that the sensor mounting sleeve would not interfere with the engine valves. The hole was drilled in between the intake and exhaust valves on the outside wall of cylinder number one. The pilot hole was drilled with the mill head at a 30 degree angle and the turn table at a 5.5 degree angle. For the second operation, a centering insert was spun on the lathe that once inserted into the pilot hole, could be used to find the center of the hole and put it in the same plane as the mill head using the tilt table setup shown in Figure 5-1. With the centering insert placed inside the pilot hole, a dial indicator was used to adjust the top surface of the insert so that it was perpendicular with the vertical axis of the mill. The counter bored hole in the center of the insert was used to center-find the pilot hole. The cylinder head was secured to the tilt table by a jig plate which contained three tapped holes for fastening the head to the jig plate through the stock head bolt holes.



Figure 5-1: Tilt table and cylinder head jig adjustment on mill

Figure 5-2 shows the tilt table dialed in on the mill, ready to drill. A through hole was drilled first for tapping the M7 x 0.75 threads for the sensor mounting sleeve. Then an end mill and 10 mm reamer were utilized to machine the counter bore for the sensor mounting sleeve.

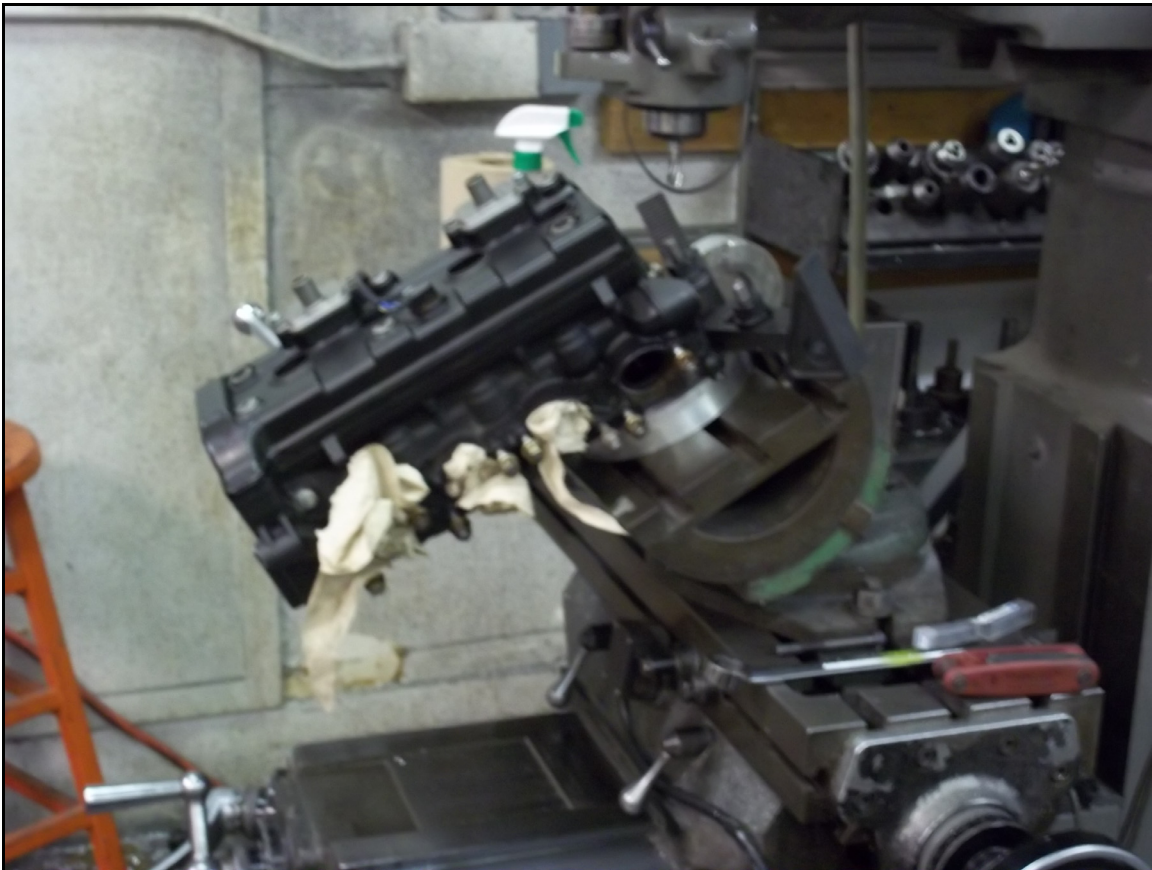


Figure 5-2: Mill setup for second cylinder head machining operation

The mounting sleeve sealed the inner combustion chamber wall from the water jacket by a 0.11 inch thick custom made copper washer. The o-ring on the mounting sleeve along with the aid of semi-liquid Honda Bond was used to seal the outer wall of the water jacket. The fitment of the mounting sleeve in the R6 head is shown in Figure 5-3 and Figure 5-4.

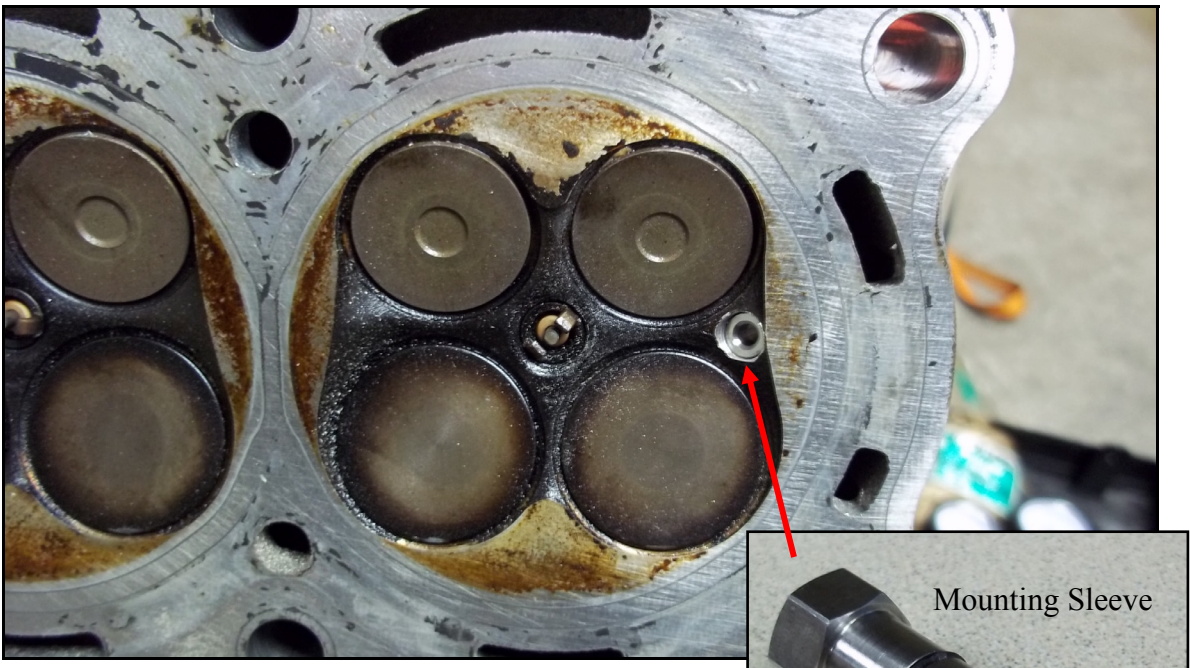


Figure 5-3: Pressure sensor communication passage

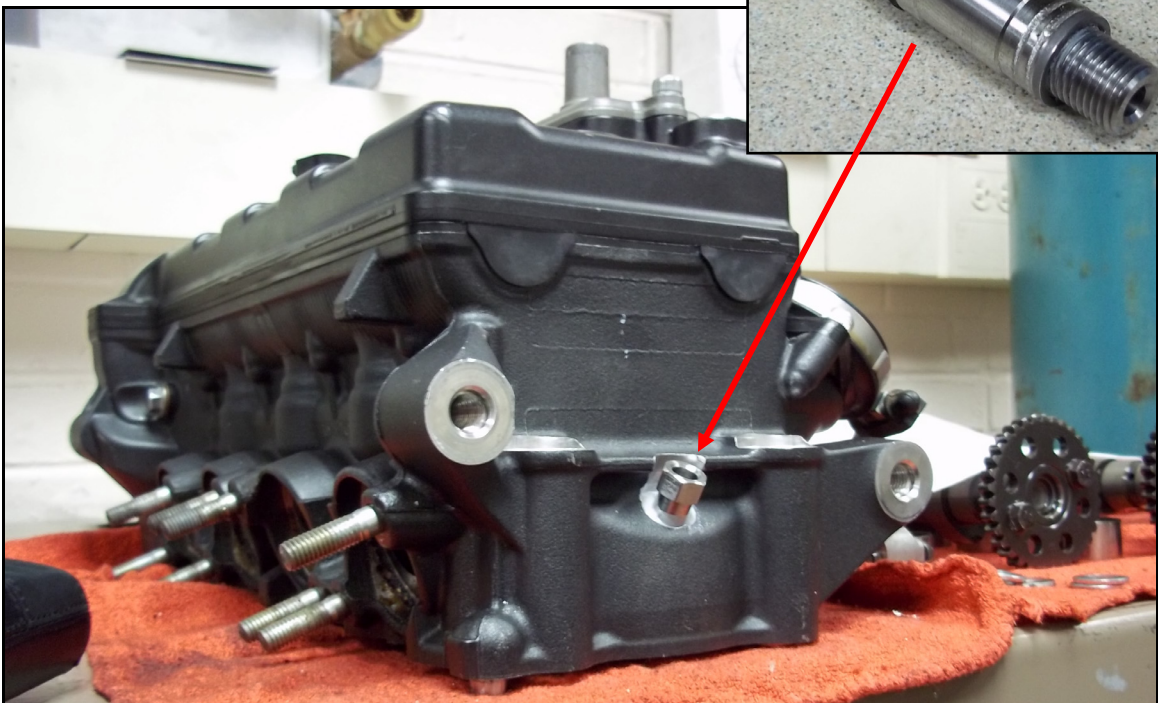


Figure 5-4: Mounting sleeve location in cylinder head

The engine run on the dynamometer for this testing was completely torn down prior to testing both to install the instrumented cylinder head and to refurbish the worn and abused power cylinder and clutch components. The teardown also offered an opportunity to

accurately measure critical geometric details of the engine's cylinder head and power cylinder components.



Figure 5-5: Disassembled upper crankcase, transmission, & power cylinder components

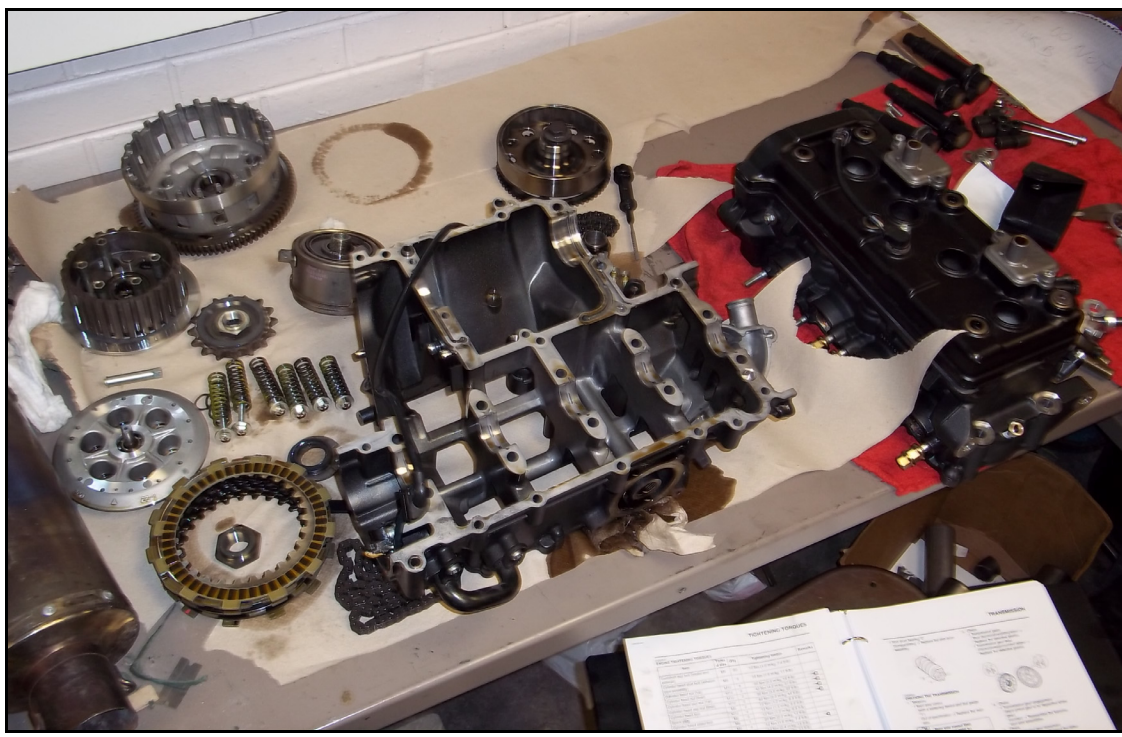


Figure 5-6: Disassembled lower crankcase, cylinder head, & clutch components

5.2 Angular Encoder Component Machining and Dynamometer Setup

Since the stock trigger wheel did not provide enough resolution for combustion analysis, an industrial encoder was mounted to the engine and directly coupled with the crankshaft. The BEI H25 incremental encoder provided 360 degrees of resolution for monitoring the crankshaft position of the engine. The picture below shows the bracket constructed for mounting the encoder to the engine as well as the mating shaft (coming out from the crankshaft), custom oil seal housing, and the flexible bellows used to couple the mating and encoder shafts.

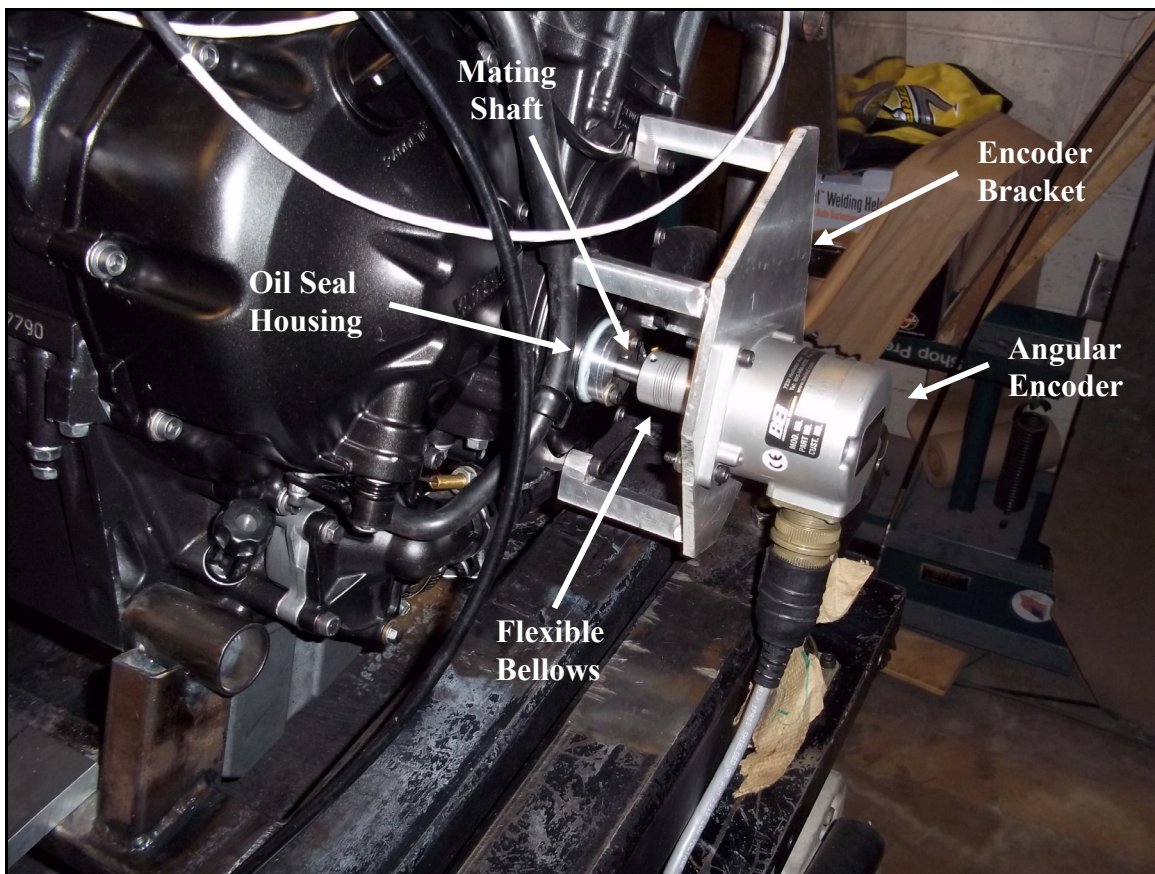


Figure 5-7: Crankshaft encoder assembly

The encoder bracket had to be constructed without the CMM coordinates of the center of the crankshaft with respect to the crankcase cover mounting holes since the engine

was not able to be measured in time by an outside source. Therefore, the feet of the bracket and a rectangular plate were machined separately. Pins for the mounting holes were spun on the lathe and used to hold the assembly together while being welded. Once the bracket was welded together, the center of the inspection hole on the crankcase cover was used to locate the mounting holes for the angular encoder on the plate so that the encoder shaft would be concentric with the crankshaft. After the drilling was complete, the corners of the plate were trimmed off to lighten the bracket assembly.



Figure 5-8: Crankshaft encoder bracket construction

The stock flange bolt that secures the trigger wheel to the crankshaft was replaced with a custom made mating shaft to provide a direct coupling to the crankshaft. The mating shaft shown in Figure 5-9 was spun on the lathe out of $\frac{1}{2}$ " stainless steel hex stock. All of the special components used for this testing were made in-house at the SAE student machine shop. The complete engine dynamometer setup is shown in Figure 5-10. The engine was managed by a MoTeC 400 ECU and was coupled to a DYNO-mite water brake dynamometer. A heat exchanger mounted underneath the engine provided the necessary heat rejection from the engine coolant system.

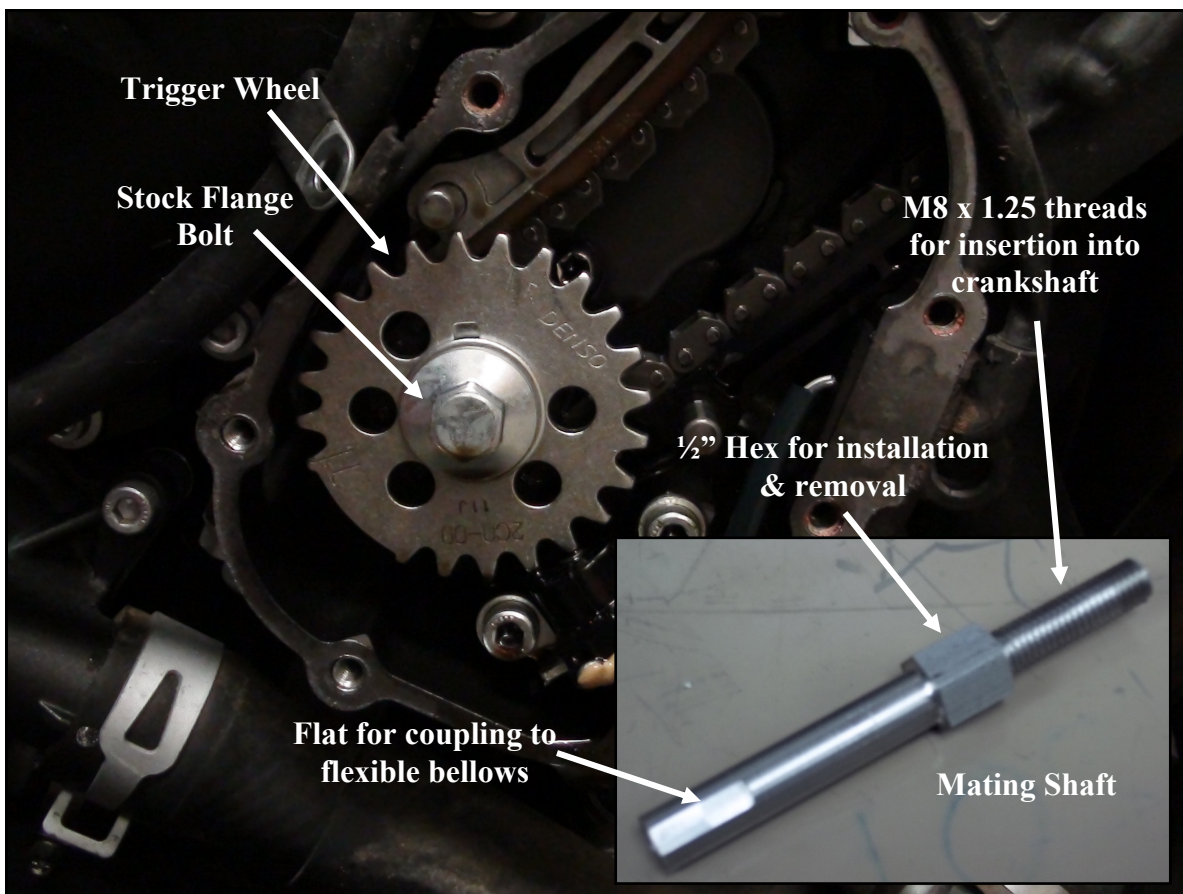


Figure 5-9: Crankshaft encoder mating shaft

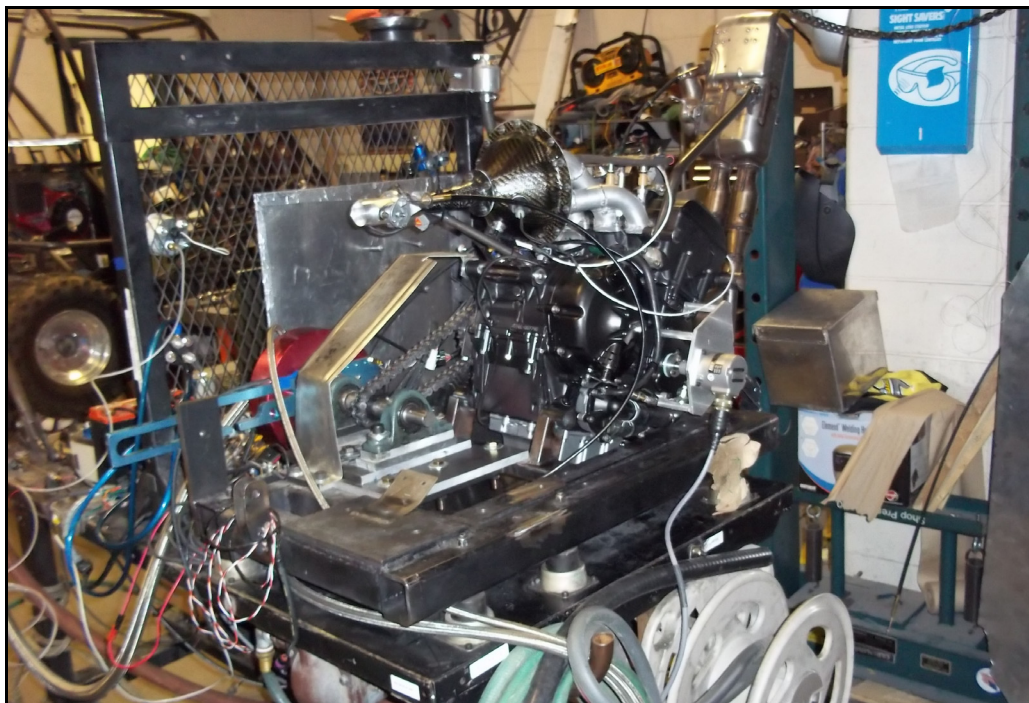


Figure 5-10: Engine dynamometer test stand

Chapter 6: Design of Experiment

6.1 15% Load, 3,000 RPM DOE

A two-level factorial design of experiment (DOE) was created to investigate the burn rate curve's response to certain engine operating parameters. Ignition timing, fuel rail pressure, injection timing, and the relative air/fuel ratio, lambda, were the four factors chosen to be investigated. The start of combustion (SOC), combustion centriod, and combustion duration were the three mass fraction burned curve responses that were examined. The experiment was designed as an eight-run, half factorial analysis to examine both the main and two factor interaction effects. Table 6-1 below lists the results of the DOE.

Table 6-1: 15% load, 3,000 RPM DOE matrix

15% Load, 3,000 RPM		Main Effects				Response				
Standard	Run	A: Ignition Timing	B: Rail Pressure	C: Injection Timing	D: Lambda	SOC	Centroid	Duration		
5	1	10	50	200	0.98	6	8.1	24		
4	2	17	70	100	0.93	12	11.3	34		
6	3	17	50	200	0.93	13	9.9	33		
1	4	10	50	100	0.93	5	10.2	25		
7	5	10	70	200	0.93	8	9.1	27		
3	6	10	70	100	0.98	8	7.9	27		
8	7	17	70	200	0.98	14	8.3	33		
2	8	17	50	100	0.98	11	8.9	30		
SOC Effect		5.75	1.75	1.25	0.25	9.6				
Centroid Effect		0.78	0.13	0.72	1.83	9.2				
Duration Effect		6.75	2.25	0.25	1.25	29.1				
		Interaction Effects								
		<i>A*B</i>	<i>A*C</i>	<i>A*D</i>						
SOC Effect		0.75	0.75	0.25		9.6				
Centroid Effect		0.53	0.28	0.17		9.2				
Duration Effect		0.25	0.75	0.75		29.1				

Half-normal plots were constructed to examine the significance of each factor on the three mass fraction burned curve parameters. Figure 6-1 displays the effects on the location of SOC. At first glance, ignition timing, fuel rail pressure, injection timing, and the interaction of ignition timing with injection timing and fuel rail pressure seem significant. However, the analysis of variance (ANOVA) shown in Table 6-2 revealed that only ignition timing, fuel rail pressure, and injection timing were important. The probability value of 0.0955 for the two interaction effects was greater than the 0.05 cutoff [18], and thus was considered to have possibly been a result of experimental noise. The model F-value of 124 implies that the model is significant. There is only a 0.80% chance that a model F-value this large could occur due to noise.

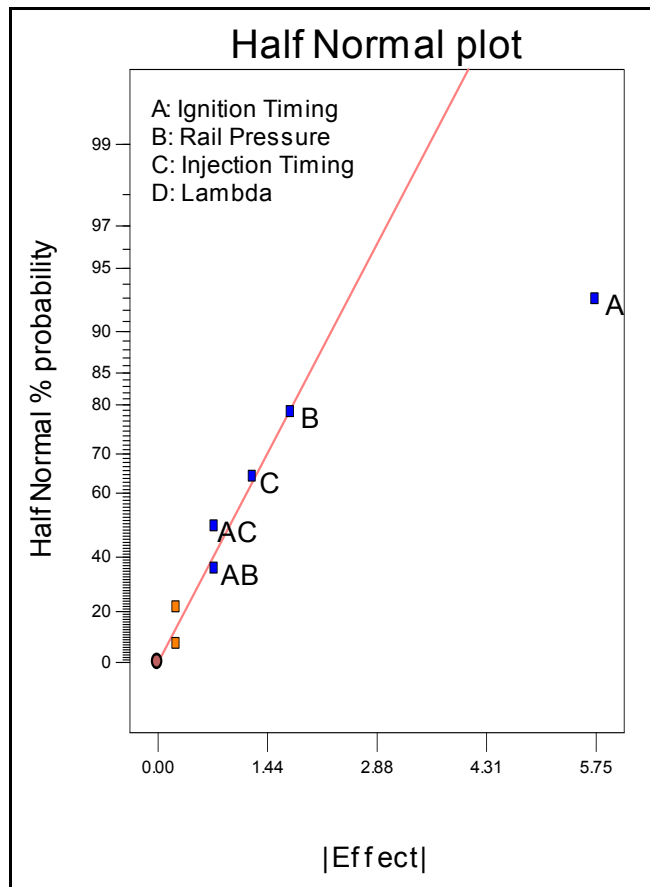


Figure 6-1: 15% load, 3,000 RPM SOC half-normal plot

Table 6-2: 15% load, 3,000 RPM SOC ANOVA

Source	Sum of Squares	DF	Mean Square	F Value	Prob > F
Model	77.63	5	15.53	124.20	0.0080
A	66.13	1	66.13	529.00	0.0019
B	6.13	1	6.13	49.00	0.0198
C	3.13	1	3.13	25.00	0.0377
AB	1.13	1	1.13	9.00	0.0955
AC	1.13	1	1.13	9.00	0.0955
Residual	0.25	2	0.13		
Corrected Total	77.88	7			

In the same fashion, a half-normal plot and ANOVA analysis were constructed for the effects on the location of the combustion centroid. Only ignition timing, injection timing, and lambda were found to be significant factors in the ANOVA analysis. The model F-value of 29 indicates that there is only a 0.98% chance that it could occur due to noise.

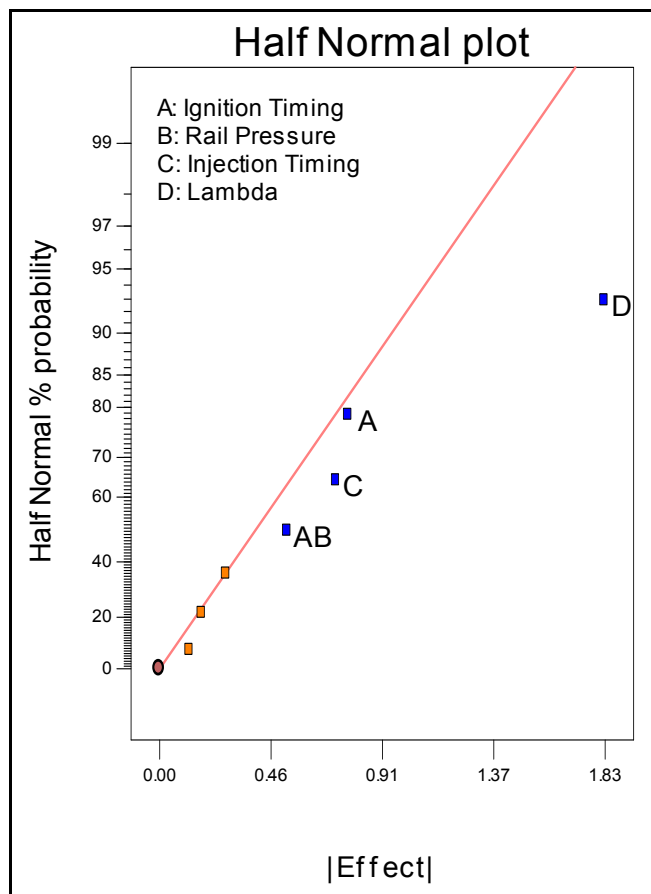


Figure 6-2: 15% load, 3,000 RPM combustion centroid half-normal plot

Table 6-3: 15% load, 3,000 RPM combustion centriod ANOVA

Source	Sum of Squares	DF	Mean Square	F Value	Prob > F
Model	9.46	4	2.37	29.12	0.0098
A	1.20	1	1.20	14.78	0.0310
C	1.05	1	1.05	12.94	0.0368
D	6.66	1	6.66	81.98	0.0028
AB	0.55	1	0.55	6.78	0.0800
Residual	0.24	3	0.081		
Corrected Total	9.71	7			

The half-normal plot and ANOVA analysis for the combustion duration yielded ignition timing, fuel rail pressure, and lambda as the key factors. The model F-value of 171 indicates that there is only a 0.58% chance that it could occur due to noise.

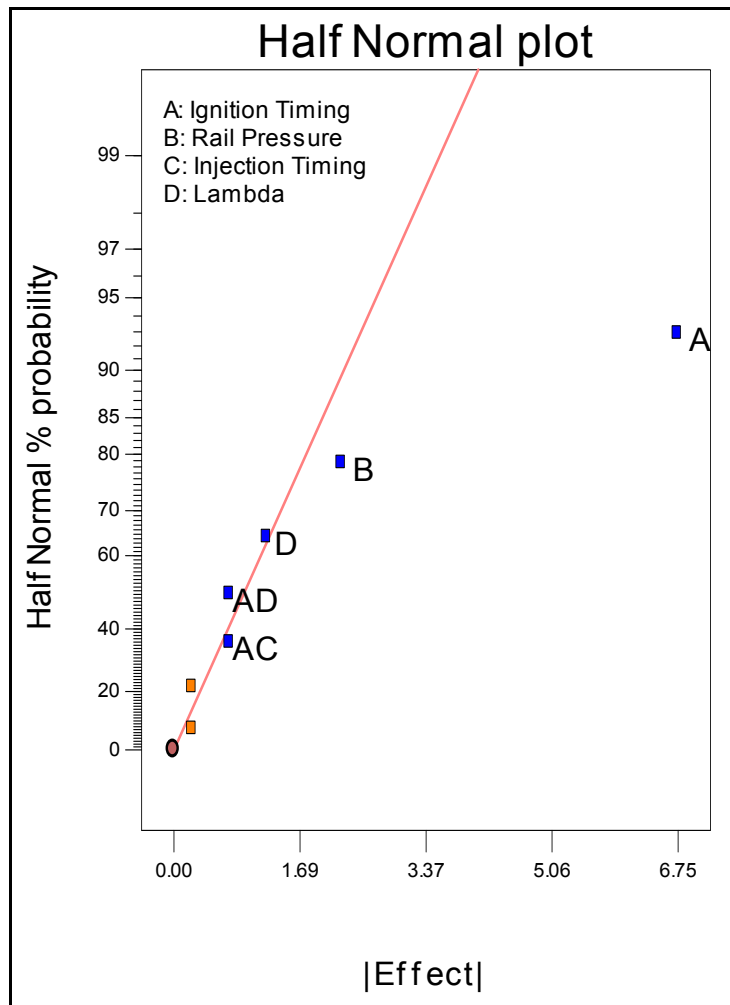


Figure 6-3: 15% load, 3,000 RPM combustion duration half-normal plot

Table 6-4: 15% load, 3,000 RPM combustion duration ANOVA

Source	Sum of Squares	DF	Mean Square	F Value	Prob > F
Model	106.63	5	21.32	170.60	0.0058
A	91.12	1	91.12	729.00	0.0014
B	10.12	1	10.12	81.00	0.0121
D	3.13	1	3.13	25.00	0.0377
AC	1.13	1	1.13	9.00	0.0955
AD	1.12	1	1.12	9.00	0.0955
Residual	0.25	2	0.12		
Corrected Total	106.88	7			

The average location of SOC for the eight DOE runs was 9.6 degrees BTDC. The average combustion centroid was 9.2 degrees ATDC, and the average combustion duration was 29.1 degrees. Figure 6-4 displays the burn rate profiles for each of the DOE runs.

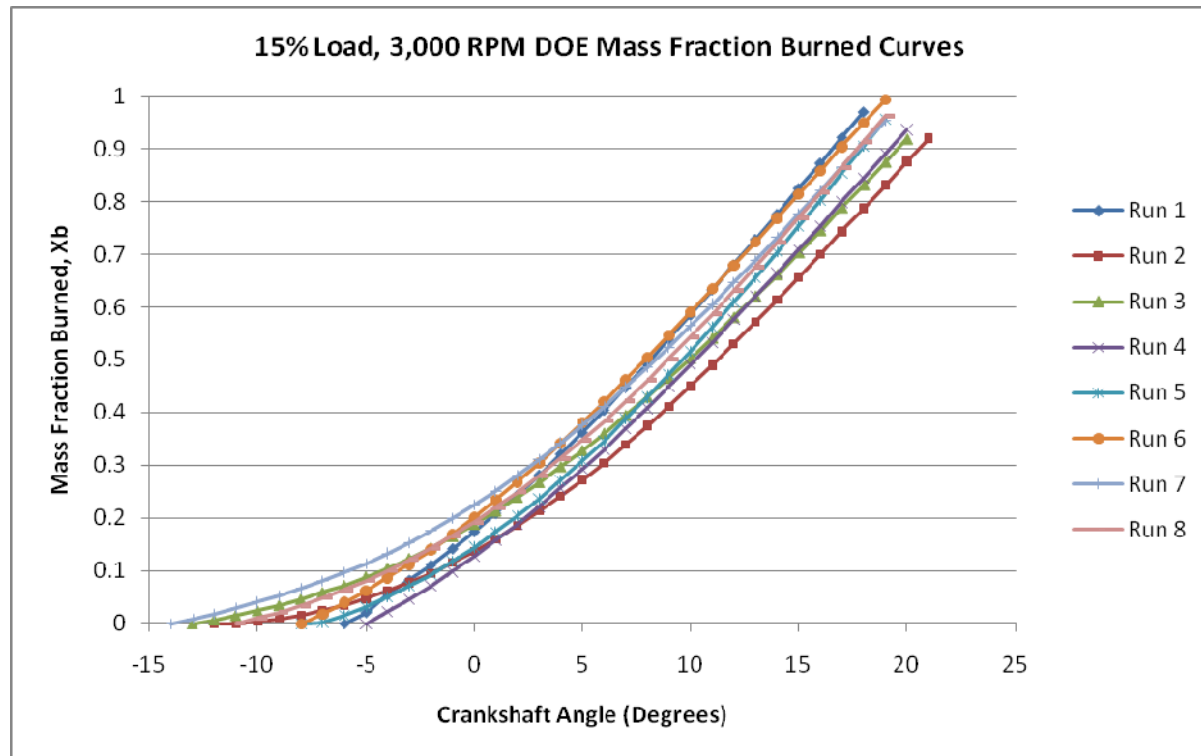


Figure 6-4: 15% load, 3,000 RPM DOE mass fraction burned curves

At the 15% load, 3,000 RPM operating point, a more homogeneous charge from higher fuel rail pressures resulted in less ignition delay. It also allowed for a more complete burn and higher fuel conversion efficiency. Commanding the fuel to be injected earlier in the

cycle also provided a decreased ignition delay as well as a combustion centroid closer to TDC. The mixtures burning close to stoichiometric at a 0.98 relative air/fuel ratio provided a centroid further from TDC.

6.2 60% Load, 3,000 RPM DOE

Another experiment was conducted to determine the effect of the four engine operating parameters on the three mass fraction burned profile quantities under study at a higher engine load. Table 6-5 lists the results of the DOE run at the 60% load, 3,000 RPM operating point.

Table 6-5: 60% load, 3,000 RPM DOE matrix

60% Load, 3,000 RPM		Main Effects				Response		
Standard	Run	A: Ignition Timing	B: Rail Pressure	C: Injection Timing	D: Lambda	SOC	Centroid	Duration
5	1	15	50	200	0.96	8	9.8	26
4	2	22	70	100	0.87	14	9.2	30
6	3	22	50	200	0.87	14	8.3	29
1	4	15	50	100	0.87	7	10.9	26
7	5	15	70	200	0.87	10	10.6	29
3	6	15	70	100	0.96	9	12.2	31
8	7	22	70	200	0.96	15	7.2	30
2	8	22	50	100	0.96	15	9.8	29
SOC Effect		6.00	1.00	0.50	0.50	11.5		
Centroid Effect		2.25	0.10	1.55	0.00		9.8	
Duration Effect		1.50	2.50	0.50	0.50			28.8
		Interaction Effects						
		<i>A*B</i>	<i>A*C</i>	<i>A*D</i>				
SOC Effect		1.00	0.50	0.50		11.5		
Centroid Effect		0.95	0.20	0.25			9.8	
Duration Effect		1.50	0.50	0.50				28.8

The half-normal plot shown in Figure 6-5 displays the effects on the location of SOC. The ANOVA revealed that ignition timing was the main factor of importance. The probability value of 0.1161 for fuel rail pressure and the interaction between fuel rail pressure and ignition timing indicated that those effects could have possibly been a result of

experimental noise. This varies slightly from the light load case in that the effects of fuel rail pressure and injection timing have been drowned out. The model F-value of 51 gives a 0.12% chance that the model could have occurred due to noise.

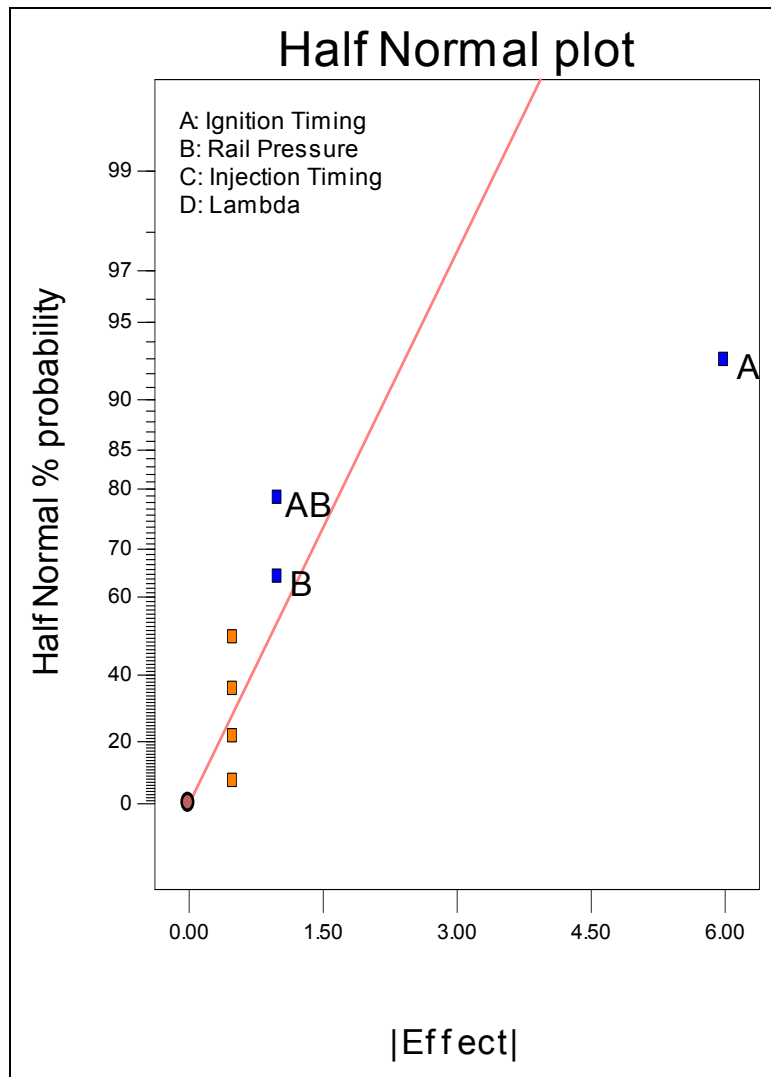


Figure 6-5: 60% load, 3,000 RPM SOC half-normal plot

Table 6-6: 60% load, 3,000 RPM SOC ANOVA

Source	Sum of Squares	DF	Mean Square	F Value	Prob > F
Model	76.00	3	25.33	50.67	0.0012
A	72.00	1	72.00	144.00	0.0003
B	2.00	1	2.00	4.00	0.1161
AB	2.00	1	2.00	4.00	0.1161
Residual	2.0	4	0.50		
Corrected Total	78.00	7			

Ignition timing, injection timing, and the interaction between ignition timing and fuel rail pressure were found to be significant factors in the placement of the combustion centroid. At the richer lambda limits, lambda was not found to be a significant factor as in the light load case (where lambda ranged from 0.93 to near stoichiometric at 0.98). This difference will be discussed later in the chapter. The model F-value of 99 indicates that there is only a 0.03% chance that it could occur due to noise.

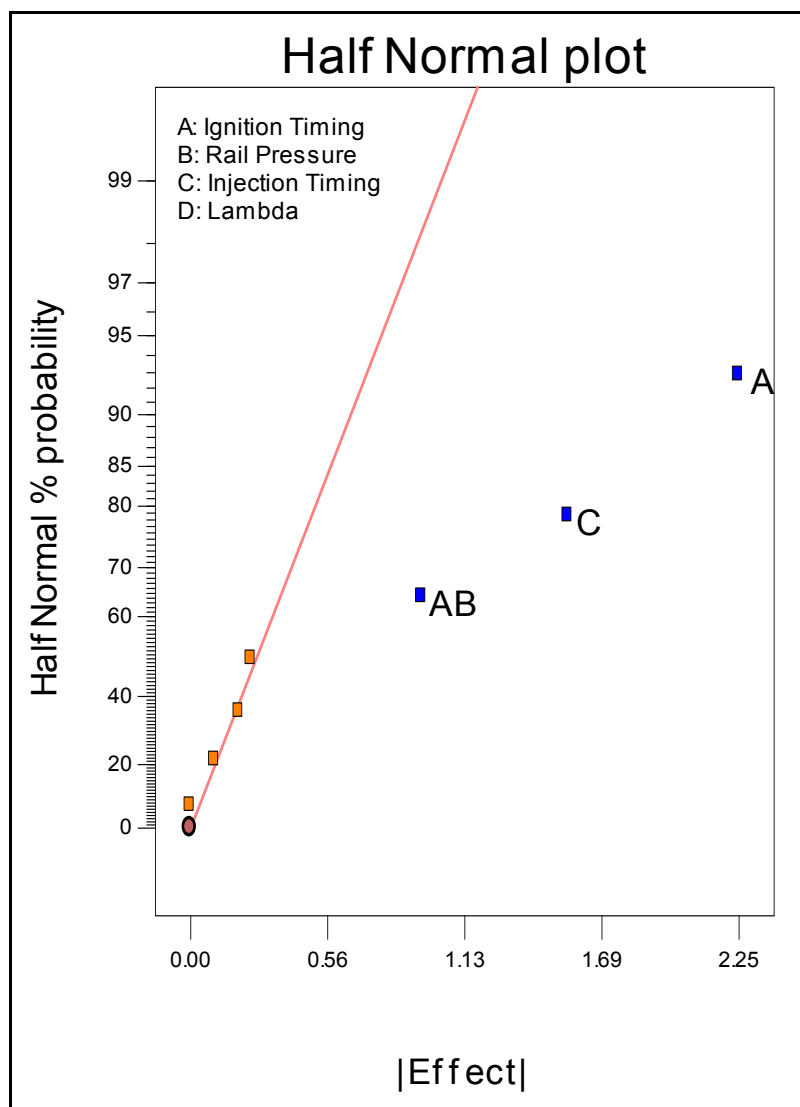


Figure 6-6: 60% load, 3,000 RPM combustion centroid half-normal plot

Table 6-7: 60% load, 3,000 RPM combustion centriod ANOVA

Source	Sum of Squares	DF	Mean Square	F Value	Prob > F
Model	16.74	3	5.58	99.17	0.0003
A	10.13	1	10.13	180.00	0.0002
C	4.81	1	4.81	85.42	0.0008
AB	1.80	1	1.80	32.09	0.0048
Residual	0.22	4	0.056		
Corrected Total	16.96	7			

The half-normal plot and ANOVA analysis for the combustion duration yielded ignition timing, fuel rail pressure, and the interaction between ignition timing and fuel rail pressure as the key factors. The model F-value of 14 indicates that there is only a 1.32% chance that it could occur due to noise.

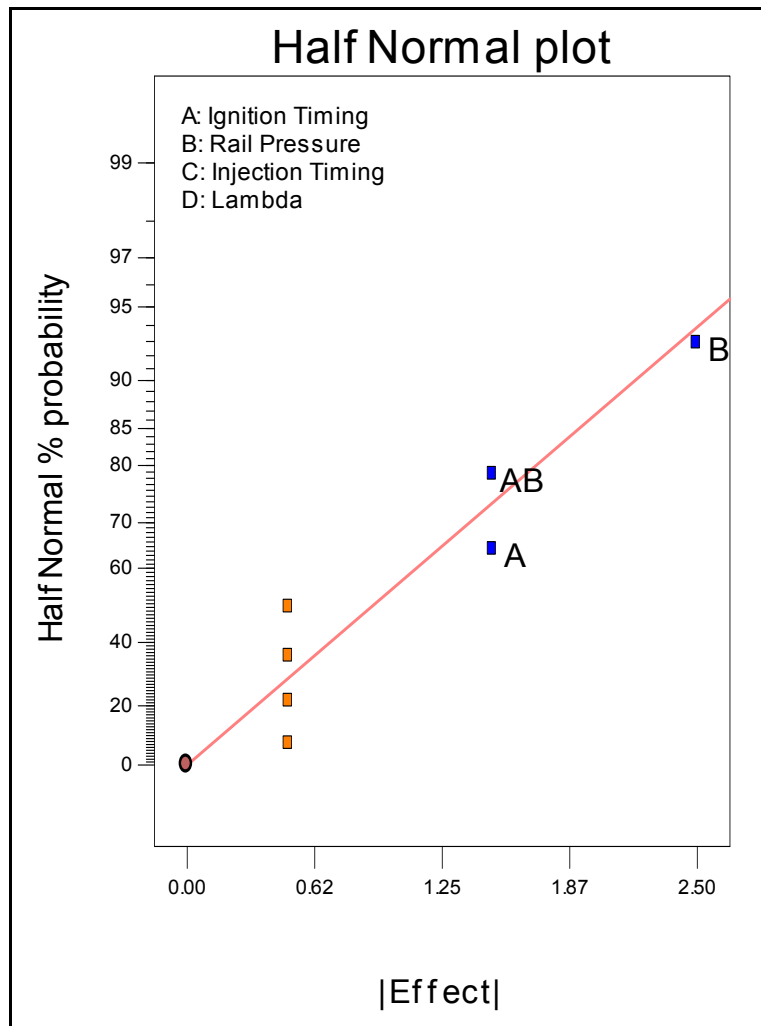


Figure 6-7: 60% load, 3,000 RPM combustion duration half-normal plot

Table 6-8: 60% load, 3,000 RPM combustion duration ANOVA

Source	Sum of Squares	DF	Mean Square	F Value	Prob > F
Model	21.50	3	7.17	14.33	0.0132
A	4.50	1	4.50	9.00	0.0399
B	12.50	1	12.50	25.00	0.0075
AB	4.50	1	4.50	9.00	0.0399
Residual	2.00	4	0.50		
Corrected Total	23.50	7			

The average location of SOC for the eight DOE runs was 11.5 degrees BTDC. The average combustion centroid was 9.8 degrees ATDC, and the average combustion duration was 28.8 degrees. Figure 6-8 displays the burn rate profiles for each of the DOE runs for the 60% load, 3,000 RPM operating point.

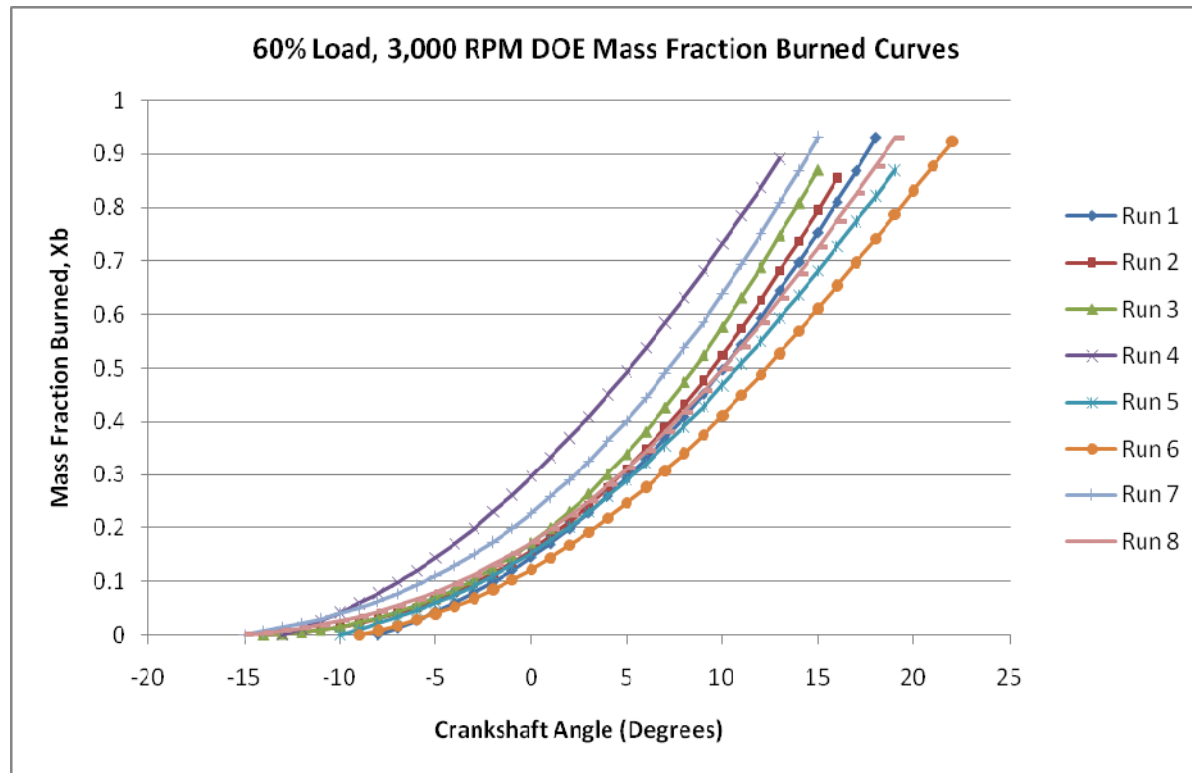


Figure 6-8: 60% load, 3,000 RPM DOE mass fraction burned curves

At the 60% load, 3,000 RPM operating point, a more homogeneous charge from higher fuel rail pressures allowed for a more complete burn and higher fuel conversion efficiency. Commanding the fuel to be injected earlier in the cycle provided a faster burn

and thus a centroid closer to TDC. Mixtures burning closer to stoichiometric at a 0.96 relative air/fuel ratio exhibited a combustion centroid further from TDC.

The influence of ignition timing on the mass fraction burned curve is illustrated in Figure 6-9. In the plot, the ignition timing of 20 degrees BTDC corresponds to MBT timing. This is where the steepest rapid burn angle is seen. If the timing is advanced or retarded slightly from MBT, the rapid burn angle is reduced and a larger amount of the mixture goes unburned. If the timing is retarded substantially, a substantial incomplete burn is seen. If the timing is advanced even further from what is shown, the engine may experience knock.

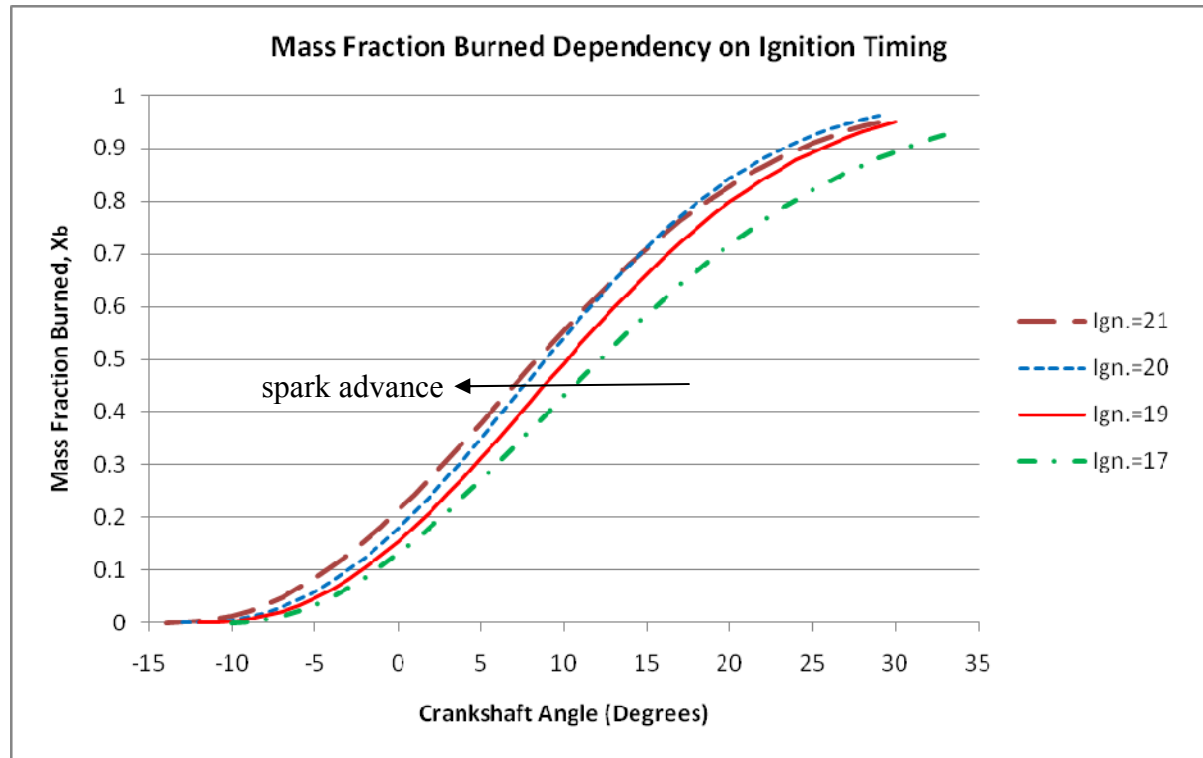


Figure 6-9: Mass fraction burned dependency on ignition timing

The influence of the excess air ratio on the mass fraction burned profile was clearly identified in the 15% load, 3,000 RPM DOE. However, in the 60% load case, the effects of lambda were not as clear. Further testing at this operating point was performed to construct Figure 6-10 which confirms that lambda does indeed influence the curve at the higher load

operating point. A change in lambda did not affect the rapid burn angle, but did shift the combustion centriod further from TDC as well as extend the duration slightly.

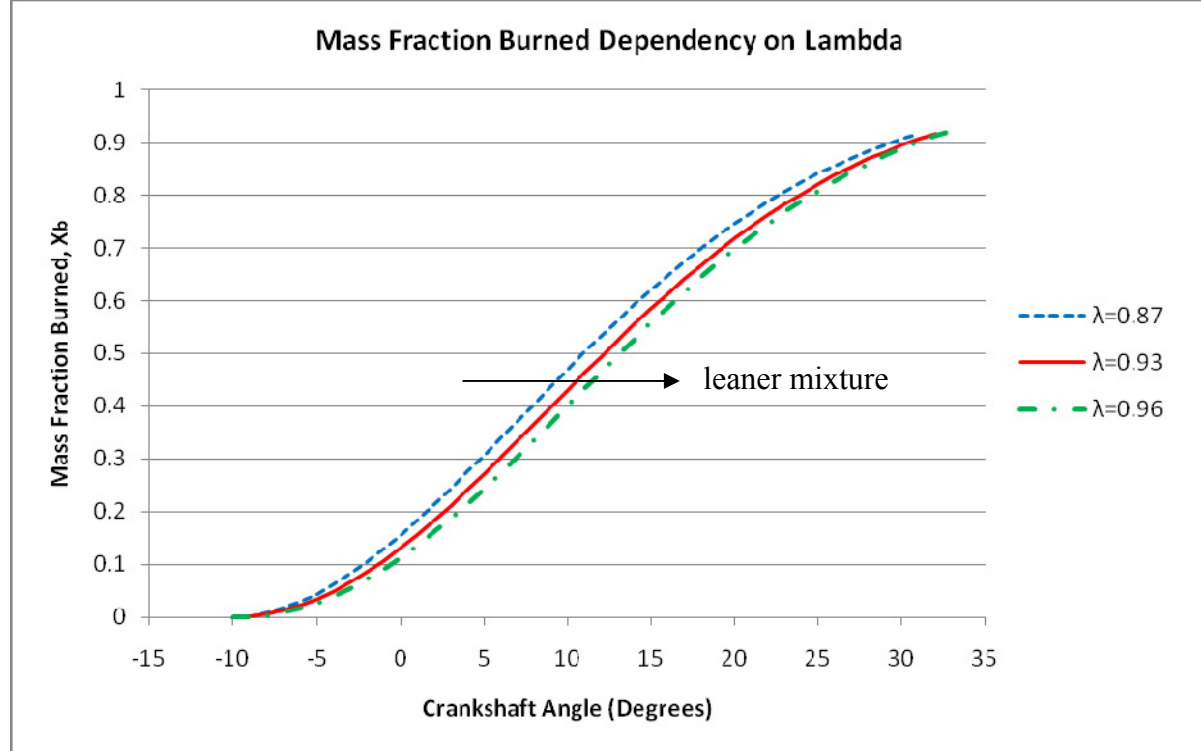


Figure 6-10: Mass fraction burned dependency on lambda

Similar mass fraction burned curve deformations due to independent changes in ignition timing and excess air ratio have been found by Vávra and Takáts [19] in their study of a SI turbocharged ML636NG six cylinder engine. These general trends discovered by the DOE and subsequent testing were utilized to uncover optimum combustion processes at both operating points under examination.

Chapter 7: Experimental Results

7.1 15% Load, 3,000 RPM Experimental Results

The DOE was constructed with limits such that the optimum engine operating points for best ISFC and IMEP would be bracketed. The statistical results were used to understand how to manipulate the mass fraction burned curve to improve engine performance and efficiency. Figure 7-1 and Figure 7-2 show the ISFC and IMEP of the engine versus the start of combustion (SOC) location. Best ISFC occurs with a SOC of 9 degrees BTDC while maximum IMEP occurs when SOC is retarded one more degree to 8 degrees BTDC.

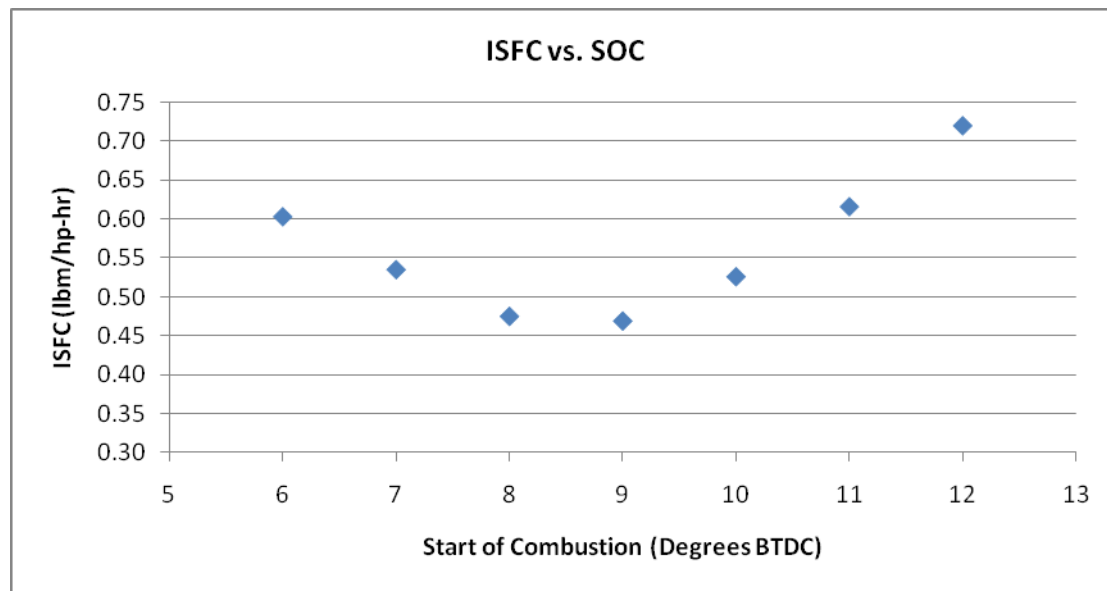


Figure 7-1: 15% load, 3,000 RPM ISFC as a function of SOC placement

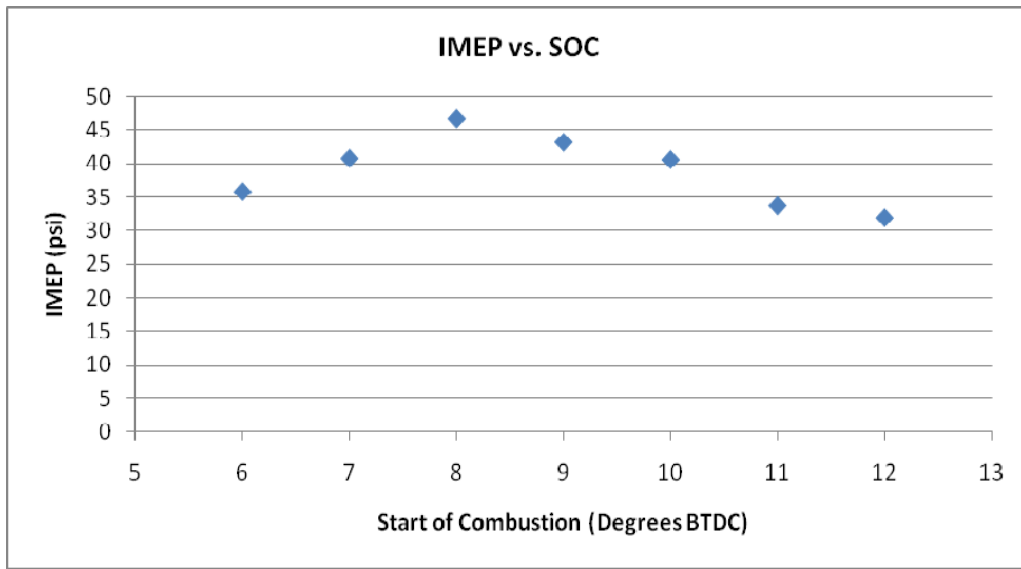


Figure 7-2: 15% load, 3,000 RPM IMEP as a function of SOC placement

The relationship between the location of SOC and ignition timing, i_t (in terms of crank angle BTDC), is shown in the ignition delay plot below. Deviation from the curve fit is caused by changes in other factors like fuel rail pressure, injection timing, and excess air ratio since these factors were not held constant for each data point. Thus, a general equation to estimate the ignition delay at this engine speed and load can be obtained.

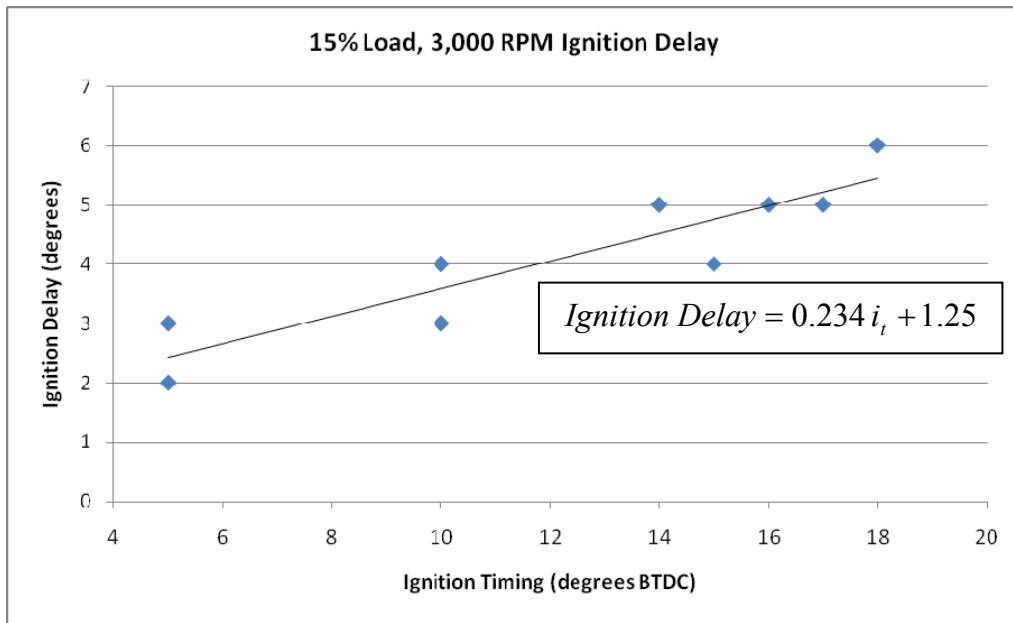


Figure 7-3: 15% load, 3,000 RPM ignition delay

The effect of the combustion centroid placement on ISFC and IMEP can be seen in Figure 7-4 and Figure 7-5. Best ISFC occurs with a combustion centroid of 8.7 degrees ATDC while maximum IMEP occurs when the combustion centroid is located at 9.1 degrees ATDC. Since ISFC is in terms of the fuel flow rate per unit power output, it is also useful to compare the shear amount of fuel being injected per cycle. The optimum ISFC point consumes 8.5% less fuel per cycle than the maximum IMEP point. There is always some kind of tradeoff to make between torque and fuel economy throughout the engine map. However, under this light load, low speed engine operating point, it is highly advantageous to choose to run at the minimum ISFC point and enjoy the maximum fuel conversion efficiency.

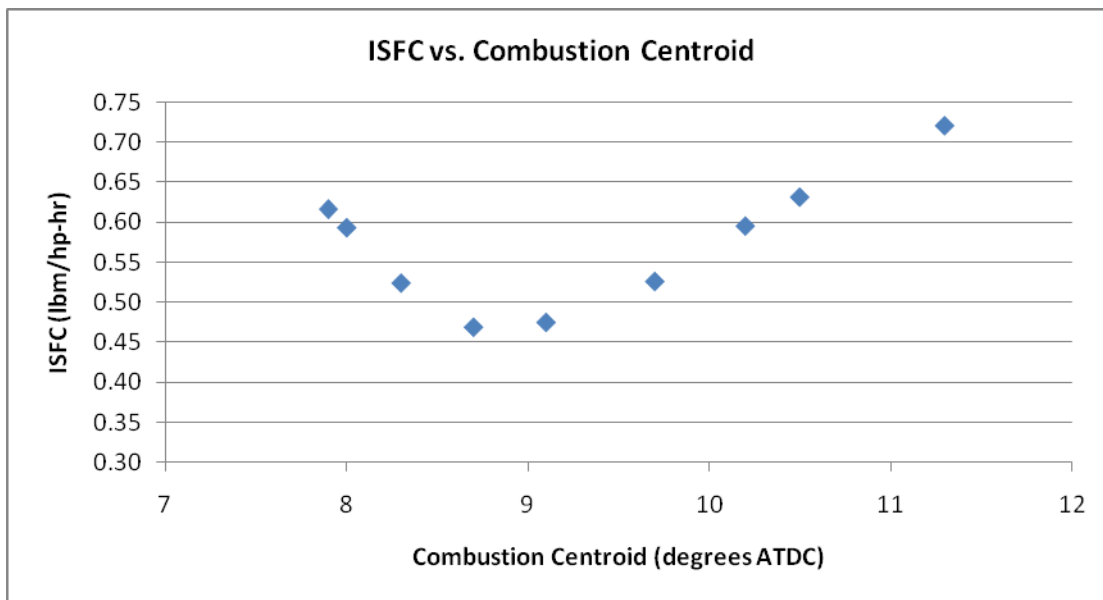


Figure 7-4: 15% load, 3,000 RPM ISFC as a function of combustion centroid placement

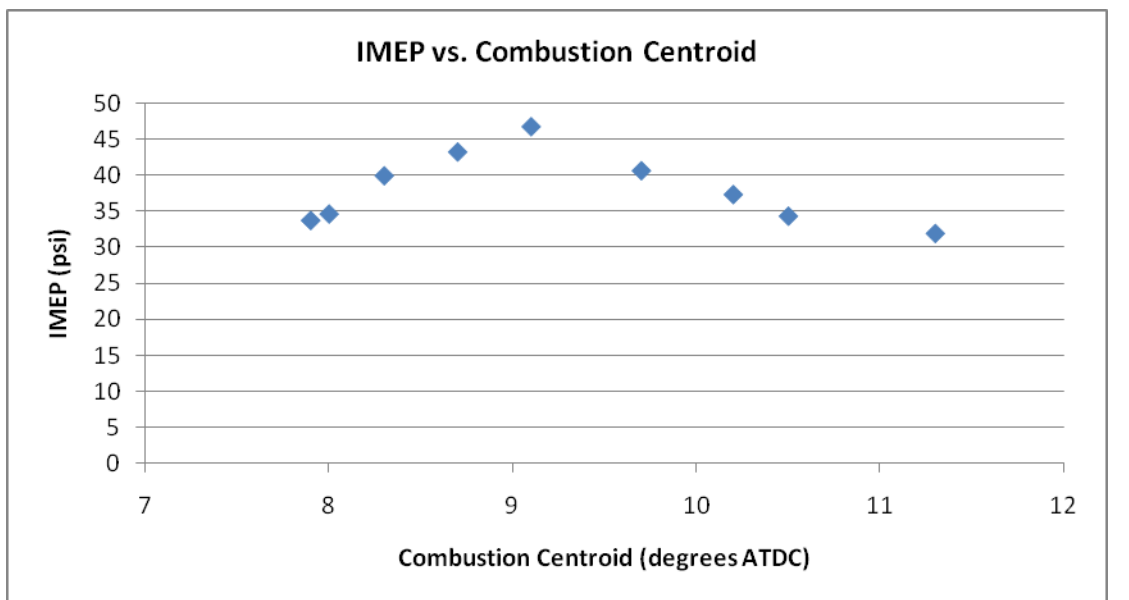


Figure 7-5: 15% load, 3,000 RPM IMEP as a function of combustion centroid placement

Figure 7-6 displays the deformation of the mass fraction burned curve due to changes in the combustion centroid location. Both the closest and furthest centroids from TDC as well as the optimum centroid from Figure 7-4 and Figure 7-5 are shown.

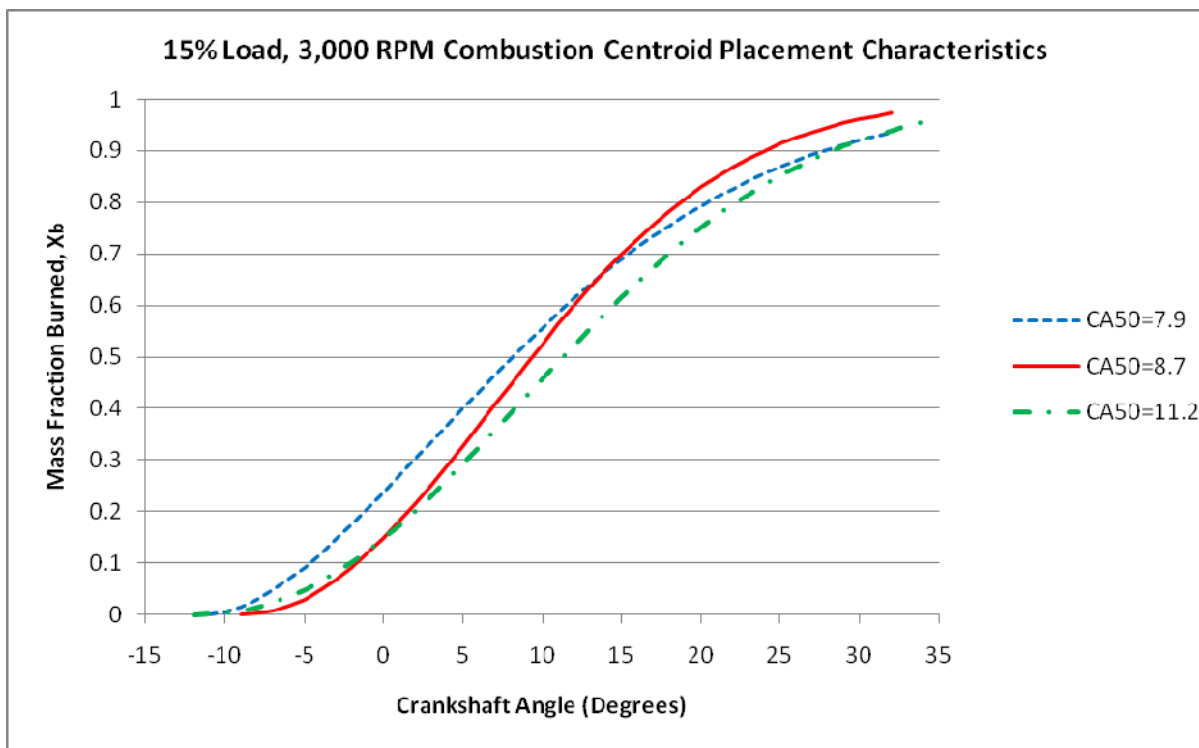


Figure 7-6: 15% load, 3,000 RPM combustion centroid placement characteristics

The mass fraction burned curve exhibiting the optimum centriod location boasts a steeper rapid burn rate and more complete burn over the other two curves. The tabulation below displays the Wiebe function curve fit parameters and performance and efficiency comparisons between the three curves.

Table 7-1: 15% load, 3,000 RPM performance and efficiency comparison

Combustion Centriod	Max Mass Burn Rate	Efficiency Parameter, a	Form Factor, m	ISFC	IMEP
7.9 deg. ATDC	0.033	3.30	1.10	0.631	34.3
8.7 deg. ATDC	0.039	3.60	1.05	0.469	43.2
11.2 deg. ATDC	0.031	2.75	0.70	0.720	31.9

The fired and motored averaged pressure traces for the optimum engine tune are shown in Figure 7-7. For the fired cycle, peak cylinder pressure was 265 psi. SOC occurred at 9 degrees BTDC. The largest standard deviation in cylinder pressure readings for the fired cycle occurred around 60 degrees ATDC where it peaked at 33 psi due to thermal shock. The standard deviations seen during the exhaust and intake events were minimal.

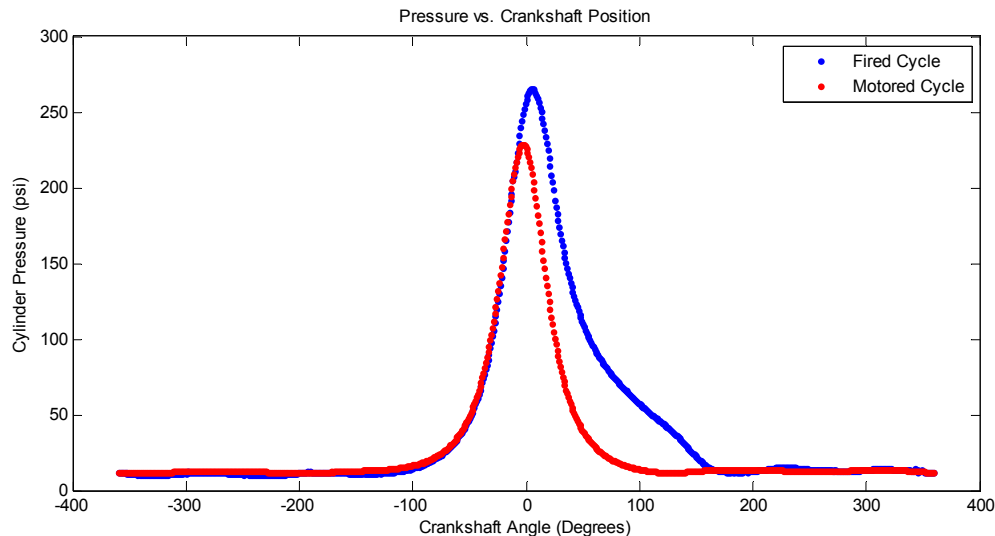


Figure 7-7: 15% load, 3,000 RPM fired and motored cycle

Figure 7-8 displays the P-V diagram for the pressure trace shown in Figure 7-7. Integration of the diagram provided 32.9 ft-lbf of indicated work per cycle per cylinder and

an IMEP of 43.2 psi. The indicated torque was 10.5 ft-lbf, and the indicated power at 3,000 RPM was 6.0 hp for the four cylinders combined.

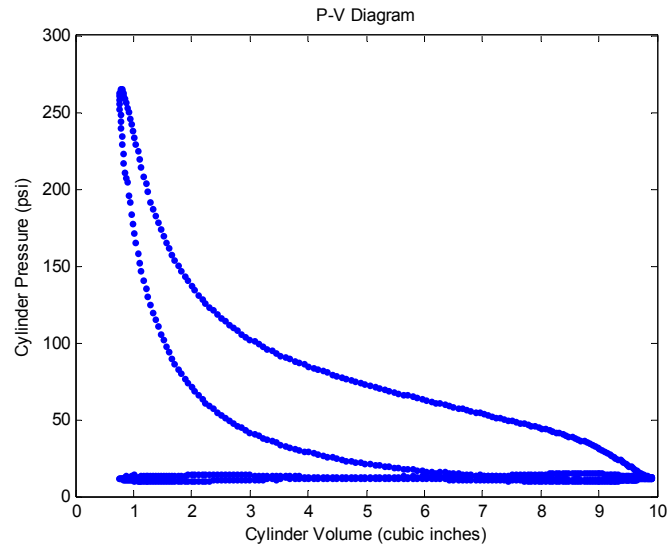


Figure 7-8: 15% load, 3,000 RPM P-V diagram

The log-log P-V diagram revealed a polytropic exponent of 1.30 on the compression stroke which matches the calculated ratio of specific heats. The line does not exhibit any curvature which implies that the engine had been allowed to reach a stable operating temperature at the time of the data acquisition.

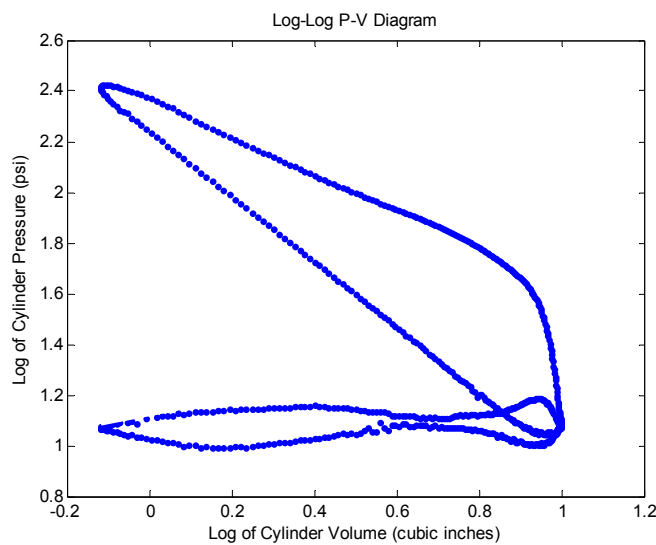


Figure 7-9: 15% load, 3,000 RPM log-log P-V diagram

The mass fraction burned curve derived from the in-cylinder pressure trace offered the desired SOC of 9 degrees BTDC and combustion centroid of 8.7 degrees ATDC. This resulted in a fast burn rate in the rapid burn portion of the curve as well as a fairly complete burn which translated into an improved fuel conversion efficiency.

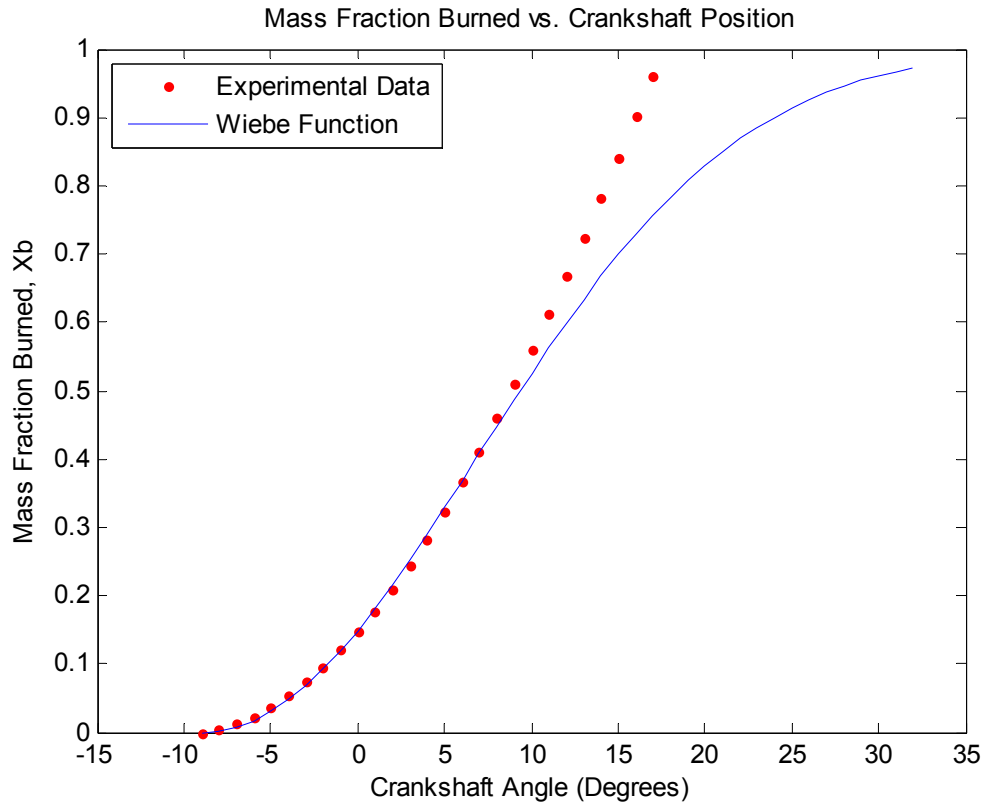


Figure 7-10: 15% load, 3,000 RPM mass fraction burned curve

7.2 60% Load, 3,000 RPM Experimental Results

In the same fashion, ISFC and IMEP as a function of SOC and combustion centroid location were examined for the 60% load, 3,000 RPM case. Figure 7-11 and Figure 7-12 show the ISFC and IMEP of the engine versus the SOC location. The relationship between the location of SOC and ignition timing, i_t (in terms of crank angle BTDC), is shown in Figure 7-13.

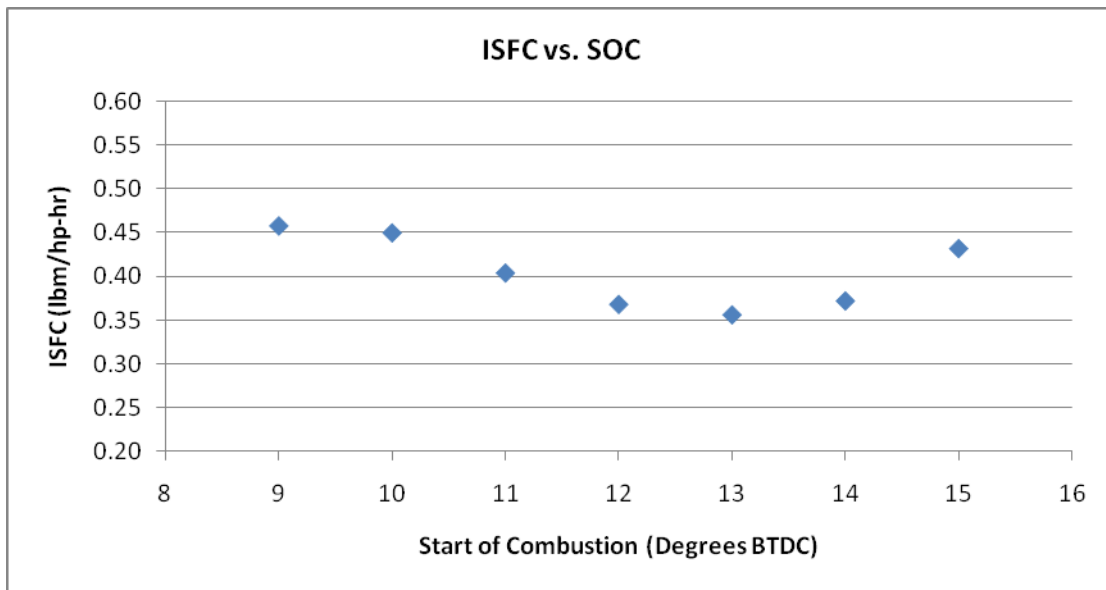


Figure 7-11: 60% load, 3,000 RPM ISFC as a function of SOC placement

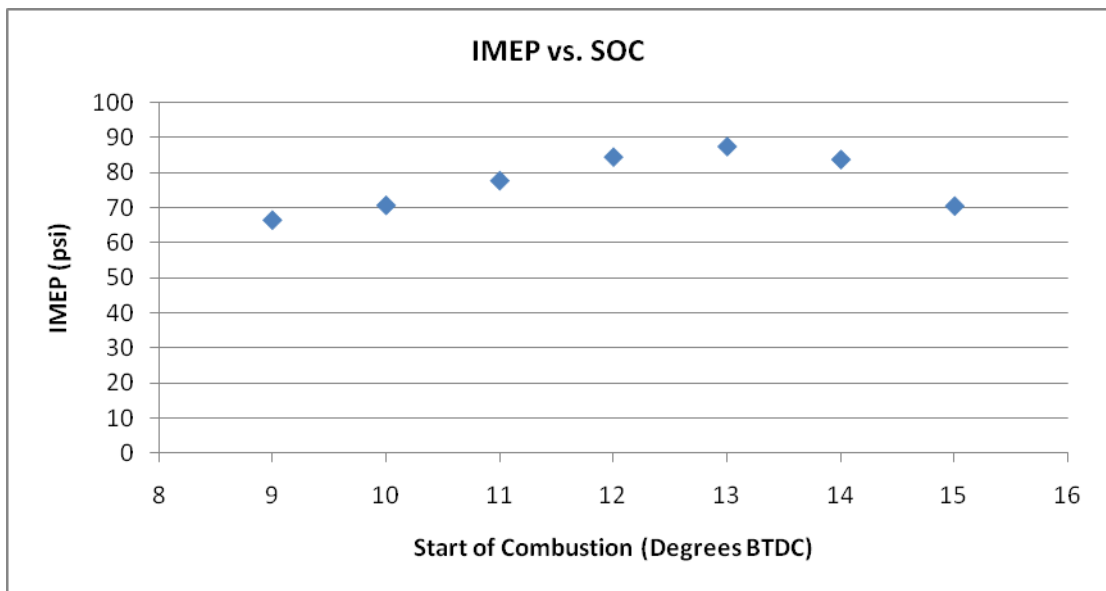


Figure 7-12: 60% load, 3,000 RPM IMEP as a function of SOC placement

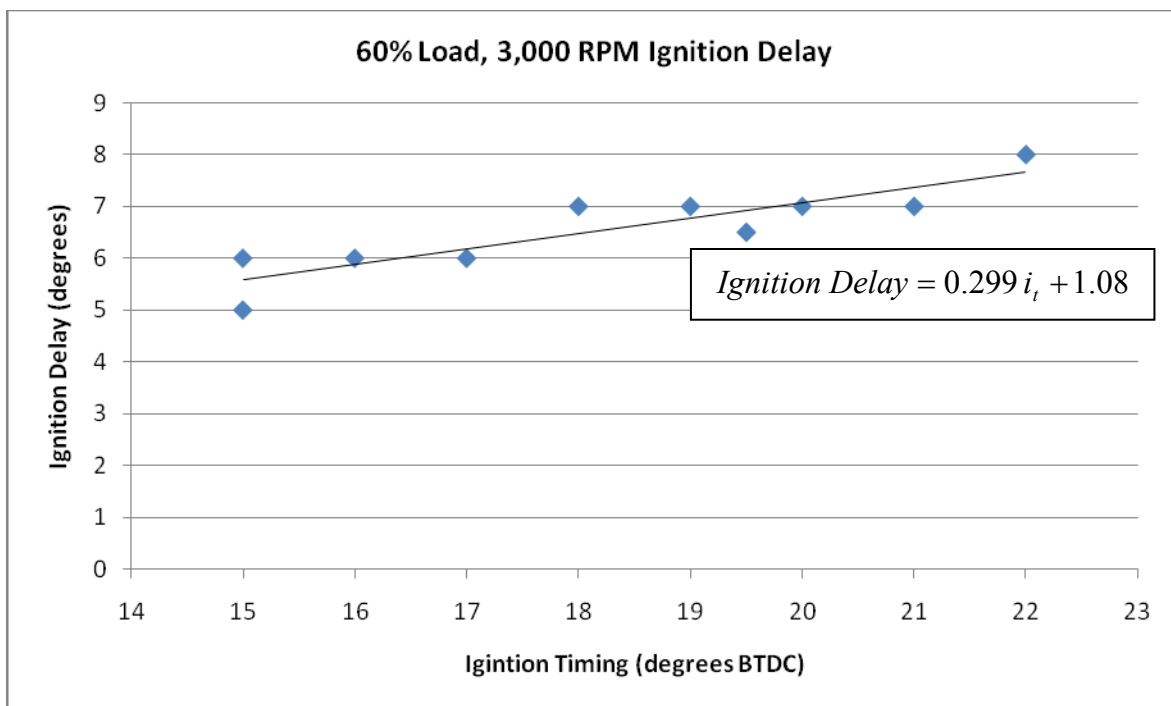


Figure 7-13: 60% load, 3,000 RPM ignition delay

The effect of the combustion centroid placement on ISFC and IMEP can be seen in Figure 7-14 and Figure 7-15. Best ISFC and IMEP occur with a combustion centroid of 8.8 degrees ATDC.

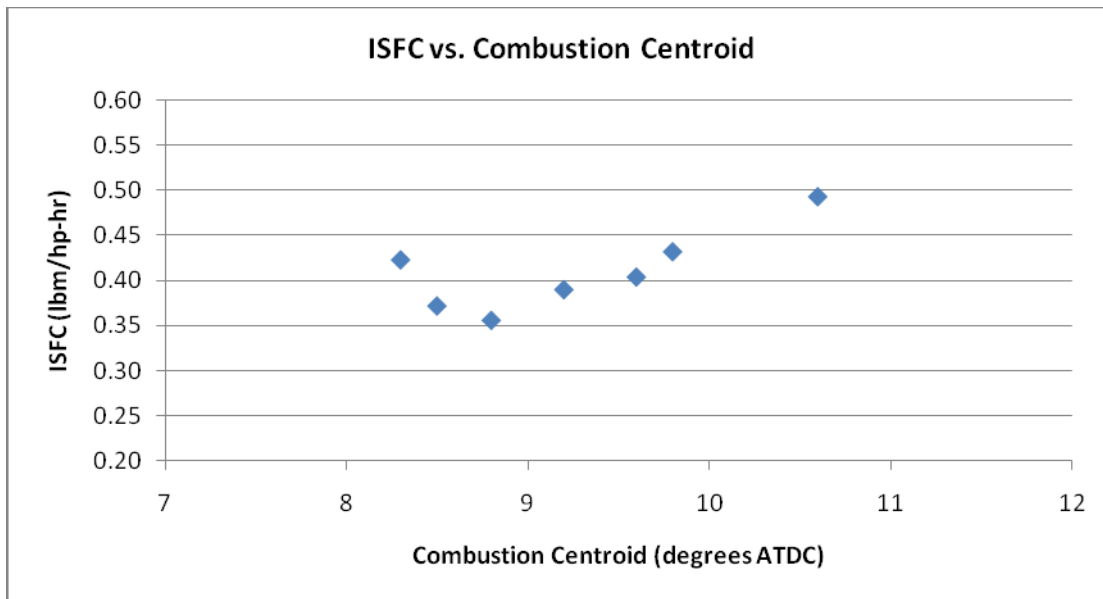


Figure 7-14: 60% load, 3,000 RPM ISFC as a function of combustion centroid placement

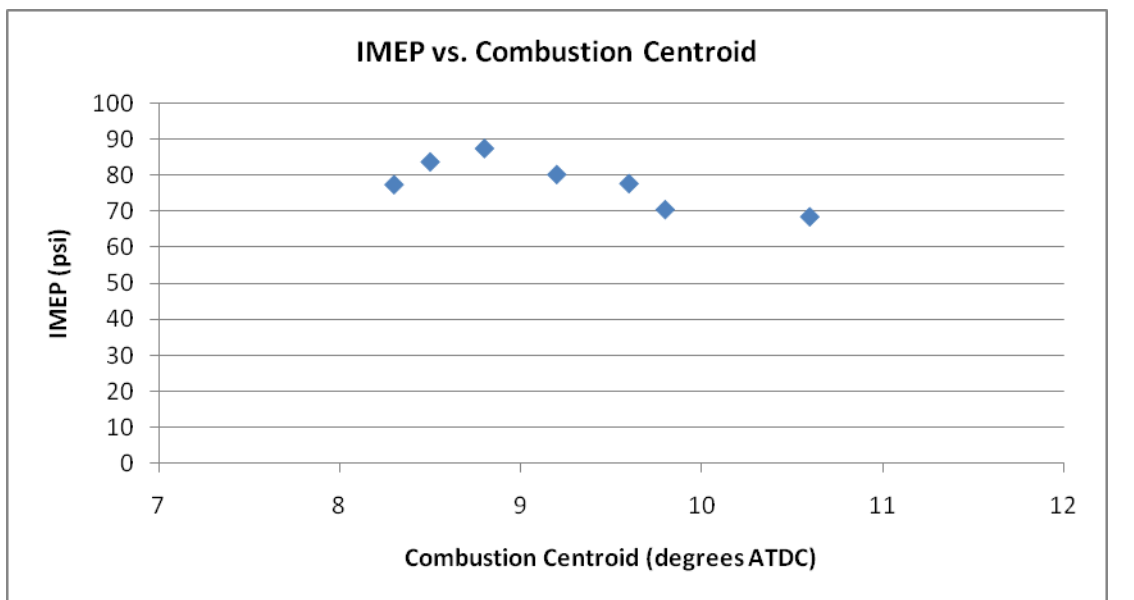


Figure 7-15: 60% load, 3,000 RPM IMEP as a function of combustion centroid placement

Figure 7-16 displays the deformation of the mass fraction burned curve due to changes in the combustion centroid location. Both the closest and furthest centroids from TDC as well as the optimum centroid from Figure 7-14 and Figure 7-15 are shown.

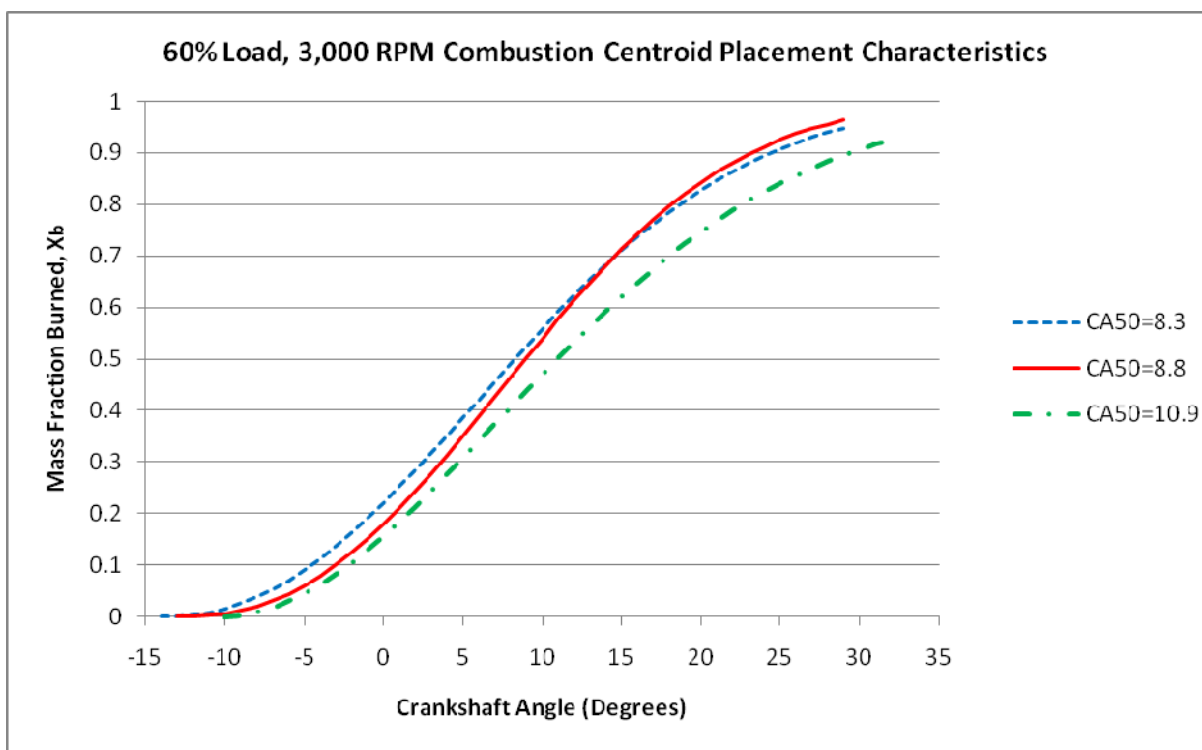


Figure 7-16: 60% load, 3,000 RPM combustion centroid placement characteristics

The mass fraction burned curve exhibiting the optimum centriod location again has a steeper rapid burn angle and more complete burn over the other two curves. The tabulation below displays the Wiebe function curve fit parameters and performance and efficiency comparisons between the three curves.

Table 7-2: 60% load, 3,000 RPM performance and efficiency comparison

Combustion Centriod	Max Mass Burn Rate	Efficiency Parameter, a	Form Factor, m	ISFC	IMEP
8.3 deg. ATDC	0.034	3.10	1.20	0.423	77.5
8.8 deg. ATDC	0.038	3.30	1.40	0.356	87.5
10.9 deg. ATDC	0.032	2.60	0.90	0.493	68.6

The fired and motored averaged pressure traces for the optimum engine tune are shown in Figure 7-17. For the fired cycle, peak cylinder pressure was 337 psi. SOC occurred at 13 degrees BTDC. The largest standard deviation in cylinder pressure readings for the fired cycle occurred around 40 degrees ATDC where it peaked at 13 psi due to thermal shock. The standard deviations seen during the exhaust and intake events were minimal.

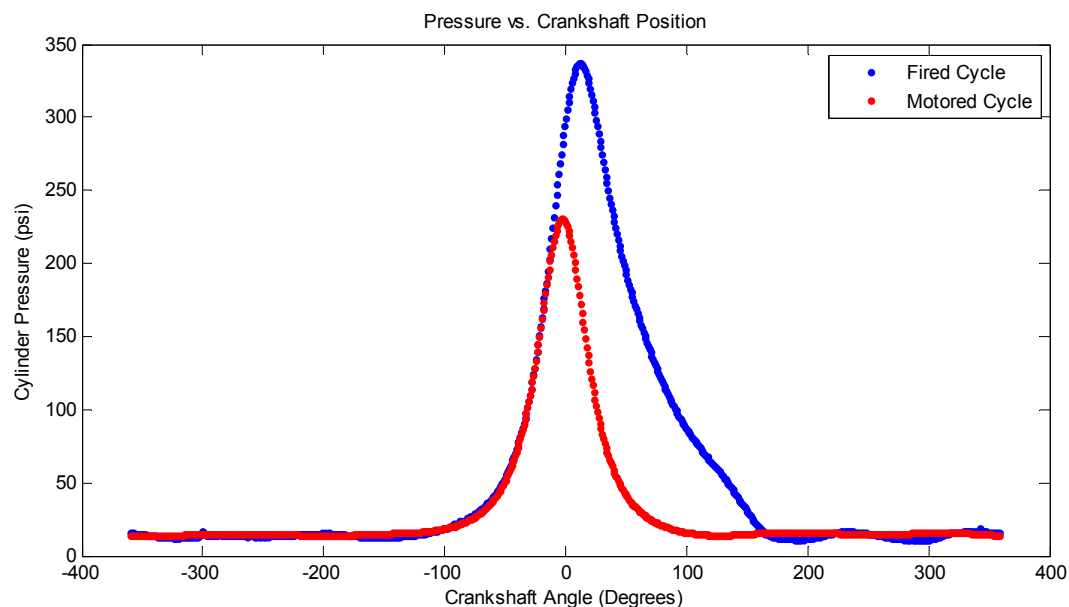


Figure 7-17: 60% load, 3,000 RPM fired and motored cycle

Figure 7-18 displays the P-V diagram for the pressure trace shown in Figure 7-17. Integration of the diagram provided 66.7 ft-lbf of indicated work per cycle per cylinder and an IMEP of 87.5 psi. The indicated torque was 21.2 ft-lbf, and the indicated power at 3,000 RPM was 11.5 hp for the four cylinders combined.

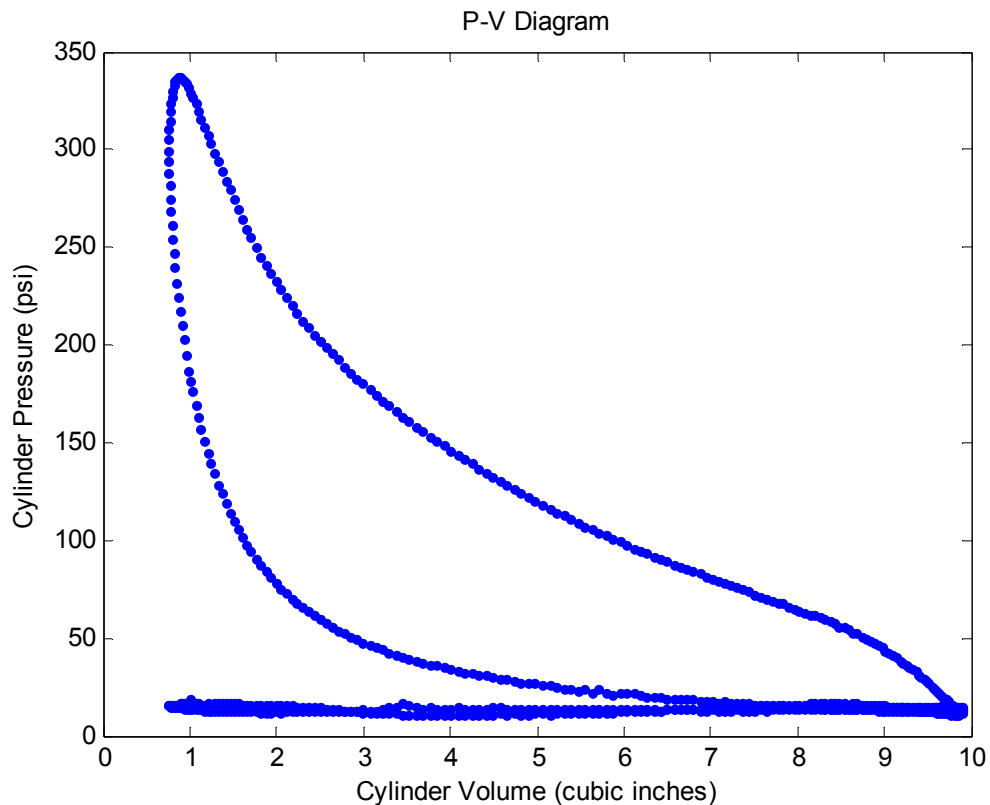


Figure 7-18: 60% load, 3,000 RPM P-V diagram

The log-log P-V diagram showed that thermal shock played more of a role during the expansion event than in any of the light load cases (more curvature). However, the compression line does not exhibit any curvature which implies that the engine had been allowed to reach a stable operating temperature at the time of the data acquisition. The polytropic exponent of 1.28 on the compression stroke matches the calculated ratio of specific heats.

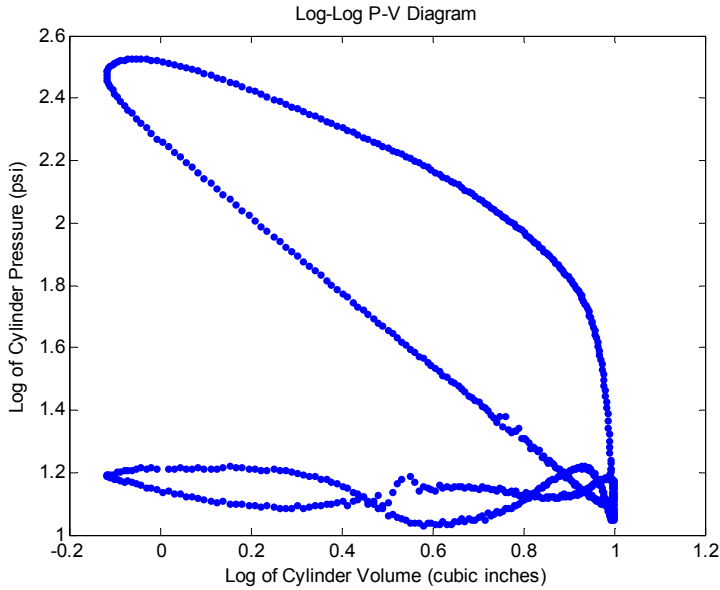


Figure 7-19: 60% load, 3,000 RPM log-log P-V diagram

The mass fraction burned curve derived from the in-cylinder pressure trace offered the desired SOC of 13 degrees BTDC and combustion centroid of 8.8 degrees ATDC. This resulted in a fast burn rate in the rapid burn portion of the curve as well as a more complete burn which resulted in an improved fuel conversion efficiency and mean effective pressure.

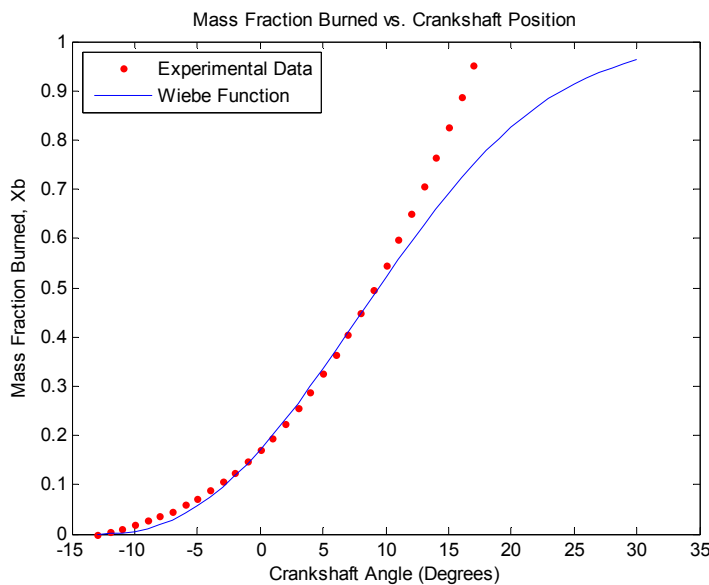


Figure 7-20: 60% load, 3,000 RPM mass fraction burned curve

The 15% load, 3,000 RPM study provided an ISFC of 0.469 lbm/hp-hr and an IMEP of 43.2 psi, while the 60% load, 3,000 RPM study provided an ISFC of 0.356 lbm/hp-hr and an IMEP of 87.5 psi. The optimum 15% and 60% load operating points provided mass burn rates of 0.039 and 0.038 respectively. These values are comparable to the maximum mass burn rate of 0.041 found by Attard, Konidaris, Hamori, Toulson, and Watson [20] for their 430 cc parallel twin PFI WATTARD engine operating at 10,000 RPM, WOT, MBT spark timing.

Chapter 8: Conclusions

The in-cylinder pressure analysis performed in this experiment proved to be more capable of improving engine performance and efficiency over tuning techniques previously used by the Auburn FSAE team. However, this type of analysis is quite computationally expensive as the data sets are large, and the analysis of the data sets must be done with care to ensure quality in the results. Few problems were experienced with the instrumentation with the exception of the thermal shock which continually occurred late in the expansion stroke. With a dry transducer, the only thing that can be done to reduce thermal shock errors is to increase the length of the communication passage between the pressure sensor and combustion chamber. This may help reduce thermal shock, but may also introduce other problems like ringing effects from resonance within the longer communication passage.

For the 15% load, 3,000 RPM case, an ISFC of 0.469 lbm/hp-hr and an IMEP of 43 psi were realized. This was done by adjusting the ignition timing to 14 degrees BTDC, fuel rail pressure to 70 psi, injection timing to 125 degrees BTDC, and relative air/fuel ratio to 0.97. For the 60% load, 3,000 RPM case, an ISFC of 0.356 lbm/hp-hr and an IMEP of 88 psi were realized. This was achieved by altering the ignition timing to 20 degrees BTDC, fuel rail pressure to 70 psi, injection timing to 175 degrees BTDC, and relative air/fuel ratio to 0.95. The adjusted settings for both cases resulted in a faster burn rates in the rapid burn portion of the curve as well as a more complete burn which translated into an improved fuel conversion efficiency and mean effective pressure. Wiebe functions fitted to the experimental

data utilized efficiency parameters of 3.60 and 3.30 and form factors of 1.05 and 1.40 respectively. Both studies shared a similar optimum combustion centroid at 8.7 and 8.8 degrees ATDC and a maximum mass burn rate of 0.039 and 0.038 correspondingly, showing good agreement between the two tests.

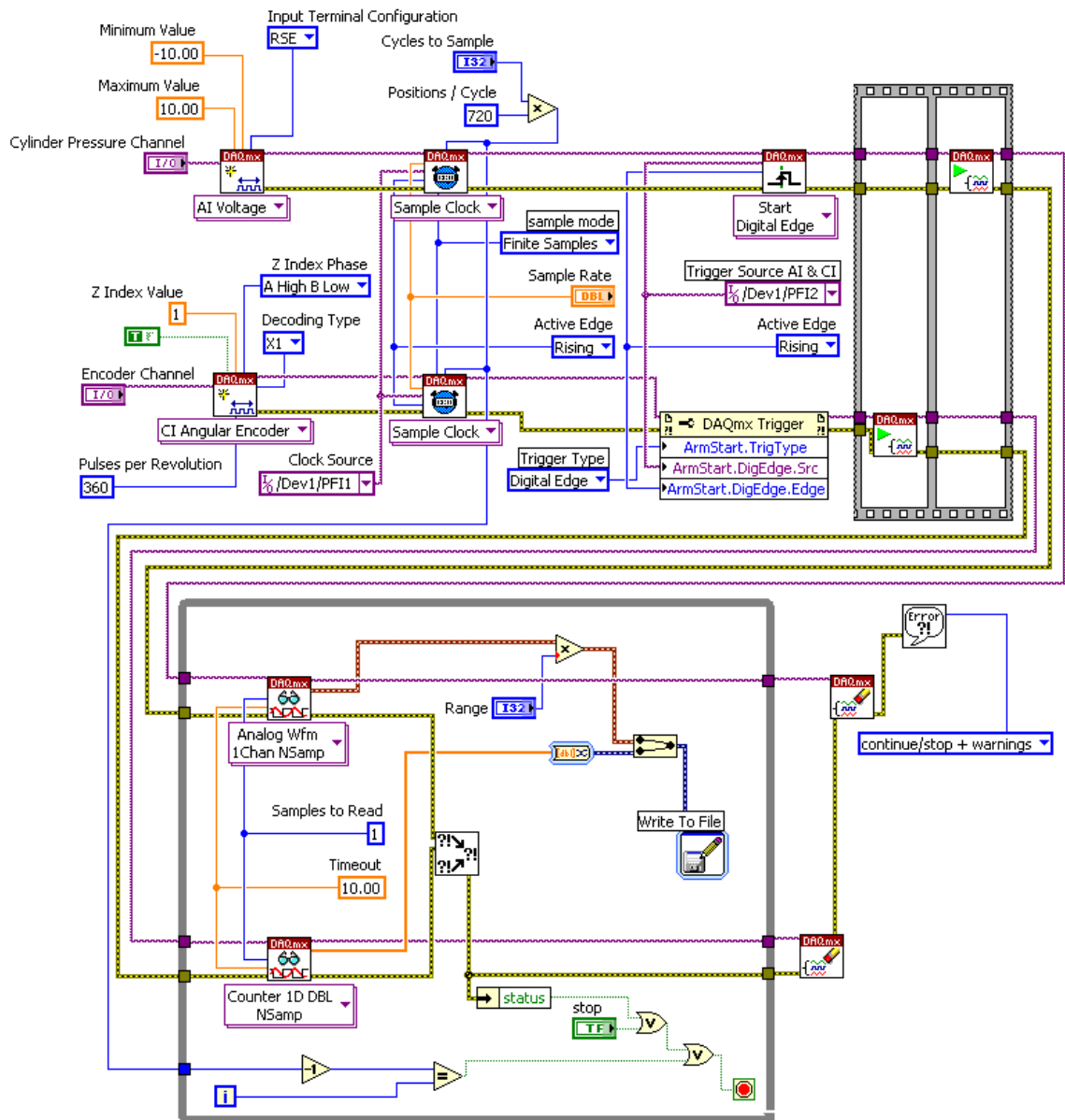
References

1. Brunt, M., Rai, H., and Emtage, A., "The Calculation of Heat Release Energy from Engine Cylinder Pressure Data," SAE paper 981052, 1998
2. Plint, M., and Martyr, A., *Engine Testing Theory and Practice*, 1995, Woburn, MA: Butterworth-Heinemann
3. Woschni, G., "A Universally Applicable Equation for the Instantaneous Heat Transfer Coefficient in the Internal Combustion Engine," SAE paper 670931, 1967
4. Stone, R., *Introduction to Internal Combustion Engines*, 1992, Warrendale, PA: SAE, Inc.
5. Iorio, B., Giglio V., Police G., and Rispoli, N., "Methods of Pressure Cycle Processing for Engine Control," SAE paper 2003-01-0352, 2003
6. Heywood, J.B., *Internal Combustion Engine Fundamentals*, 1988, New York, NY: McGraw-Hill, Inc.
7. Atkins, R., *An Introduction to Engine Testing and Development*, 2009, Warrendale, PA, SAE International
8. Ferguson, C.R., *Internal Combustion Engines – Applied Thermosciences*, 1986, Toronto, Canada: John Wiley & Sons, Inc.
9. Rassweiler, G.M., and Withrow, L., "Motion Pictures of Engine Flames Correlated with Pressure Cards," SAE paper 670931, 1967
10. Gatowski, J.A., Balles, E.N., Chun, K.M., Nelson, F.E., Ekchian, J.A., and Heywood, J.B., "Heat Release Analysis of Engine Pressure Data," SAE paper 841359, 1984
11. Cheung, H.M., Heywood, J.B., "Evaluation of a One-Zone Burn-Rate Analysis Procedure Using Production SI Engine Pressure Data," SAE paper 932749, 1993
12. Cengel, Y. and Boles, M., *Thermodynamics An Engineering Approach*, 2008, New York, NY: McGraw-Hill, Inc.

13. Eriksson, L., “Requirements for and a Systematic Method for Identifying Heat-Release Model Parameters,” SAE paper 980626, 1998
14. Jones, P., *MECH 4410 Engines*, Summer 2010 course notes, Auburn, AL, Auburn University, Department of Mechanical Engineering
15. Rogers, D., *Engine Combustion: Pressure Measurement and Analysis*, 2010, Warrendale, PA: SAE, International
16. *Kistler Instruction Manual*, 2003, Winterthur, Switzerland, Kistler Instrument Corporation
17. “The Piezoelectric Effect, Theory, Design, and Usage”,
http://www.designinfo.com/kistler/ref/tech_text.htm, Winterthur, Switzerland,
Kistler Instrument Corporation
18. Anderson, M. and Whitcomb, P., *DOE Simplified: Practical Tools for Effective Experimentation*, 2000, Portland, OR: Productivity, Inc.
19. Vávra, J. and Takáts, M., “Heat Release Regression Model for Gas Fuelled SI Engines,”
SAE paper 2004-01-1462, 2004
20. Attard, W., Konidaris, S., Hamori, F., Toulson, E., Watson, H., “Compression Ratio Effects on Performance, Efficiency, Emissions and Combustion in a Carbureted and PFI Small Engine,” SAE paper 2007-01-3623, 2007

Appendix

LabView 2009 Data Acquisition Block Diagram



LabView 2009 Data Acquisition Front Panel



MATLAB R2009a Data Analysis Code

```
%% R6_Peg_Shift_Awesome.m
% Performs post processing of text file output from LabView
% NOTE: first import fired pressure data file into MATLAB
% 1. Go to File\Import Data...
% 2. Set delimiting type (tab)
% 3. Set "Number of text header lines" to 23 for typical file
% 4. Ensure that the first values of the file are included in the preview
%     (i.e. crank=1 deg.), if not, adjust the "Number of text header
lines" to the appropriate value
% 5. Click "Next"; check "create variables matching preview"
% 6. Remove checks from everything BUT the data matrix; click "Finish"
% 7. Repeat steps 1-6 for the motored pressure data file, then right-
click & rename the data matrix as "data2"
% 8. Edit pressure and position data column callouts below to obtain data
in the sorting loop (if necessary)
% 9. Enter engine speed, number of cycles sampled, & lambda for the test
% 10. Enter any other appropriate values (i.e. Tim, Twall, EGT, mfdot,
%     Woschini calibration parameters, etc.)
% 11. Adjust any other parameters as necessary

clc;

% global statements
global Ru fuel phi EGT Tim

% Data column callouts (for both fired & motored)
Pcol=2; % Pressure data column
Ccol=3; % Position data column

% Enter combustion analysis start and end values [degrees from TDC]
polystrt1=-91; % start for analyzing polytropic index
polyend1=-28; % end for analyzing polytropic index
polystrt2=(-1*polyend1)+3; % start for analyzing polytropic index
polyend2=(-1*polystrt1)-39; % end for analyzing polytropic index

% tolerance for SOC & EOC detection
tolerance=0.005;
% duration for combustion centroid calculation
rapdbrnstrt=6;
rapdbrnend=13;
combstrt720=349;
combend720=378;

% Enter engine speed
rpm=3150;

% Enter MAP, plenum temperature, & volumetric efficiency
MAP=89; % [kPa]
Trefc=20; % intake reference temperature [C]
etav=0.33; % volumetric efficiency
```

```

% Enter # of cycles sampled
cycles=99;
mcycles=99;

% Enter lambda value
lambda=0.96;

% Enter angular encoder shift
shift=166; % [degrees]
mshift=166; % [degrees]

% Engine Geometry
bore=6.7; % [cm]
stroke=4.25; % [cm]
Rc=13.1; % compression ratio
numcyl=4; % number of cylinders
Vd=(pi*((bore/2)^2)*stroke); % displaced volume [cc]
Vdm=Vd/(100^3); % displaced volume [m^3]
Vc=Vd/(Rc-1); % clearance volume [cc]
Vcm=Vc/(100^3); % clearance volume [m^3]

% Valve Timing (adjusted to Theta matrix "1-720 degrees")
IVO=721-39;
IVC=181+65;
EVO=541-64;
EVC=721-24;

% Fluid Properties
Timf=164; % intake manifold temperature [F]
Twallf=500; % cylinder wall temperature [F]
EGTf=1200; % exhaust gas temperature [F]
Tim=((Timf-32)/1.8)+273; % intake manifold temperature [K]
Twall=((Twallf-32)/1.8)+273; % cylinder wall temperature [K]
EGT=((EGTf-32)/1.8)+273; % exhaust gas temperature [K]
fuel=2; % fuel type (1-CH4; 2-C7H17; 3-C14.4H24.9; 4-CH3OH; 5-CH3NO2)
Ru=8314.34; % universal gas constant [J/kmolK]
Pref=MAP*1000; % intake reference pressure [Pa]
Tref=Trefc+273; % intake reference temperature [K]
phi=1/lambda; % fuel/air equivalency ratio

% Woschini's correlation for engine heat transfer
Rs=2.5; % swirl ratio
N=rpm/60; % angular velocity of crank [rot/s]
strokem=stroke/100; % converting to meters
borem=bore/100; % converting to meters
ws=Rs*2*pi*N; % angular velocity of fluid [rad/s]
vs=(borem*ws)/2; % swirl velocity term [m/s]
Sp=2*strokem*(rpm/60); % mean piston speed [m/s]
c11=6.18+(0.417*(vs/Sp)); % calibration parameter (gas exchange period)
c12=2.28+(0.308*(vs/Sp)); % calibration parameter (rest of cycle)
c2=3.24e-03; % calibration parameter (only valid for combustion & expansion period)
Rem=0.5; % Reynold's number exponent
cal1=1; % Woschini convection coefficient calibration parameter
cal2=1; % Woschini convection coefficient calibration parameter

```

```

% Allocating 23for space
Pm=zeros(720,cycles);
Pdata=zeros(720,cycles);
Cdata=zeros(720,cycles);
Mdata=zeros(720,mcycles);
MCdata=zeros(720,mcycles);
Pmeas=zeros(720,cycles);
RunPm=zeros(720,cycles);
RunTm=zeros(720,cycles);
Pmot=zeros(720,mcycles);
Pmeasmot=zeros(720,mcycles);
RunPmot=zeros(720,mcycles);
RunTmot=zeros(720,mcycles);
Diff=zeros(5,1);
Diffmot=zeros(5,1);
Diffavg=zeros(5,1);
Diffmotavg=zeros(5,1);
allval1=zeros(1,cycles);
allval2=zeros(1,mcycles);
Pavg=zeros(720,1);
Pavgmot=zeros(720,1);
Pmode=zeros(720,1);
Pmedian=zeros(720,1);
Pstd=zeros(720,1);
Theta=zeros(720,1);
Vol=zeros(720,1);
fpos=zeros(180,1);
fneg=zeros(179,1);
wpos=zeros(179,1);
wneg=zeros(178,1);
fposR=zeros(180,cycles);
fnegR=zeros(179,cycles);
wposR=zeros(179,cycles);
wnegR=zeros(178,cycles);
MEPR=zeros(1,cycles);
Pspl1=zeros(abs(polystrt1)-abs(polyend1)+1,1);
Vspl1=zeros(abs(polystrt1)-abs(polyend1)+1,1);
Pspl2=zeros(abs(polystrt2)-abs(polyend2)+1,1);
Vspl2=zeros(abs(polystrt2)-abs(polyend2)+1,1);
T=zeros(720,1);
w=zeros(720,1);
h=zeros(720,1);
Acyl=zeros(720,1);
dQdT=zeros(720,1);
PdVdt=zeros(720,1);
VdPdt=zeros(720,1);

% Shift pressure values to TDC
j=1;
for i=1:1:shift
    Pdata(i,1)=data(i,Pcol);
    Cdata(i,1)=data(i,Ccol)-shift;
    j=j+1;
end
j=1;

```

```

for i=1:1:mshift
    Mdata(i,1)=data2(i,Pcol);
    MCdata(i,1)=data2(i,Ccol)-mshift;
    j=j+1;
end
for i=shift+1:1:720
    Pdata(i,1)=data(i,Pcol);
    if j<=360
        Cdata(i,1)=data(i,Ccol);
    else
        Cdata(i,1)=data(i,Ccol)+360;
    end
end
for i=mshift+1:1:720
    Mdata(i,1)=data2(i,Pcol);
    if j<=360
        MCdata(i,1)=data2(i,Ccol);
    else
        MCdata(i,1)=data2(i,Ccol)+360;
    end
end
% Calculate # of double crank positions for fired cycle
fend=(720*cycles);
for i=721:1:fend
    if data(i,Ccol)==data(i-1,Ccol)
        fend=fend+1;
    end
end
% Sort reamaining data values for fired cycle
j=1;
k=2;
for i=721:1:fend
    if data(i,Ccol)>data(i-1,Ccol)
        Pdata(j,k)=data(i,Pcol);
        if j<=360
            Cdata(j,k)=data(i,Ccol);
        else
            Cdata(j,k)=data(i,Ccol)+360;
        end
        if j<720
            j=j+1;
        else
            j=1;
            k=k+1;
        end
    elseif data(i,Ccol)==1
        Pdata(j,k)=data(i,Pcol);
        if j<=360
            Cdata(j,k)=data(i,Ccol);
        end
        if j<720
            j=j+1;
        else
            j=1;
            k=k+1;
        end
    end
end

```

```

        end
% Calculate # of double crank positions for motored cycle
mend=(720*mcycles);
for i=721:1:mend
    if data2(i,Ccol)==data2(i-1,Ccol)
        mend=mend+1;
    end
end
% Sort remaining data values for motored cycle
j=1;
k=2;
for i=721:1:mend
    if data2(i,Ccol)>data2(i-1,Ccol)
        Mdata(j,k)=data2(i,Pcol);
        if j<=360
            MCdata(j,k)=data2(i,Ccol);
        else
            MCdata(j,k)=data2(i,Ccol)+360;
        end
        if j<720
            j=j+1;
        else
            j=1;
            k=k+1;
        end
    elseif data2(i,Ccol)==1
        Mdata(j,k)=data2(i,Pcol);
        if j<=360
            MCdata(j,k)=data2(i,Ccol);
        end
        if j<720
            j=j+1;
        else
            j=1;
            k=k+1;
        end
    end
end
%Pegging Pressure Traces
for i=1:1:cycles
    for j=178:1:182
        Diff(j-177,i)=Pdata(j,i)-(MAP*(14.696/101.325));
    end
end

for i=1:1:cycles
    for j=1:1:5
        Diffavg(j,i)=mean(Diff(j,i));
    end
end

for i=1:1:mcycles
    for j=178:1:182
        Diffmot(j-177,i)=Mdata(j,i)-(MAP*(14.696/101.325));
    end

```

```

end

for i=1:1:mcycles
    for j=1:1:5
        Diffmotavg(j,i)=mean(Diffmot(j,i));
    end
end

Peg=mean(Diffavg);
Peg2=mean(Peg);
Pegmot=mean(Diffmotavg);
Pegmot2=mean(Pegmot);

for i=1:1:cycles
    for j=1:1:720
        Pm(j,i)=Pdata(j,i)-Peg2;
    end
end

for i=1:1:mcycles
    for j=1:1:720
        Pmot(j,i)=Mdata(j,i)-Pegmot2;
    end
end

% Calculating mean, median, mode, & std
for k=1:1:720
    for m=1:1:cycles
        allval1(1,m)=Pm(k,m);
    end
    for j=1:1:mcycles
        allval2(1,j)=Pmot(k,j);
    end
    Pavg(k,1)=mean(allval1);
    Pavgmot(k,1)=mean(allval2);
    Pmode(k,1)=mode(allval1);
    Pmedian(k,1)=median(allval1);
    Pstd(k,1)=std(allval1);
end

% Calculating PCP and LPP
Peak=0;
Peakmot=0;
for k=1:1:720
    if Pavg(k,1)>Peak
        Peak=Pavg(k,1);
        Locatefire=k-1;
    end
    if Pavgmot(k,1)>Peakmot
        Peakmot=Pavgmot(k,1);
        Locatemot=k-1;
    end
end

Locatecorr=Locatefire-360;

```

```

Locatemotcorr=Locatemot-360;

fprintf('\n')
fprintf('Fired PCP %6.1f psi \n',Peak) % fired PCP
fprintf('Fired LPP %6.0f degrees \n',Locatecorr) %
fired LPP
fprintf('Motored PCP %6.1f psi \n',Peakmot) % motored
PCP
fprintf('Motored LPP %6.0f degrees \n',Locatemotcorr) %
motored LPP

Pstd180p=Pstd(180,1); % standard deviation of pressure @ -180 degrees
Pstd180m=Pstd(540,1); % standard deviation of pressure @ +180 degrees

fprintf('\n')
fprintf('STD of Pressure -180 degrees %6.1f psi \n',Pstd180p) % standard
deviation of pressure @ -180 degrees
fprintf('STD of Pressure +180 degrees %6.1f psi \n',Pstd180m) % standard
deviation of pressure @ +180 degrees

% Creating theta & volume matrices
r=stroke/2; % crankshaft throw [cm]
l=9.1; % connecting rod length [cm]
for i=-360:1:359
    q=i+361;
    Theta(q,1)=i;
    s(q,1)=(r*cos(Theta(q,1)*(pi/180)))+(((l^2)-
((r^2)*((sin(Theta(q,1)*(pi/180)))^2)))^0.5);
    Ach=(pi*((stroke/2)^2)+(2*pi*(stroke/2)*0.087785);
    Ap=(pi*((stroke/2)^2));
    A(q,1)=Ach+Ap+(pi*bore*(l+r-s(q,1)));
    Vol(q,1)=(Vc+((pi*(bore^2))/4)*(l+r-s(q,1)))*(1/(2.54^3));
end

% Integrating P-V diagram (averaged data)
j=1;
for i=1:1:180
    fpos(j,1)=abs(Pavg(i+361,1)-Pavg(361-i,1));
    j=j+1;
end
j=1;
for i=1:1:179
    wpos(j,1)=abs((Vol(i+361,1)-
Vol(i+362,1))*(fpos(i,1)+fpos(i+1,1))/2));
    j=j+1;
end
j=1;
for i=1:1:179
    fneg(j,1)=-1*(abs(Pavg(181-i,1)-Pavg(541+i,1)));
    j=j+1;
end
j=1;
for i=1:1:178
    wneg(j,1)=-1*abs((Vol(i+179,1)-
Vol(i+178,1))*(fneg(i,1)+fneg(i+1,1))/2));
    j=j+1;

```

```

end
W=0;
for i=1:1:178
    W=W+wpos(i,1)+wneg(i,1);
end
Work=W/12; % per cylinder
MEP=W/(Vol(181,1)-Vol(1,1)); % total for 4 cylinders
Power=(rpm*numcyl*Work)/(60*2*550); % total for 4 cylinders
Torque=(Power*550*60)/(rpm*2*pi); % total for 4 cylinders
fprintf('\n')
fprintf('Work/Cycle/Cylinder           %6.1f ft-lbf \n',Work) % per
cylinder
fprintf('IMEP                         %6.1f psi \n',MEP) % total for 4
cylinders
fprintf('Indicated Power             %6.1f hp \n',Power) % total for 4
cylinders
fprintf('Indicated Torque            %6.1f ft-lbf \n',Torque) % total
for 4 cylinders

% Integrating P-V diagram (raw data)
for c=1:1:cycles
    j=1;
    for i=1:1:180
        fposR(j,c)=abs(Pm(i+361,c)-Pm(361-i,c));
        j=j+1;
    end
    j=1;
    for i=1:1:179
        wposR(j,c)=abs((Vol(i+361,1)-
Vol(i+362,1))*(fposR(i,c)+fposR(i+1,c))/2));
        j=j+1;
    end
    j=1;
    for i=1:1:179
        fnegR(j,c)=-1*(abs(Pm(181-i,c)-Pm(541+i,c)));
        j=j+1;
    end
    j=1;
    for i=1:1:178
        wnegR(j,c)=-1*abs((Vol(i+179,1)-
Vol(i+178,1))*(fnegR(i,c)+fnegR(i+1,c))/2));
        j=j+1;
    end
    WR=0;
    for i=1:1:178
        WR=WR+wposR(i,c)+wnegR(i,c);
    end
    MEPR(1,c)=WR/(Vol(181,1)-Vol(1,1)); % total for 4 cylinders
end

IMEPstd=std(MEPR); % standard deviation of IMEP
COVIMEP=(IMEPstd/MEP)*100; % coefficient of variation of IMEP (COV)
IMEPmin=min(MEPR); % minimum IMEP value
LNVIMEP=(IMEPmin/MEP)*100; % lowest normalized value of IMEP (LNV)

```

```

fprintf('\n')
fprintf('STD of IMEP          %6.1f psi \n',IMEPstd)    % per cycle
fprintf('COV of IMEP          %6.1f percent \n',COVIMEP)  % per
cycle
fprintf('LNV of IMEP          %6.1f percent \n',LNVIMEP)  % per
cycle

% Creating log-log P-V data
Plog=log10(Pavg);
Vlog=log10(Vol);

% Calculating polytropic index using least squares regression
n=polyend1-polystrt1+1;
sumx=0;
sumy=0;
sumxy=0;
sumx2=0;
for i=polystrt1+361:1:polyend1+361
    sumx=sumx+Vlog(i,1);
    sumy=sumy+Plog(i,1);
    sumxy=sumxy+(Vlog(i,1)*Plog(i,1));
    sumx2=sumx2+(Vlog(i,1)^2);
end
gamma1=-1* ((n*sumxy)-(sumx*sumy)) / ((n*sumx2)-(sumx^2));

sumx=0;
sumy=0;
sumxy=0;
sumx2=0;
for i=polystrt2+361:1:polyend2+361
    sumx=sumx+Vlog(i,1);
    sumy=sumy+Plog(i,1);
    sumxy=sumxy+(Vlog(i,1)*Plog(i,1));
    sumx2=sumx2+(Vlog(i,1)^2);
end
gamma2=((n*sumxy)-(sumx*sumy)) / ((n*sumx2)-(sumx^2));

fprintf('\n')
fprintf('Polytropic Index 1      %6.2f \n',gamma1)
fprintf('Polytropic Index 2      %6.2f \n',gamma2)

% Calculating SOC
slope=-0.5;
start=polyend1+361;
while slope>-gamma1-tolerance
    slope=(Plog(start+1,1)-Plog(start,1))/(Vlog(start+1,1)-Vlog(start,1));
    start=start+1;
end

% combstrt720=start-1;
SOC=combstrt720-360;

% Calculating EOC and combustion duration
slope2=1;
endburn=polystrt2+361;

```

```

while slope2>gamma2-tolerance
    slope2=(Plog(endburn-1,1)-Plog(endburn,1))/(Vlog(endburn-1,1)-
Vlog(endburn,1));
    endburn=endburn-1;
end

% combend720=endburn-1;
EOC=combend720-360;
combdur=combend720-combstrt720;
fprintf('\n')
fprintf('SOC %6.0f degrees \n',SOC)
fprintf('EOC %6.0f degrees \n',EOC)
fprintf('Combustion Duration %6.0f degrees \n',combdur)

% Allocating for space
Xb=zeros(combdur,1);
deg=zeros(combdur,1);
Xb2=zeros(combdur,1);
HR2=zeros(combdur,1);
deg2=zeros(combdur,1);
deg3=zeros(combdur,1);
Wiebe=zeros(combdur,1);

% Calculating mass fraction burned (Rassweiler & Withrow Method)
j=1;
Theta1=SOC;
for i=combstrt720:1:combend720
    Xb(j,1)=(((Pavg(i,1)^(1/gamma1))*Vol(i,1))-...
        ((Pavg(combstrt720,1)^(1/gamma1))*Vol(combstrt720,1)))/...
        (((Pavg(combend720,1)^(1/gamma1))*Vol(combend720,1))-...
        ((Pavg(combstrt720,1)^(1/gamma1))*Vol(combstrt720,1)));
    deg(j,1)=Theta1;
    j=j+1;
    Theta1=Theta1+1;
end

% Beginning 1st Law of Thermodynamics analysis on system
Psi=Pavg.* (101325/14.696); % convert pressure to SI units [Pa]
Pmsi=Pavgmot.* (101325/14.696); % convert pressure to SI units [Pa]
Volsi=Vol.* ((2.54^3)/(100^3)); % convert volume to SI units [m^3]

% Calculating charge mass
[FA,Mch,cvch,cPch,uch,hch,soch,dsodTch]=properties(fuel,phi,0,Tim);
Rch=Ru/Mch; % specific gas constant for charge [J/kgK]
mch=etav*((Pref*Vdm)/(Rch*Tref)); % charge mass [kg]

% Calculating residual mass
[FA,Mr,cvr,cPr,ur,hr,sor,dsodTr]=properties(fuel,phi,1,EGT);
Rr=Ru/Mr; % specific gas constant for residual [J/kgK]
mr=(Psi(EVC,1)*Vcm)/(Rr*EGT); % residual mass [kg]
xr=mr/(mr+mch); % residual mass fraction
xch=1-xr; % charge mass fraction

% Calculating temperature profile using ideal gas law
mt=mch+mr; % total mass in cylinder [kg]

```

```

for i=1:1:720
    T(i,1)=((Psi(i,1)*Volsi(i,1))/((Rch*mch)+(Rr*mr))), % [K]
end

% Woschni's correlation for engine heat transfer
Ahead=pi*(borem/2)^2; % combustion chamber area of head [m^2]
Apiston=pi*(borem/2)^2; % area of piston crown [m^2]
for i=1:1:720
    % Calculating average cylinder gas velocity [m/s]
    if i>combstrt720 && i<EVO % (combustion & expansion period)
        w(i,1)=(c12*Sp)+(cal2*((Vdm*T(combstrt720,1))/...
            (Psi(combstrt720,1)*Volsi(combstrt720,1)))*(Psi(i,1)-
Pmsi(i,1)));
    elseif i>IVC && i<combstrt720 % (compression period)
        w(i,1)=(c12*Sp);
    else % (gas exchange period)
        w(i,1)=c11*Sp;
    end
    % Calculating Woshini's convection coefficient [KJ/kg]
    h(i,1)=(3.26*cal1*(borem^Rem-1)*(Psi(i,1)^Rem)*(T(i,1)^(0.75-
(1.62*Rem)))*(abs(w(i,1))^Rem))/1000;
    % Calculating area of cylinder wall [m^2]
    Acyl(i,1)=2*pi*(borem/2)*((strokem/2)-
((strokem/2)*(cosd(Theta(i,1)))));
    % Calculating the heat transfer rate across the system boundary [KW/s]
    dQdT(i,1)=(h(i,1)*(Acyl(i,1)+Ahead+Apiston)*(T(i,1)-Twall));
end

% Calculating the rate of work transfer done by the system [Nm/s]
for i=1:1:719
    PdVdt(i,1)=Psi(i,1)*((Volsi(i+1,1)-Volsi(i,1))/(Theta(i+1,1)-
Theta(i,1)))*(2*pi*N);
end

% Calculating mass fraction burned (1st Law of Thermodynamics Approach)
Xbo=0;
j=1;
Theta2=SOC;
for i=combstrt720:1:combend720
    [FA,Mch,cvch,cPch,uch,hch,soch,dsodTch]=properties(fuel,phi,0,Tim);
    [FA,Mbg,cvbg,cPbg,ubg,hbg,sobg,dsodTbg]=properties(fuel,phi,1,EGT);
    [FA,Mr,cvr,cPr,ur,hr,sor,dsodTr]=properties(fuel,phi,1,EGT);
    dXbdo=((((dQdT(i,1)-PdVdt(i,1))/(2*pi*N))-((mch*cvch)+(mr*cvr))*((T(i+1,1)-T(i,1))/...
        (Theta(i+1,1)-Theta(i,1))))/(mt)*(ubg-uch));
    if j==1
        Xb2(j,1)=0;
    else
        Xb2(j,1)=Xb2(j-1,1)+dXbdo;
    end
    deg2(j,1)=Theta2;
    j=j+1;
    Theta2=Theta2+1;
end

```

```

% 50% Burn Location Calculation
n=rapdbrnend-rapdbrnstrt+1;
sumx=0;
sumy=0;
sumxy=0;
sumx2=0;
for i=rapdbrnstrt-SOC:1:rapdbrnend-SOC
    sumx=sumx+deg2(i,1);
    sumy=sumy+Xb2(i,1);
    sumxy=sumxy+(deg2(i,1)*Xb2(i,1));
    sumx2=sumx2+(deg2(i,1)^2);
end
rapdbrnslp=((n*sumxy)-(sumx*sumy))/((n*sumx2)-(sumx^2));
rapdbrnoffst=(1/n)*(sumy-(rapdbrnslp*sumx));
Centroid=((0.50-rapdbrnoffst)/rapdbrnslp);

fprintf('Combustion Centroid           %6.1f degrees \n',Centroid)

% ISFC calculation
AF=lambda*14.7; % air/fuel ratio
mf=mch/AF; % mass of fuel inducted per cycle
TotE=mf*44E6; % total energy of fuel (J)
Wc=(Work*12*2.54*4.4482)/100; % work per cycle (J)
nf=Wc/TotE; % fuel conversion efficiency
sfc=(2545/(nf*19000)); % specific fuel consumption (lbm/hp-hr)
nfperc=nf*100; % fuel conversion efficiency to percentage

% Wiebe Function
a=2.5; % curve fit efficiency parameter
m=0.7; % curve fit form factor
durfac=14;
Theta3=SOC;
j=1;
for i=combstrt720:1:combend720+durfac
    Wiebe(j,1)=1-exp(-a*((Theta3-SOC)/(combdur+durfac))^(m+1));
    deg3(j,1)=Theta3;
    Theta3=Theta3+1;
    j=j+1;
end
Wiebedur=j-1;

fprintf('\n')
fprintf('Fuel Conversion Efficiency      %6.1f percent \n',nfperc) % per
cylinder
fprintf('ISFC                           %6.3f lbm/hp-hr \n',sfc) % per
cylinder
fprintf('Mass of Fuel per Cycle        %e kg \n',mf) % 1 cylinder
fprintf('\n')
fprintf('Wiebe Efficiency Parameter    %6.2f \n',a) % a parameter
fprintf('Wiebe Form Factor             %6.2f \n',m) % b parameter
fprintf('Wiebe Duration                 %6.0f degrees \n',Wiebedur) %
Wiebe combustion duration

```

```

% Plotting Data
figure (1)
plot(Theta,Pavg,'.b');
hold on
plot(Theta,Pavgmot,'.r');
xlabel('Crankshaft Angle (Degrees)');
ylabel('Cylinder Pressure (psi)');
title('Pressure vs. Crankshaft Position');
legend('Fired Cycle','Motored Cycle');
hold off
figure (2)
plot(Theta,Pavg,'.k');
hold on
plot(Theta,Pmedian,'.b');
plot(Theta,Pmode,'.r');
xlabel('Crankshaft Angle (Degrees)');
ylabel('Mean, Median, Mode of Cylinder Pressure (psi)');
title('Statistical Check for Cylinder Pressure Data');
legend('Mean','Median','Mode');
hold off
figure (3)
plot(Theta,Pstd,'.b');
xlabel('Crankshaft Angle (Degrees)');
ylabel('Cylinder Pressure Standard Deviation (psi)');
title('Standard Deviation of Pressure vs. Crankshaft Position');
figure (4)
plot(Vol,Pavg,'.b');
xlabel('Cylinder Volume (cubic inches)');
ylabel('Cylinder Pressure (psi)');
title('P-V Diagram');
figure (5)
plot(Vlog,Plog,'.b');
xlabel('Log of Cylinder Volume (cubic inches)');
ylabel('Log of Cylinder Pressure (psi)');
title('Log-Log P-V Diagram');
figure (6)
% plot(deg,Xb,'.k');
% hold on
plot(deg2,Xb2,'.r');
hold on
plot(deg3,Wiebe,'b');
hold off
ylim([0 1])
xlim([-15 35])
xlabel('Crankshaft Angle (Degrees)');
ylabel('Mass Fraction Burned, Xb');
title('Mass Fraction Burned vs. Crankshaft Position');
legend('Experimental Data','Wiebe Function',2);

```

MATLAB R2009a JANAF Table Thermodynamic Data Code

`%% properties.m [14]`

```

function [far,molwt,cv,cP,u,h,so,dsdT]=properties(fuel,phi,xb,T)
global Ru
Ru      = 8314.34; % universal gas constant [J/kmolK]
global atomCO2   aCO2
global atomH2O   aH2O
global atomN2    aN2
global atomO2    aO2
global atomCO    aCO
global atomH2    aH2
global atomH     aH
global atomO     aO
global atomOH   aOH
global atomNO   aNO
global atomfuel afuel
atomCO2 =[ 0.10000e+01  0.00000e+01  0.20000e+01  0.00000e+01];
aCO2    =[ 0.24008e+01  0.87351e-02 -0.66071e-05  0.20022e-08  0.63274e-15
-0.48378e+05  0.96951e+01;
            0.44608e+01  0.30982e-02 -0.12393e-05  0.22741e-09 -0.15526e-13
-0.48961e+05 -0.98636e+00];
atomH2O =[ 0.00000e+01  0.20000e+01  0.10000e+01  0.00000e+01];
aH2O    =[ 0.40701e+01 -0.11084e-02  0.41521e-05 -0.29637e-08  0.80702e-12
-0.30280e+05 -0.32270e+00;
            0.27168e+01  0.29451e-02 -0.80224e-06  0.10227e-09 -0.48472e-14
-0.29906e+05  0.66306e+01];
atomN2  =[ 0.00000e+01  0.00000e+01  0.00000e+01  0.20000e+01];
aN2    =[ 0.36748e+01 -0.12082e-02  0.23240e-05 -0.63218e-09 -0.22577e-12
-0.10612e+04  0.23580e+01;
            0.28963e+01  0.15155e-02 -0.57235e-06  0.99807e-10 -0.65224e-14
-0.90586e+03  0.61615e+01];
atomO2  =[ 0.00000e+01  0.00000e+01  0.20000e+01  0.00000e+01];
aO2    =[ 0.36256e+01 -0.18782e-02  0.70555e-05 -0.67635e-08  0.21556e-11
-0.10475e+04  0.43053e+01;
            0.36220e+01  0.73618e-03 -0.19652e-06  0.36202e-10 -0.28946e-14
-0.12020e+04  0.36151e+01];
atomCO  =[ 0.10000e+01  0.00000e+01  0.10000e+01  0.00000e+01];
aCO    =[ 0.37101e+01 -0.16191e-02  0.36924e-05 -0.20320e-08  0.23953e-12
-0.14356e+05  0.29556e+01;
            0.29841e+01  0.14891e-02 -0.57900e-06  0.10364e-09 -0.69354e-14
-0.14245e+05  0.63479e+01];
atomH2  =[ 0.00000e+01  0.20000e+01  0.00000e+01  0.00000e+01];
aH2    =[ 0.30575e+01  0.26765e-02 -0.58099e-05  0.55210e-08 -0.18123e-11
-0.98890e+03 -0.22997e+01;
            0.31002e+01  0.51119e-03  0.52644e-07 -0.34910e-10  0.36945e-14
-0.87738e+03 -0.19629e+01];
atomH   =[ 0.00000e+01  0.10000e+01  0.00000e+01  0.00000e+01];
aH     =[ 0.25000e+01  0.00000e+00  0.00000e+00  0.00000e+00  0.00000e+00
0.25472e+05 -0.46012e+00;
            0.25000e+01  0.00000e+00  0.00000e+00  0.00000e+00  0.00000e+00
0.25472e+05 -0.46012e+00];
atomO   =[ 0.00000e+01  0.00000e+01  0.10000e+01  0.00000e+01];
aO     =[ 0.29464e+01 -0.16382e-02  0.24210e-05 -0.16028e-08  0.38907e-12
0.29148e+05  0.29634e+01];

```

```

          0.55420e+01 -0.27551e-04 -0.31028e-08  0.45511e-11 -0.43680e-15
0.29231e+05  0.49203e+01];
atomOH = [ 0.00000e+01  0.10000e+01  0.10000e+01  0.00000e+01];
aOH     =[ 0.38376e+01 -0.10779e-02  0.96830e-06  0.18714e-09 -0.22571e-12
0.36413e+04  0.49370e+00;
            0.29106e+01  0.95932e-03 -0.19442e-06  0.13757e-10  0.14224e-15
0.39354e+04  0.54423e+01];
atomNO = [ 0.00000e+01  0.00000e+01  0.10000e+01  0.10000e+01];
aNO     =[ 0.40459e+01 -0.34182e-02  0.79819e-05 -0.61139e-08  0.15919e-11
0.97454e+04  0.29975e+01;
            0.31890e+01  0.13382e-02 -0.52899e-06  0.95919e-10 -0.64848e-14
0.98283e+04  0.67458e+01];
atomfuel=[ 0.10000e+01  0.40000e+01  0.00000e+01  0.00000e+01;
            0.70000e+01  0.17000e+02  0.00000e+01  0.00000e+01;
            0.14400e+02  0.24900e+02  0.00000e+01  0.00000e+01;
            0.10000e+01  0.40000e+01  0.10000e+01  0.00000e+01;
            0.10000e+01  0.30000e+01  0.20000e+01  0.10000e+01];
afuel    =[ 0.19713e+01  0.78716e-02 -0.10486e-05  0.00000e+00  0.00000e+00
-0.99304e+04  0.88737e+01;
            0.40652e+01  0.60977e-01 -0.18801e-04  0.00000e+00  0.00000e+00
-0.35880e+05  0.15450e+02;
            0.79710e+01  0.11954e+00 -0.36858e-04  0.00000e+00  0.00000e+00
-0.19385e+05 -0.17879e+01;
            0.17798e+01  0.12625e-01 -0.36249e-05  0.00000e+00  0.00000e+00
-0.25254e+05  0.15088e+02;
            0.14126e+01  0.20871e-01 -0.81421e-05  0.00000e+00  0.00000e+00
-0.10264e+05  0.19171e+02];
if T<1000
    arange=1;
else
    arange=2;
end
t      = T/1000;
lnK    = 2.743-1.761/t-1.611/t^2+0.2803/t^3;
K      = exp(lnK);
as     = atomfuel(fuel,1)+atomfuel(fuel,2)/4-atomfuel(fuel,3)/2;
if phi<1
    nCO2 = atomfuel(fuel,1);
    nH2O = atomfuel(fuel,2)/2;
    nN2  = atomfuel(fuel,4)/2+3.773*as/phi;
    nO2  = as*(1/phi-1);
    nCO  = 0;
    nH2  = 0;
else
    d1   = 2*as*(1-1/phi);
    a1   = 1-K;
    b1   = atomfuel(fuel,2)/2+K*atomfuel(fuel,1)-d1*(1-K);
    c1   = -atomfuel(fuel,1)*d1*K;
    nCO  = (-b1+sqrt(b1^2-4*a1*c1))/2/a1;
    nCO2 = atomfuel(fuel,1)-nCO;
    nH2O = atomfuel(fuel,2)/2-d1+nCO;
    nN2  = atomfuel(fuel,4)+3.773*as/phi;
    nO2  = 0;
    nH2  = d1-nCO;
end
yfuelch = 1/(1+4.773*as/phi);
yO2ch   = as/phi/(1+4.773*as/phi);

```

```

yN2ch      = 3.773*as/phi/(1+4.773*as/phi);
yCO2bg     = nCO2/(nCO2+nH2O+nN2+nO2+nCO+nH2);
yH2Obg     = nH2O/(nCO2+nH2O+nN2+nO2+nCO+nH2);
yN2bg      = nN2/(nCO2+nH2O+nN2+nO2+nCO+nH2);
yO2bg      = nO2/(nCO2+nH2O+nN2+nO2+nCO+nH2);
yCObg      = nCO/(nCO2+nH2O+nN2+nO2+nCO+nH2);
yH2bg      = nH2/(nCO2+nH2O+nN2+nO2+nCO+nH2);
molwtfuel=
atomfuel(fuel,1)*12.01115+atomfuel(fuel,2)*1.00797+atomfuel(fuel,3)*15.999
4+atomfuel(fuel,4)*14.0067;
molwtCO2 = atomCO2(1)*12.01115 +atomCO2(2)*1.00797 +atomCO2(3)*15.9994
+atomCO2(4)*14.0067;
molwtH2O = atomH2O(1)*12.01115 +atomH2O(2)*1.00797 +atomH2O(3)*15.9994
+atomH2O(4)*14.0067;
molwtN2   = atomN2(1)*12.01115 +atomN2(2)*1.00797 +atomN2(3)*15.9994
+atomN2(4)*14.0067;
molwtO2   = atomO2(1)*12.01115 +atomO2(2)*1.00797 +atomO2(3)*15.9994
+atomO2(4)*14.0067;
molwtCO   = atomCO(1)*12.01115 +atomCO(2)*1.00797 +atomCO(3)*15.9994
+atomCO(4)*14.0067;
molwtH2   = atomH2(1)*12.01115 +atomH2(2)*1.00797 +atomH2(3)*15.9994
+atomH2(4)*14.0067;
molwtch   = yfuelch*molwtfuel+yO2ch*molwtO2 +yN2ch*molwtN2;
molwtbg   = yCO2bg*molwtCO2 +yH2Obg*molwtH2O+yN2bg*molwtN2...
            +yO2bg*molwtO2 +yCObg*molwtCO +yH2bg*molwtH2;
xfuelch   = yfuelch*molwtfuel/molwtch;
xO2ch     = yO2ch*molwtO2/molwtch;
xN2ch     = yN2ch*molwtN2/molwtch;
far        = xfuelch/(xO2ch+xN2ch);
xCO2bg    = yCO2bg*molwtCO2/molwtbg;
xH2Obg    = yH2Obg*molwtH2O/molwtbg;
xN2bg     = yN2bg*molwtN2/molwtbg;
xO2bg     = yO2bg*molwtO2/molwtbg;
xCObg     = yCObg*molwtCO/molwtbg;
xH2bg     = yH2bg*molwtH2/molwtbg;
xfuel     = (1-xb)*xfuelch;
xO2       = (1-xb)*xO2ch+xb*xO2bg;
xN2       = (1-xb)*xN2ch+xb*xN2bg;
xCO2      = xb*xCO2bg;
xH2O      = xb*xH2Obg;
xCO       = xb*xCObg;
xH2       = xb*xH2bg;
molwt     = 1/((1-xb)/molwtch)+(xb/molwtbg));
cPfuel    =
afuel(fuel,1)+afuel(fuel,2)*T+afuel(fuel,3)*T^2+afuel(fuel,4)*T^3+afuel(fu
el,5)*T^4;
cPfuel    = cPfuel*Ru/molwtfuel;
hfuel     =
afuel(fuel,1)+afuel(fuel,2)/2*T+afuel(fuel,3)/3*T^2+afuel(fuel,4)/4*T^3+af
uel(fuel,5)/5*T^4+afuel(fuel,6)/T;
hfuel     = hfuel*Ru/molwtfuel*T;
sofuel    =
afuel(fuel,1)*log(T)+afuel(fuel,2)*T+afuel(fuel,3)/2*T^2+afuel(fuel,4)/3*T
^3+afuel(fuel,5)/4*T^4+afuel(fuel,7);
sofuel    = sofuel*Ru/molwtfuel;
dsodTfuel= cPfuel/T;

```

```

cPCO2      =
aCO2(arange,1)+aCO2(arange,2)*T+aCO2(arange,3)*T^2+aCO2(arange,4)*T^3+aCO2
(arange,5)*T^4;
cPCO2      = cPCO2*Ru/molwtCO2;
hCO2       =
aCO2(arange,1)+aCO2(arange,2)/2*T+aCO2(arange,3)/3*T^2+aCO2(arange,4)/4*T^
3+aCO2(arange,5)/5*T^4+aCO2(arange,6)/T;
hCO2      = hCO2*Ru/molwtCO2*T;
soCO2      =
aCO2(arange,1)*log(T)+aCO2(arange,2)*T+aCO2(arange,3)/2*T^2+aCO2(arange,4)
/3*T^3+aCO2(arange,5)/4*T^4+aCO2(arange,7);
soCO2      = soCO2*Ru/molwtCO2;
dsodTCO2   = cPCO2/T;
cPH2O      =
aH2O(arange,1)+aH2O(arange,2)*T+aH2O(arange,3)*T^2+aH2O(arange,4)*T^3+aH2O
(arange,5)*T^4;
cPH2O      = cPH2O*Ru/molwtH2O;
hH2O       =
aH2O(arange,1)+aH2O(arange,2)/2*T+aH2O(arange,3)/3*T^2+aH2O(arange,4)/4*T^
3+aH2O(arange,5)/5*T^4+aH2O(arange,6)/T;
hH2O      = hH2O*Ru/molwtH2O*T;
soH2O      =
aH2O(arange,1)*log(T)+aH2O(arange,2)*T+aH2O(arange,3)/2*T^2+aH2O(arange,4)
/3*T^3+aH2O(arange,5)/4*T^4+aH2O(arange,7);
soH2O      = soH2O*Ru/molwtH2O;
dsodTH2O   = cPH2O/T;
cPN2       =
aN2(arange,1)+aN2(arange,2)*T+aN2(arange,3)*T^2+aN2(arange,4)*T^3+aN2(aran
ge,5)*T^4;
cPN2      = cPN2*Ru/molwtN2;
hN2        =
aN2(arange,1)+aN2(arange,2)/2*T+aN2(arange,3)/3*T^2+aN2(arange,4)/4*T^3+aN
2(arange,5)/5*T^4+aN2(arange,6)/T;
hN2      = hN2*Ru/molwtN2*T;
soN2       =
aN2(arange,1)*log(T)+aN2(arange,2)*T+aN2(arange,3)/2*T^2+aN2(arange,4)/3*T
^3+aN2(arange,5)/4*T^4+aN2(arange,7);
soN2      = soN2*Ru/molwtN2;
dsodTN2   = cPN2/T;
cPO2       =
aO2(arange,1)+aO2(arange,2)*T+aO2(arange,3)*T^2+aO2(arange,4)*T^3+aO2(aran
ge,5)*T^4;
cPO2      = cPO2*Ru/molwtO2;
hO2        =
aO2(arange,1)+aO2(arange,2)/2*T+aO2(arange,3)/3*T^2+aO2(arange,4)/4*T^3+aO
2(arange,5)/5*T^4+aO2(arange,6)/T;
hO2      = hO2*Ru/molwtO2*T;
soO2       =
aO2(arange,1)*log(T)+aO2(arange,2)*T+aO2(arange,3)/2*T^2+aO2(arange,4)/3*T
^3+aO2(arange,5)/4*T^4+aO2(arange,7);
soO2      = soO2*Ru/molwtO2;
dsodTO2   = cPO2/T;
cPCO      =
aCO(arange,1)+aCO(arange,2)*T+aCO(arange,3)*T^2+aCO(arange,4)*T^3+aCO(aran
ge,5)*T^4;
cPCO      = cPCO*Ru/molwtCO;

```

```

hCO      =
aCO(arange,1)+aCO(arange,2)/2*T+aCO(arange,3)/3*T^2+aCO(arange,4)/4*T^3+aC
O(arange,5)/5*T^4+aCO(arange,6)/T;
hCO      = hCO*Ru/molwtCO*T;
soCO     =
aCO(arange,1)*log(T)+aCO(arange,2)*T+aCO(arange,3)/2*T^2+aCO(arange,4)/3*T
^3+aCO(arange,5)/4*T^4+aCO(arange,7);
soCO     = soCO*Ru/molwtCO;
dsodTCO  = cPCO/T;
cPH2     =
aH2(arange,1)+aH2(arange,2)*T+aH2(arange,3)*T^2+aH2(arange,4)*T^3+aH2(aran
ge,5)*T^4;
cPH2     = cPH2*Ru/molwtH2;
hH2      =
aH2(arange,1)+aH2(arange,2)/2*T+aH2(arange,3)/3*T^2+aH2(arange,4)/4*T^3+aH
2(arange,5)/5*T^4+aH2(arange,6)/T;
hH2      = hH2*Ru/molwtH2*T;
soH2     =
aH2(arange,1)*log(T)+aH2(arange,2)*T+aH2(arange,3)/2*T^2+aH2(arange,4)/3*T
^3+aH2(arange,5)/4*T^4+aH2(arange,7);
soH2     = soH2*Ru/molwtH2;
dsodTH2  = cPH2/T;
cP       =
xfuel*cPfuel+xCO2*cPCO2+xH2O*cPH2O+xN2*cPN2+xO2*cPO2+xCO*cPCO+xH2*cPH2;
h       =
xfuel*hfuel+xCO2*hCO2+xH2O*hH2O+xN2*hN2+xO2*hO2+xCO*hCO+xH2*hH2;
so      =
xfuel*sofuel+xCO2*soCO2+xH2O*soH2O+xN2*soN2+xO2*soO2+xCO*soCO+xH2*soH2;
dsodT   =
xfuel*dsodTfuel+xCO2*dsodTCO2+xH2O*dsodTH2O+xN2*dsodTN2+xO2*dsodTO2+xCO*ds
odTCO+xH2*dsodTH2;
cv      = cP-Ru/molwt;
u       = h-Ru/molwt*T;

```